Study by Proteomics of a Transgenic Mouse Model of Alzheimer's Disease Tau Pathology

Dissertation

zur

Erlangung der naturwissenschaftlichen Doktorwürde

(Dr. sc. nat.)

vorgelegt der

Mathematisch-naturwissenschaftlichen Fakultät

der

Universität Zürich

Von

Della Crystal David

aus Grossbritannien

Promotionskomitee

Prof. Dr. Josef Jiricny (Vorsitz)

PD Dr. Jürgen Götz (Leitung der Dissertation)

Dr. Luc Buée

Zürich 2005

To my Father

TABLE OF CONTENTS:

ZUSAMMENFASSUNG

Die Alzheimer'sche Erkrankung (AD) ist gekennzeichnet durch zwei wesentliche histopathologische Merkmale, extrazelluläre aus fibrillärem Aβ-Peptid bestehenden Amyloid Plaques und intrazelluläre Neurofibrillenbündel (NFT), welche aus hyperphosphoryliertem Tau-Protein bestehen. Bei der mit AD verwandten neurodegenerativen Erkrankung namens Frontotemporale Demenz mit Parkinsonismus gekoppelt mit Chromosom 17 (FTDP-17) finden sich viele NFT ohne eine gleichzeitige Anhäufung von Plaques. Transgene Mäuse, welche das Tau-Protein mit der Mutation P301L überexprimieren, sind ein Modell für die Taupathologie in vivo. Diese Mäuse zeigen sowohl eine Anhäufung von hyper-phosphoryliertem Tau-Protein als auch eine NFT-Bildung, ähnlich wie bei den humanen Krankheitsbildern AD und FTDP-17.
In unserem Labor wurde eine Proteomik-Arbeitsstation eingerichtet, um die Konsequenzen der Taupathologie in diesen Mäusen zu untersuchen. Sowohl die sequentielle Extraktion als auch die zweidimensionale Gelelektrophorese wurden für unsere Untersuchungen am Maushirn optimiert. Die Analyse der P301L Tau-transgenen und Wildtyp-Kontrollhirne zeigte drei prinzipielle Kategorien differentiell regulierter Proteine als Folge der P301L Tau-Expression auf: Proteine mit einer Rolle im Stoffwechsel wie beispielsweise Komponenten der mitochondriellen Atmungskette, Proteine im Zusammenhang mit oxidativem Stress und Funktionen in der Reaktive Sauerstoff-Spezies (ROS) Detoxifikation sowie synaptische Proteine. Es ist bedeutsam, dass die Reduktion der Mengen an mitochondrialem Komplex V in den P301L Tau-transgenen Mäusen - wie in der Proteomanalyse aufgezeigt - in humanen P301L FTDP-17 Gehirnen bestätigt werden konnte. Eine eingehende funktionelle Analyse zeigte eine mitochondriale Dysfunktion in P301L Tau-transgenen Mäusen zusammen mit einer reduzierten Aktivität der NADH-Ubiquinon-Oxidoreduktase und, als Funktion des Alters, eine reduzierte mitochondriale Atmung und ATP Synthese. Die mitochondriale Dysfunktion war assoziiert mit erhöhten Mengen an ROS in alten transgenen Mäusen. Die verstärkte Taupathologie in alten homozygoten P301L Tau-transgenen Mäusen zeigte modifizierte Mengen an Lipidperoxidation und die Hochregulation antioxidanter Enzyme als Antwort auf den oxidativen Stress auf. Ausserdem zeigten die P301L Tau-Mitochondrien eine erhöhte Vulnerabilität nach Behandlung mit Aβ, was auf eine synergistische Wirkung von Tau und Aβ im Hinblick auf die mitochondriale Pathologie hinweist.
Zusammengefasst schliessen wir aus unseren Untersuchungen, dass die durch Tau bewirkte

Pathologie eine mitochondriale und mit oxidativem Stress zusammenhängende ist, und sich möglicherweise von der durch das Aβ-Peptid ausgelösten unterscheidet.

Zusätzlich hat unsere Arbeitsgruppe für AD ein Tier- und ein zelluläres Modell entwickelt, das sowohl die Tau- als auch die Aβ-Pathologie einschliesst. Im zellulären Modell werden P301L Tau überexprimierende Neuroblastomzellen mit oder ohne Aβ-Peptid behandelt und im Mausmodell werden P301L Tau-transgene Mäuse intrazerebral mit Aβ-Peptid injiziert. Beide Modelle wurden proteomisch untersucht und spezifische Modifikationen konnten als Folge der Aβ-Behandlung gefunden werden.

Schliesslich haben wir das mit Streptogramin reprimierbare PipOFF Genregulations-system in der Maus evaluiert. In der Abwesenheit von Streotograminen wird PIT exprimiert und bindet an seinen P_{PIR} Ziel-Promoter, was schliesslich die Transkription eines Reportergens aktiviert. Es wurden EF1α-PIT und PPIR8-YFP doppel-transgene Mäuse hergestellt, aber es gelang uns nicht, die Expression von PIT bzw YFP nachzuweisen. Wir modifizierten den die PIT-Expression regulierenden Promoter und die Reportergene in CMV/β-Aktin-PIT und PPIR8-LacZ, konnten aber auch dadurch nicht PIT bzw LacZ Expression in den Mäusen nachweisen. Wir schliessen aus unseren Untersuchungen, dass sich das PipOFF-System in seiner gegenwärtigen Form nicht für eine regulierte Genexpression im Mausmodell eignet.

SUMMARY

Alzheimer's disease (AD) is characterised by two major histopathological hallmarks, extracellular plaques of fibrillar β-amyloid peptides and intracellular neurofibrillary tangles (NFT) composed of hyperphosphorylated tau protein. Mutations in tau have been identified in a related neurodegenerative disorder called frontotemporal dementia with parkinsonism linked to chromosome 17 (FTDP-17) with NFT formation in the absence of plaque formation. Transgenic mice overexpressing the P301L mutant human tau protein model tau pathology in vivo. These mice show an accumulation of hyperphosphorylated tau and NFT formation similar to those in FTDP-17 and AD. A proteomics working station was established in the laboratory to analyse the consequences of tau pathology in these mice. A sequential extraction and two-dimensional electrophoresis related methods were optimised for the study of the mouse brains. Analysis of P301L tau transgenic and wild-type control mouse brains revealed three principal categories of proteins differentially regulated by P301L tau expression: metabolism related proteins including mitochondrial respiratory chain complex components, oxidative stress related enzymes implicated in reactive oxygen species (ROS) detoxification and synaptic related proteins. Significantly, the reduction in mitochondrial complex V levels in the P301L tau mice shown using proteomics was also confirmed as decreased in human P301L FTDP-17 brains. Functional analysis demonstrated a mitochondrial dysfunction in P301L tau mice together with reduced NADH-ubiquinone oxidoreductase activity and, with age, impaired mitochondrial respiration and ATP synthesis. Mitochondrial dysfunction was associated with higher levels of reactive oxygen species in aged transgenic mice. Increased tau pathology as in aged homozygous P301L tau mice revealed modified lipid peroxidation levels and the up-regulation of antioxidant enzymes in response to oxidative stress. Furthermore, P301L tau mitochondria displayed increased vulnerability towards β-amyloid peptide insult, suggesting a synergistic action of tau and β-amyloid peptide pathology on the mitochondria. Taken together, we conclude that tau pathology involves a mitochondrial and oxidative stress disorder possibly distinct from that caused by β-amyloid peptide.

In addition our group has generated a cellular and mouse model for AD which incorporates both the β-amyloid and tau pathology. In the cellular model, P301L tau overexpressing neuroblastoma cells were treated with or without β-amyloid peptide and in the mouse model, P301L tau transgenic mice were intracranially injected with β-amyloid peptide. Proteomic

analysis of both models was carried out and we detected specific modifications caused by β-amyloid peptide treatment.

Finally we evaluated the streptogramin-repressible gene regulation system, PipOFF, in the mouse model. In the absence of streptogramins, PIT is expressed, binds to its target P_{PIR} promoter and activates transcription of the reporter gene. EF1α-PIT and PPIR8-YFP double transgenic mice were generated but we could not detect the presence of PIT or YFP. We modified the promoter controlling PIT expression and the reporter gene to CMV/β-actin-PIT and PPIR8-LacZ. However we could still not detect PIT or LacZ expression in these mice either. Therefore we conclude that the PipOFF system is not suitable in its present form, to regulate gene expression in the mouse model.

1 INTRODUCTION

1.1 General background on Alzheimer's disease

1.1.1 Alzheimer's Disease - A Major Health Problem

The sporadic form of Alzheimer's disease (AD) is the most common neurodegenerative disorder among people over 65. From this age on, its prevalence doubles every 5 years and reaches about 30% of the population aged 85. Since this age group is the most rapidly increasing part of the population in most industrialised countries, the impact of the disease on society becomes increasingly important. The annual cost of care for a patient with moderate AD is estimated to be around $30,000. AD not only affects patients but also presents a heavy physical and psychological burden to their relatives who take care of them for most of the time while observing the constant, irreversible aggravation of symptoms, until hospitalisation becomes inevitable.

1.1.2 Clinical symptoms and cognitive tests

AD is characterised by the progressive loss of memory. Patients have more and more difficulty in remembering names of common objects and familiar persons (agnosy), fail to carry out simple tasks (apraxy), develop dysfunctional speech (aphasy) and eventually lose their complete reasoning ability. The progress of the disease is correlated with abnormal behaviour, personality changes and often with depressions. Finally patients become bedridden, completely dependent on caretakers and develop opportunistic diseases. Most AD patients die from pneumonia. The impact of AD has become even more evident since an established network of collaborations has produced a standardised diagnosis of dementia (DSM IV, APA 1996), preclinical and clinical AD (criteria of the NINCDS-ADRDA, (McKhann et al., 1984)), and the associated histopathology (CERAD, (Mirra et al., 1994)). The aforementioned criteria allow a distinction between "possible", "probable" or "certain" AD. Assessing the cognitive abilities in patients requires a constant follow-up, because not the absolute level of cognitive performance, but its constant pace of decline is indicative for AD. Cognitive tests like the Mini-Mental State exam or the Blessed Dementia Scale are available to monitor the development of the patient's cognitive abilities and to distinguish it from normal age-related decline. These tests are usually supported by the patient's history, interviews with relatives and neuropsychological exercises. However, the error rate of

"possible" or "probable" AD diagnosis in the best specialised medical centres is estimated to be 10-20%.

1.1.3 Neurodegeneration and molecular markers of Alzheimer's disease

Alzheimer's disease is characterised by an increasing shrinkage (atrophy) of the brain. Positron emission tomography (PET) can be used to find zones of neuronal death by monitoring the metabolisation of radioactively marked glucose in the neurones. Another imaging technique, magnetic resonance imaging (MRI), becomes increasingly important for measuring the hippocampal volume and establishing an early AD diagnosis in patients with memory impairment.

However, only after the patient has deceased will the autopsy of the brain provide the definite histopathological evidence of the two molecular hallmarks of AD and a confirmation of the diagnosis. The final stage of AD is characterised by the massive deposition of extracellular neuritic plaques and intracellular neurofibrillary tangles (NFT). Neuritic plaques consist mainly of amyloid deposits of Aβ peptide, an extracellular proteolytic fragment of the transmembrane amyloid precursor protein (APP)(review in (Selkoe, 1998)). NFT are proteinaceous aggregates consisting mainly of paired helical filaments (PHF), a fibrillary polymer of the microtubule-associated protein tau. Apart from these two unconditional signs associated with AD, Lewy bodies and cerebrovascular amyloid can also be found.

1.2 General review on ß-amyloid pathology

1.2.1 β-Amyloid generation

In the AD brain, β-amyloid is deposited around meningeal and cerebral vessels, and in the grey matter as β-amyloid plaques (reviewed in (Gotz et al., 2004a)). The major proteinaceous component of these deposits is a 40-42 amino acid aggregated polypeptide termed Aβ ($A\beta_{40}$ and $A\beta_{42}$), which is derived by proteolysis from the larger amyloid precursor protein, APP (Fig. 1) (Glenner and Wong, 1984; Masters et al., 1985).

APP can be proteolytically cleaved by the membrane-associated α-secretase, which cleaves APP within the Aβ domain. This pathway is non-amyloidogenic, as this cleavage precludes the formation of Aβ. Alternatively, cleavage may occur in the amyloidogenic, endosomal-lysosomal pathway, first by β-secretase and then by γ-secretase, which together generates the highly fibrillogenic Aβ peptide. β-secretase activity has been attributed to a single protein, BACE,

whereas γ-secretase activity was shown to depend on the presence of a total of four components: presenilin, nicastrin, APH-1 and PEN-2 (Edbauer et al., 2003; Vassar et al., 1999).

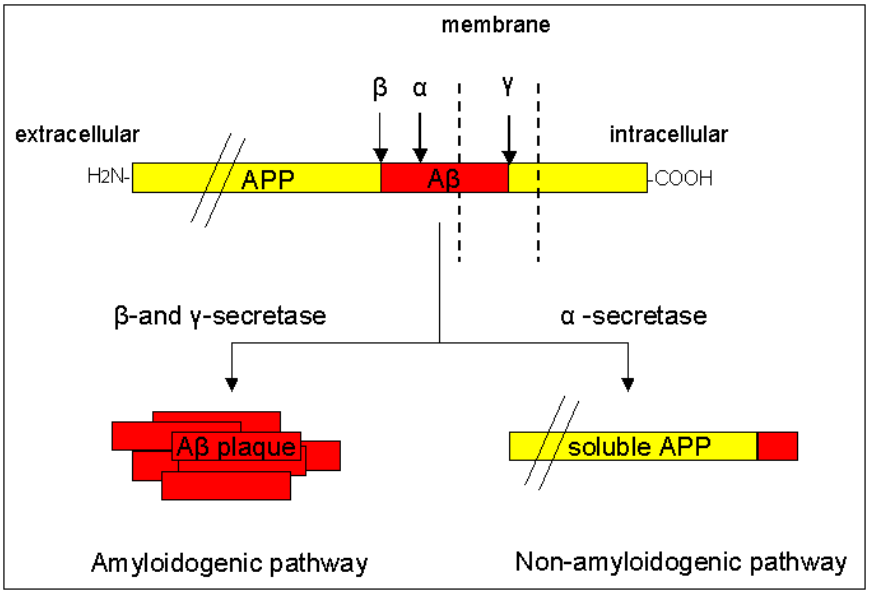

Figure 1.: Aβ generation from APP

1.2.2 β-Amyloid function and toxicity

The exact physiological function of Aβ remains unclear. It has been proposed that Aβ might act as a physiological regulator of ion channel function in neurones, based on studies using exogenously added Aβ peptides and neuronal primary cultures (Ramsden et al., 2002; Ramsden et al., 2001). Furthermore non-fibrillary Aβ peptides have been demonstrated to block α7-containing nicotinic receptors on rat hippocampal neurones in culture. Recently neuronal activity has been shown to modulate the formation and secretion of Aβ peptides in hippocampal slice neurones that overexpress APP (Kamenetz et al., 2003). Indeed increased neuronal activity causes increased Aβ secretion which in turn down-regulates excitatory synaptic transmission. Furthermore this study reveals that Aβ production impairs long-term potentiation (LTP). Therefore Aβ could function as a synaptic transmission and plasticity regulator.
On the other hand, numerous toxic functions have been imputed to Aβ (review (Small et al., 2001). Aβ has been shown, among other, to increase ER stress (Nakagawa et al., 2000), induce apoptosis (Loo et al., 1993), increase reactive oxygen species (ROS) (Behl et al., 1994), inhibit

ATP levels through inhibition of cytochrome c oxidase activity (Keil et al., 2004; Parker et al., 1994) and to mediate neurotoxicity by interacting with APP (Lorenzo et al., 2000).

1.2.3 Genetic involvement of amyloid precursor protein in Alzheimer's disease

In the complex etiology of AD, in addition to environmental conditions, genetic factors play a major role. Twin studies support the notion that 70-80% of the risk to develop AD is determined by genetic factors (Gatz et al., 1997). Early-onset familial forms of AD (FAD) make up 1% of the total number of AD cases (Delacourte et al., 2002). These forms of AD are characterised by specific mutations, in the APP gene itself, and in the presenilin 1 (PS1) and presenilin 2 (PS2) genes. Mutations in the APP gene are estimated to account for up to 5% of FAD, the most well-known being the "Swedish mutation" consisting of a double base pair substitution K670D/M671L (Mullan et al., 1992) and the "London mutation" consisting of the mutation V717I (Goate et al., 1991). Until today, a total of 16 pathogenic mutations has been identified in the APP gene (Finckh et al., 2005).

1.2.4 Amyloid precursor protein transgenic mouse models

The first APP transgenic animals to show extensive AD-like neuropathology, expressed high levels of the disease-linked V717F mutant form of APP, under control of the platelet-derived growth factor (PDGF) mini-promoter (Games et al., 1995; Gotz et al., 2004b). These PDAPP mice showed many of the pathological features of AD, including extensive deposition of extracellular amyloid plaques, astrocytosis and neuritic dystrophy. Moreover, the β-amyloid load in the hippocampus increased as a function of age. Morris water maze testing showed memory impairment. A second transgenic model by Hsiao et al. expressed the APP swedish mutation inserted into a hamster prion protein (PrP) cosmid vector (Hsiao et al., 1996). The resulting Tg2576 line developed numerous β-amyloid plaques that could be stained with the Congo red dye. Learning was assessed in the Y-maze, a spatial alternation task, and in the Morris water maze. At nine months of age and older, impairment in learning and memory became apparent in these transgenic mice. Since many other groups have generated APP transgenic mouse models. Furthermore Aβ induced pathology can be enhanced by co-expressing both the APP swedish mutant and the presenilin M146L PS1 mutant (Holcomb et al., 1998).

1.2.5 Anti-β-amyloid vaccination trials in humans

Currently, there are no cures for AD. Available drugs only alleviate the symptoms but are ineffective against cognitive decline. As transgenic animal models provided evidence that both active and passive Aβ immunisation can reduce cognitive dysfunction in APP transgenic mouse models without any side effects, an immunisation trial was initiated in humans (review (Gotz et al., 2004b)).

Phase I clinical trials were initiated with the AN-1792 vaccine, a pre-aggregated synthetic $A\beta_{42}$ preparation, and the adjuvant QS-21 (Schenk, 2002). It could be shown that approximately 25% of the patients produced Aβ-specific antibodies. In October 2001, a phase IIa clinical trial was started and patients were randomised to receive AN1792/QS-21 or placebo (Orgogozo et al., 2003). However, the dosing was prematurely halted in January 2002 when four patients who had received the AN-1792/QS-21 vaccine developed signs of subacute meningoencephalitis (Check, 2002; Senior, 2002).

Among a cohort of 30 patients from one of the centres, 24 patients were shown to have developed specific antibodies against Aβ, which did not cross-react with human full-length APP. These antisera stained Aβ plaques in brain slices from APP transgenic mice and post-mortem brain sections from patients with AD (Hock et al., 2002). Among the 24 patients, the specific immune reaction against Aβ was still stable after one year. Moreover, this immune reaction showed a significant correlation with slowed cognitive decline. These beneficial clinical effects could also be demonstrated in two of three patients who had experienced immunisation-related aseptic meningoencephalitis (Hock et al., 2003). Together, these results indicate that vaccination against Aβ might be a potential treatment for AD, provided that a safe treatment modality can be introduced. It is important to note that immunisation against Aβ does not seem to remove neurofibrillary pathology as shown in post-mortem studies of three patients having received the AN-1792 vaccine (Ferrer et al., 2004; Masliah et al., 2005; Nicoll et al., 2003).

1.3 General review on tau pathology

1.3.1 Molecular function of tau protein

Tau is the major microtubule-associated protein in axons and plays a role in neurite outgrowth, axonal stability and transport functions in the nervous system. It belongs to the family of microtubule-binding proteins that also comprises its close relatives, MAP2a, MAP2b (expressed

in dendrites only, with the much shorter foetal isoform MAP2c) and MAP4 (only expressed in peripheral tissue). These proteins range from 42kDa to 280kDa and share the common features of 3-5 C-terminal microtubule-binding repeat domains and an N-terminal projection domain.
The tau gene is present in humans in a single copy spanning 100kb at 17q21 and contains 16 exons (Andreadis et al., 1992). It is regulated by the TATA-less type promoter often found in housekeeping genes. Of the 16 putative exons, exons 8 is never found in any human tau mRNA (reviewed in (Andreadis, 2005). Exon 4A is only included in tau from peripheral tissue, and exons -1 and 14 are transcribed but never translated. Foetal tau [2-,3-,10-] is the only transcript during early brain development and contains the exons 1, 4, 5, 7, 9, 11, 12 and 13. In adult brain, the additional exon cassettes 2, 3, and 10 can be spliced in, exon 3 never being present without exon 2. Alternative splicing therefore leads to six different tau translation products ([2-,3-,10-]; [2+,3-,10-]; [2+,3+,10-]; [2-,3-,10+]; [2+,3-,10+]; [2+,3+,10+]). Exons 9, 11, 12 and the alternatively spliced cassette 10 code the four microtubule-binding repeats. This alternative splicing is developmentally regulated and different neuronal subpopulations in cortical layers have different sets of tau isoforms.
One of the best studied roles of tau is its interaction with tubulin through three to four conserved microtubule binding repeats located in the C-terminal half of the protein. Tau shows non-saturable, biphasic binding behaviour to tubulin *in vitro*, and a higher affinity is found with the four-repeat isoform containing an additional binding site (Ackmann et al., 2000). The N-terminal projection domain of tau is highly acidic. Its length is determined by alternative splicing of cassettes 2 and 3 and may be responsible for the spacing between microtubules. The projection domain is thought to interact with other cytoskeletal proteins and the plasma membrane to confer stability to the axons. Tau also seems to play a significant role in cellular transport. Indeed overexpressed tau bound to microtubules inhibits anterograde kinesin-dependent transport of mitochondria and vesicles along microtubules (Ebneth et al., 1998; Mandelkow et al., 2003; Stamer et al., 2002).

1.3.2 Normal tau phosphorylation and abnormal phosphorylation linked to Alzheimer's disease

Physiological phosphorylation of tau is thought to regulate its microtubule binding proprieties. The potential tau phosphorylation sites can be separated into two categories: the Ser-Pro (S-P) or Thr-Pro (T-P) motifs, and the non-S/T-P motifs as for example, KXGS. The S/T-P motifs are

phosphorylated by proline-directed kinases, for example, MAPK, GSK3β and cyclin-dependent kinases like cdc2 and cdk5. The non S/T-P motifs have been found to be potentially phosphorylated by MARK, PKA, CaMK II and casein kinase II. Tau phosphorylation is an active process, as well as being developmentally regulated. Indeed tau from fetal brain is phosphorylated at more sites than tau from adult brain, implying selective dephosphorylation of the shortest isoform during brain maturation (Goedert et al., 1995).

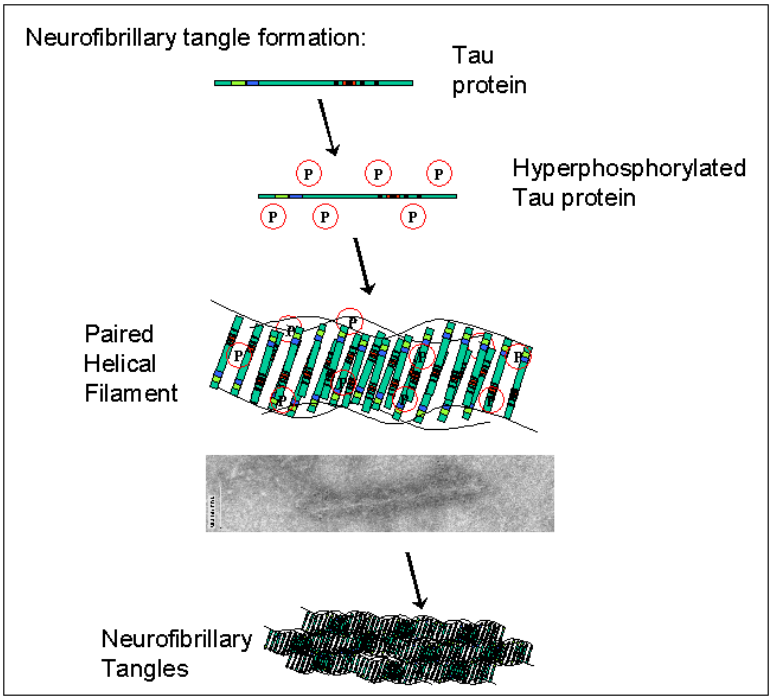

Figure 2.: Neurofibrillary tangle formation

In pathological circumstances, tau has been shown to be hyperphosphorylated compared to normal adult brain tau phosphorylation. Thus, phosphorylation sites have been classified into physiological and pathological sites. The latter include the R145d/AP422 epitope Ser-422, the AT100 epitope Thr-212/Ser-214, and the conformation- and phosphorylation-dependent epitope AT180/PHF-27/TG3 (Thr-231/Ser-235) (Bussiere et al., 1999; Hasegawa et al., 1996; Hoffmann et al., 1997; Jicha et al., 1997). Hyperphosphorylation of tau reduces its binding to the microtubules and causes its translocation from the axon to the somatodendritic domain in AD neurones, where it forms paired helical filaments and straight filaments and finally NFT (Fig. 2). It remains unclear whether hyperphosphorylation enhances tau assembly into PHF or not, as contradictory studies have been published (Alonso et al., 2001; Schneider et al., 1999). Still little

is known about the molecular basis of tau's destructive actions. One hypothesis is that the intracellular aggregation of tau and the formation of NFT causes cell death through gain of function. The second or concomitant hypothesis would be that tau hyperphosphorylation and sequestration in the cytoplasm leads to the dysregulation of the cellular microtubule dynamics ((Alonso et al., 1994), review (Feinstein and Wilson, 2005)).

1.3.3 Human tauopathies

Tau-positive filamentous lesions can be found in a wide range of neurodegenerative diseases that are commonly regrouped as "tauopathies". With the exception of AD, Aβ is usually absent in most of these diseases. Accounting for the wide variety of symptoms, NFT can be found in different parts of the brain depending on the tauopathie, can affect either neuronal cells or glial cells or both and can occur in only certain types of neuronal cells. Often tauopathies will be distinguished according to which isoforms accumulate to form PHF, which produces a characteristic band pattern in gel electrophoresis. In AD, all six isoforms compose PHF. In Pick's disease, a rare frontotemporal dementia characterised by Pick bodies in both cortical and subcortical structures, predominantly three-repeat tau isoforms are found in the abnormal filaments. In contrast to that, only four-repeat tau isoforms are present in NFT in neuronal and glial cells in the cases of corticobasal degeneration (CBD), characterised by frontoparietal atrophy, and in progressive supranuclear palsy (PSP), a late-onset atypical Parkinsonian disorder. For some of the tauopathies, a hereditary form of the disease linked to the tau locus has been discovered and named frontotemporal dementia with parkinsonism linked to chromosome 17 (FTDP-17) (Foster et al., 1997; Hutton et al., 1998). The characteristics of FTDP-17 diseases depend on the nature and location of the specific mutation and sometimes give rise to the same clinical picture as found in various sporadic tauopathies (Spillantini et al., 2000).
The FTDP-17 mutations can be classified into three groups (Table 1) (Barghorn et al., 2000; Ingram and Spillantini, 2002). The list represented in Table 1 is not extensive. One group of missence mutations affects the microtubule-binding function of tau and enhances its propensity to form fibrils. A second variant encompasses mutations in exon 10 that are only found in tau proteins with four repeats. In this group, fibrillisation is greatly increased and tau binding to microtubules is inhibited. The third group of mutations affects the splicing of exon 10, leading to a shift only in the ratio of four-repeat to three-repeat tau. These mutations cause only a mild increase in the propensity to aggregation of the tau protein.

Table 1.: Classification of FTDP-17 mutations and effect on the assembly of microtubules and the formation of tau filaments *in vitro* (non-extensive list).

FTDP mutations	*Exon affected and effect on isoform ratio*	*Inhibitory effect on tau-promoted microtubule assembly*	*Stimulatory effect on formation of tau filaments*
wt	-	0	+
Missense mutations that alter the function of all tau isoforms			
G272V	9 (normal ratio)	++	++
V337M	12 (normal ratio)	++	++
R406W	13 (normal ratio)	+	+
Missense mutations in exon 10 that alter the function of four-repeat tau isoforms only			
P301L	10 (normal ratio)	+++	+++
P301S	10 (normal ratio)	+++	+++
Mutations that shift the four-repeat/three-repeat tau ratio			
ΔK280	10 (mostly spliced out)	+++	+
L284L	10 (always included)	0	+
N279K	10 (always included)	0	+
S305N	10 (always included)	0	+
+3, +12, +13, +14, +16, +33	intron behind exon 10 (largely included)	0	+

1.3.4 Tau transgenic mouse models

The first tau transgenic model was established in 1995 in mice by expression of the longest human brain tau isoform under control of the hThy1 promoter (Gotz et al., 1995) (review (Gotz, 2001; Gotz et al., 2004b)). At that time, pathogenic mutations in tau had not yet been identified. Despite the lack of NFT pathology, these mice modelled aspects of human AD, such as somatodendritic localisation and hyperphosphorylation of tau and, therefore, represented an early pre-NFT AD-like phenotype. The subsequent use of stronger promoters to drive transgene expression caused a more pronounced phenotype (Ishihara et al., 1999; Probst et al., 2000; Spittaels et al., 1999). In these mice, tau protein extracted from transgenic brain and spinal cord became increasingly insoluble as the mice became older. Despite the decreased solubility of tau, NFT did not form, unless the mice reached a very old age (Ishihara et al., 2001). With the identification in 1998 of pathogenic mutations in tau in FTDP-17 (Hutton et al., 1998), several groups achieved NFT formation both in neurones (Allen et al., 2002; Gotz et al., 2001a; Lewis et al., 2000; Tanemura et al., 2001; Tatebayashi et al., 2002) and in glial cells of transgenic mice (Gotz et al., 2001c; Higuchi et al., 2002). When a human tau isoform lacking the two amino-terminal inserts, was expressed together with the P301L mutation by using the murine PrP

promoter (Lewis et al., 2000), in a line with high expression levels, 90% of the mice developed motor and behavioural disturbances by 10 months of age. In these mice, NFT were identified in brain and spinal cord, and motor neurones were reduced twofold in spinal cord (Lewis et al., 2000). The P301L mutation was also expressed in a second model using the longest human tau isoform. In this model, the mThy1.2 promoter was chosen instead of the PrP promoter, which may account for different expression patterns in these mice (Gotz et al., 2001a). Expression levels of tau are high in the amygdala, hippocampus, cortex but not detectable in the cerebellum. NFT were identified in these transgenic mice by Gallyas silver staining and thioflavin S-fluorescent microscopy.

1.4 Amyloid cascade hypothesis: connection between tau and ß-amyloid

The pathogenic relationship of the two major lesions of AD, Aβ-plaques and NFT, and their relative contribution to the clinical features of AD is one of the most crucial and controversial topics in AD research. Patients bearing APP mutations develop both hallmarks, whereas tau mutation carriers only develop NFT, providing evidence that Aβ might induce NFT formation but not the opposite. These findings lead to the amyloid cascade hypothesis (Hardy and Higgins, 1992), which claims that (at least in familial AD) Aβ causes or enhances the NFT pathology (review ((Gotz et al., 2004b)). Although this concept at first sight seems consistent, it is difficult to combine it with the highly puzzling finding that plaques and NFT are neuroanatomically separated. NFT develop in specific sites of the brain and spread in a predictable, non-random manner across it. Six stages of disease progression based on the tau pathology have been distinguished (Braak and Braak, 1991; Braak and Braak, 1995): the transentorhinal stages I-II representing clinically silent cases; the limbic stages III-IV of incipient AD; and the neocortical stages V-VI of fully developed AD. A comparative study of Aβ-associated pathology defined five phases which differ strikingly from the NFT-stages. These findings suggest that Aβ-deposition expands anterogradely into regions that receive neuronal projections from regions already exhibiting Aβ (Thal *et al.*, 2002).

Numerous correlation studies failed to demonstrate a clear relationship between the severity of dementia and Aβ deposition in human AD brain whereas correlation between NFT numbers and severity of dementia has been reported (Arriagada *et al.*, 1992; Bierer *et al.*, 1995; Crystal *et al.*, 1988; Nagy *et al.*, 1996). It was shown that total NFT counts in specific brain areas such as the entorhinal and frontal cortex, as well as neurone numbers in the CA1 region of the hippocampus

were the best predictors of cognitive deficits in brain ageing and AD (Giannakopoulos *et al.*, 2003).

However, a synergistic interaction between the APP- and the tau-related pathology, despite the different spatiotemporal distribution of plaques and NFT, has been proposed (Delacourte *et al.*, 1999; Delacourte *et al.*, 2002). It was shown that whenever Aβ aggregates were detected, tau pathology was found, at least in the entorhinal cortex. The opposite was not true because cases were found with advanced tau pathology, with no trace of Aβ aggregates (Delacourte *et al.*, 2002). To address the issue of Aβ driven tau pathogenesis, our group stereotaxically injected pre-aggregated Aβ fibrils into the somatosensory cortex and the hippocampus (CA1) of P301L tau transgenic mice (Gotz et al., 2001b). This stereotaxic approach caused a fivefold increase in the numbers of NFT in the amygdala of P301L mice, but not in wild-type tau transgenic or control mice. NFT formation was associated with the pathological phosphorylation of tau at the epitopes Thr-212/Ser-214 (AT100) and Ser-422 (pS422).

An alternative approach was pursued by intercrossing Aβ-producing APP-mutant mice (Tg2576 mice overexpressing the APP swedish mutation) with P301L tau transgenic mice (JNPL3-line) (Lewis *et al.*, 2001). Double transgenic mice showed a more than sevenfold increase in NFT numbers in the olfactory bulb, the entorhinal cortex and the amygdala compared to P301L single transgenic mice. In contrast, plaque formation was unaffected by the presence of the tau mutation compared to APP swedish single transgenic mice. Recently, a triple transgenic model was generated expressing mutant M146V PS1, P301L tau and the swedish APP mutation (Oddo et al., 2003). These mice show an age-related deposition of intracellular and extracellular Aβ which occurs before accumulation of tau protein, thus also supporting the amyloid cascade hypothesis. Together, although these data do not prove a causal relationship between Aβ and tau pathology, they demonstrate that Aβ can significantly accelerating the NFT formation in P301L tau mice.

Based on the *in vivo* data of the tau transgenic mice, our group established a cellular system using the human SH-SY5Y neuroblastoma cell line. P301L mutant human tau was stably overexpressed in these cells. Treatment with extracellular pre-aggregated Aβ-peptides for five days caused the development of numerous AD-like tau filaments (Ferrari et al., 2003).

1.5 Proteomics

The significance of purely genomic approaches is undermined by a poor mRNA/protein correlation observed in numerous studies and possibly due to mechanisms such as translational

control, post-translational modification and regulation of protein stability (Gygi et al., 1999b). Therefore measuring gene expression at the protein level is potentially more informative than the corresponding measurement at the mRNA level. By definition, the proteome is the full complement of proteins produced by a particular genome of a cell, tissue or species at a given time. It represents a higher complexity than the transcriptome, and it displays a higher degree of dynamics due to posttranslational modifications.

The field of proteomics has been rapidly changing over the past few years. Two-dimensional technology has significantly improved as well as the detection limits of current mass spectrometers. New non-gel based technologies have emerged using either a series of liquid chromatography (LC) separations as in multidimensional protein identification technology (MudPIT) or combining peptide labelling and LC separation such as ICAT, iTRAQ and stable isotope labelling with amino acids in cell culture (SILAC) technologies (Gygi et al., 1999a; Krijgsveld et al., 2003; Ross et al., 2004). Importantly, peptide labelling allows for the first time the quantification of changes between two differently treated samples without using two-dimensional electrophoresis (2-DE). However the implementation of non gel-based proteomics is mainly limited by the sample complexity, which demands a significant amount of sample fractionation, and the subsequent peptide identification by mass spectrometry (MS) normally electrospray ionisation MS, which is very time consuming. The latter requires the availability of considerable machine time which is generally not available in shared resource environments such as those in functional genomic centres. Therefore 2-DE remains the current workhorse for statistical quantitative comparison of complex samples.

1.5.1 Two-dimensional electrophoresis

In 2-DE, proteins are first separated according to charge and then in the second dimension by mass (Hoerndli et al., 2005) (Fig. 3). 2-DE routinely allows the detection of over 3000 proteins per gel and as little as 1 ng per protein spot. In principal, this method is capable of resolving up to 10,000 proteins in a single gel (Klose, 1975; O'Farrell, 1975).

In the first phase of 2-DE, proteins are separated by isoelectric focusing using immobilised pH gradients (IPG) in a thin gel strip. Proteins migrate through the IPG strip until their net charge is neutral (the isoelectric point, pI). Different IPG strips can be used, from wide pH range and covering many pH units which allows low resolution of a large number of proteins, to narrow pH ranges covering just one or two pH units which allows high resolution of a small number of

proteins (Hoving et al., 2002). Following separation in the first dimension, proteins are separated in the orthogonal direction using electrophoresis in acrylamide gels containing sodium dodecyl sulfate (SDS), where SDS imparts a net negative charge, allowing protein separation by molecular weight (SDS-PAGE). Once proteins are separated, they can be visualised using a variety of stains, such as the highly sensitive Silver staining or the less sensitive Coomassie blue staining. Alternatives are fluorescent dyes such as the SYPRO stain which is more compatible with protein identification by MS, since the proteins are not covalently modified by the dye. Moreover, the signal is linear over a wide range of spot intensities, allowing a more precise quantification (Berggren et al., 2002).

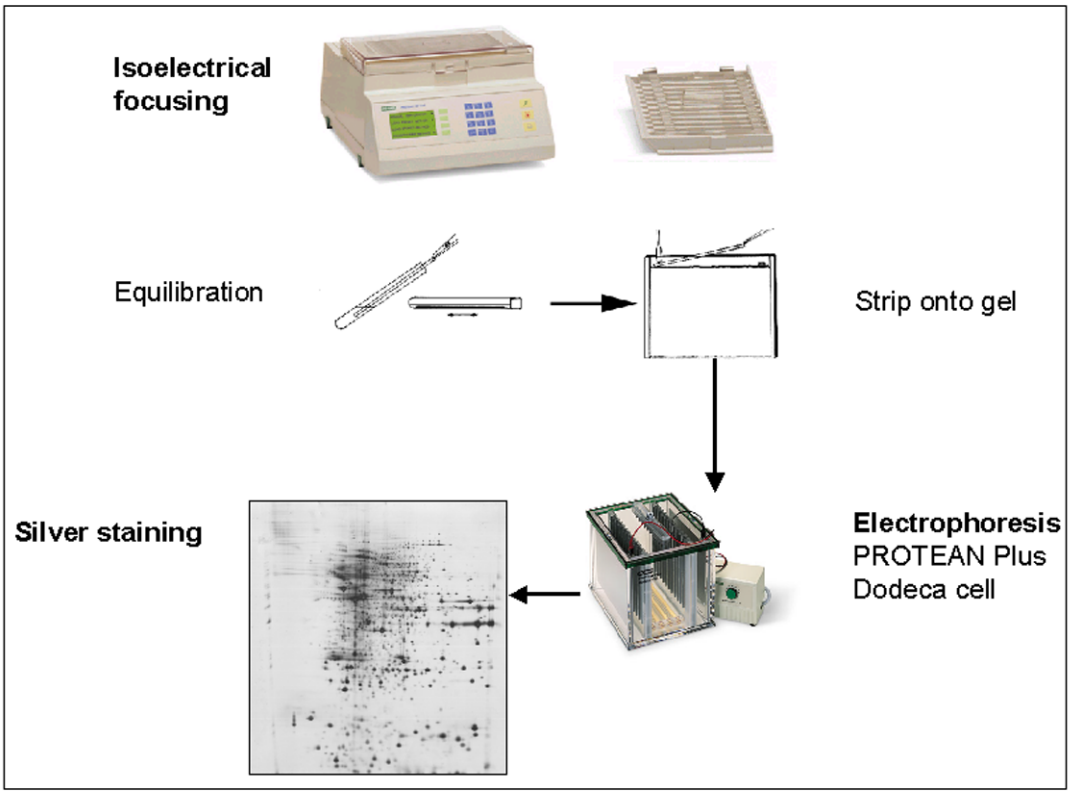

Figure 3.: Two-dimensional electrophoresis: From isoelectrical focusing to 2-D gels.

1.5.2 Mass spectrometry

MS (reviewed in (Griffin and Aebersold, 2001; Steen and Mann, 2004)) is used to identify proteins following separation by 2-DE or LC. 15 years ago, the two major techniques were developed: matrix-assisted laser desorption ionisation (MALDI) time-of-flight (TOF) MS, and

electrospray ionisation (ESI) MS (Banks and Whitehouse, 1996; Fenn et al., 1989; Hillenkamp et al., 1991; Karas and Hillenkamp, 1988). The development of these relatively non-destructive, soft ionisation methods made it possible to convert proteins into volatile ions. Usually, for peptide mass fingerprint (PMF) analysis, the protein to be analysed is purified, and digested enzymatically, generally by trypsin, to cleave the protein at specific bonds giving a reproducible pattern of digestion. For ESI-MS, the resulting peptides are injected into a reverse phase HPLC column that is directly coupled to the mass spectrometer.

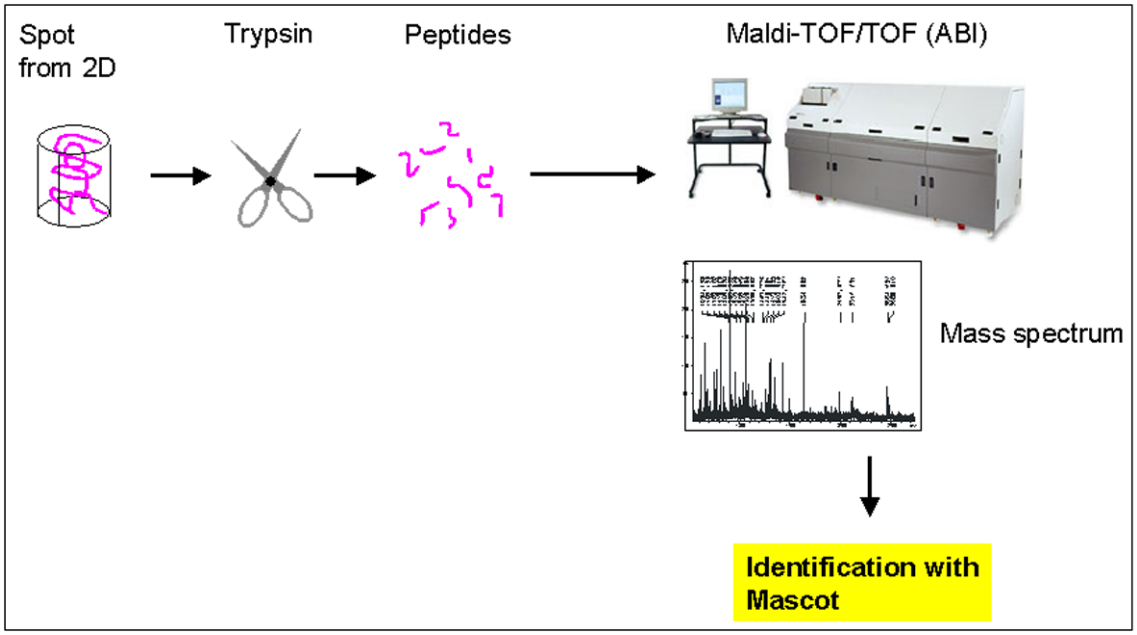

Figure 4.: Identification of protein spots with the MALDI-TOF/TOF MS

For MALDI-MS, tryptic peptides are combined with a matrix on a MALDI target and then analysed (Fig. 4). Gaseous ions are produced by accelerating an ionised particle, in this case a peptide, through a rarefied atmosphere and the mass-to-charge (m/z) ratio is measured by the detector. A further analysis step can be carried out by MS/MS, where the ionised peptides are fragmented by collision induced dissociation and the m/z of each product ion is detected, constituting a MS/MS spectrum for each peptide. Using software packages such as Mascot or Sequest, the MS and if available, the MS/MS fingerprints are then compared to databases containing the theoretical mass of cleaved protein and a list of the closest matching proteins is produced.

1.5.3 Proteomic analysis of Alzheimer's disease

A few studies have analysed changes in the proteome associated with the progression of Alzheimer's disease. However the application of proteomics to the study of human brain is undermined by post-mortem delays (Tsuji et al., 2002). Less abundant proteins are probably the most affected by protease activity in post-mortem delays and the post-translational modifications such as phosphorylation are prone to dephosphorylation as phosphatases remains active post-mortem for longer than kinases. Proteomic characterisation of AD has revealed the modification and potential dysregulation of certain categories of proteins such as metabolic, antioxidant, synaptic, apoptotic and anti-apoptotic, and chaperone related (review (Butterfield et al., 2003)). Furthermore increased nitration and oxidation of certain proteins in AD have also been shown by proteomics (Castegna et al., 2002; Castegna et al., 2003; Korolainen et al., 2002).
Until now very few proteomic studies have been carried out on AD mouse models (Tilleman et al., 2002; Vercauteren et al., 2004), although the use of these models presents several advantages. Indeed post-mortem delays are avoided, the pathology is greatly simplified and both Aβ and tau pathologies can be dissociated.

1.6 PipOFF transactivation system

Transgenic mice are used in many areas of research to model diseases and evaluate the function of specific genes. However, the classical transgenic approach involves either the expression of the transgene throughout the life-span or the knock-out of the gene of interest. The tetracycline-inducible gene regulation system has answered this limitation by allowing the reversible and temporary control of gene expression. Recently, a novel system, the streptogramin-based gene regulation system, has been established in mammalian cells in cell culture (Fussenegger et al., 2000). This system, named Pip system, exhibits superior inducibility and background expression properties compared to the tetracycline-based system (for review see (Fussenegger, 2001)). Furthermore, the Pip system is compatible with the tetracycline system and both could be used in parallel to control independently more than one gene. In view of the advantages offered by this new system, it would be essential to investigate its application to the mouse model.

1.6.1 Pristinamycin Resistance in *Streptomyces*

In *Streptomyces pristinaespiralis*, pristinamycin production and resistance are strictly co-regulated. Pip acts as a repressor of the pristinamycin resistance determinant (*ptr*) by binding to

three dyad symmetrical sites of the P_{PTR} promoter. Pip is released from P_{PTR} in the presence of streptogramins and the bacterial resistance gene is expressed (Fig. 5).

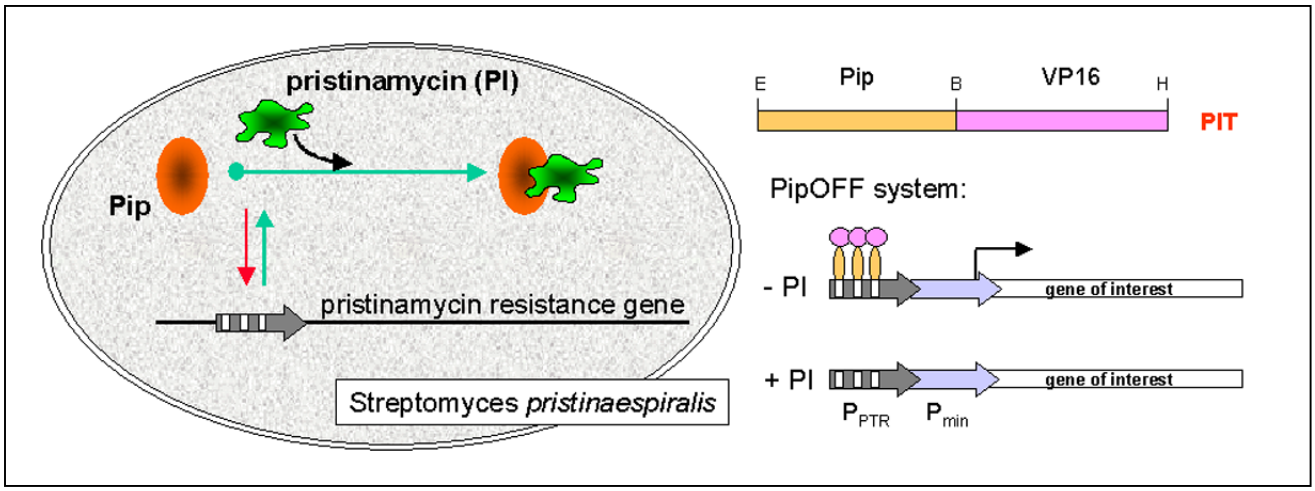

Figure 5.: Pip System. Right: Regulation of Pip binding to pristinamycin resistance gene promoter. Left: PipOFF system using Pip fused to the transactivation domain VP16 (PIT protein).

1.6.2 Pristinamycin-responsive mammalian expression system

1.6.2.1 The streptogramin-repressible gene regulation system: PipOFF

The *Streptomyces* regulatory elements Pip and P_{PTR} were adapted for use in a eukaryotic context by the construction of two chimeric determinants: The pristinamycin (PI)-inhibited transactivator (PIT, Pip fused to the VP16 transactivation domain of *Herpes simplex* virus) and the PI-responsive promoter (P_{PIR}) (P_{PTR} fused to the minimal TATA box-containing version of the hCMV intermediate early minimal promoter). In the absence of streptogramins, PIT is expressed, binds to its target P_{PIR} promoter and activates transcription of the reporter gene. After the addition of streptogramins such as pristinamycin, PIT dissociates from P_{PIR} and no transcription occurs (Fig. 5).

1.6.2.2 The streptogramin-inducible gene regulation system: PipON

The "ON" configuration was constructed to offer the advantages of gene expression after the addition of antibiotics instead of the constitutive expression in the "OFF" configuration. The streptogramin-induced promoter P_{PIR}ON consists of a strong constitutive viral P_{SV40} promoter that harbours between its TATA box and the ATG start codon of the gene of interest, an operator sequence consisting of a PIR3 Pip-binding module. In the absence of pristinamycin, Pip binds to

PIR3 and suppresses transcription while with the addition of PI, Pip is released and P_{PIR}ON-driven expression is induced.

1.7 Objectives of the Ph. D. Project

1.7.1 What are the consequences of tau pathology alone?

Little is known about the distinct intracellular mechanisms underlying the consequences of tau pathology. This insight could help us to understand the selective vulnerability of cells with tau pathology and thereby the pathogenesis in AD. To examine the contribution of tau to these neurodegenerative processes, we wanted to carry out a proteomic analysis of our P301L tau transgenic mice. To zoom in on proteins relevant to the pathology, we sequentially extracted whole brains from six pairs of P301L tau and wild-type (WT) mice into three fractions according to protein solubility. Comparative analysis of 2-D gels run for each fraction revealed statistically significant differences between P301L tau and WT mice. We characterised these differences by functional assays.

1.7.2 How does ß-amyloid influence tau pathology?

Both Gotz et al. and Lewis et al. (Gotz et al., 2001b; Lewis et al., 2001) have demonstrated that Aβ pathology accelerates the onset of tau pathology following the amyloid cascade hypothesis (see 1.4). We wanted to study the molecular mechanisms behind this process using proteomics. We analysed the action of Aβ in two models established in the laboratory. In the cell culture model (Ferrari et al., 2003), neuroblastoma SH-SY5Y cells stably overexpressing P301L tau, were treated for five days with either fibrillary Aβ or reverse non-fibrillary Aβ. Cells were extracted and fractionated before being analysed by 2-D gels. In the mouse model, P301L tau transgenic mice were intracranially injected in the hippocampal CA1 region of both hemispheres with either fibrillar Aβ or reverse non-fibrillary Aβ. As the strongest effect of Aβ on tau pathology was observed in the amygdala, we dissected the amygdala and analysed possible differences between Aβ and control reverse Aβ treatment by 2-D gels.
We hope that this study will reveal categories of proteins which are up- or down-regulated by Aβ and that could influence tau pathology.

1.7.3 Can the PipOFF transactivation system be adapted to the mouse model?

The PipOFF system was assayed in the mouse initially by co-injecting the PIT construct under the control of the EF1α promoter and the yellow fluorescent protein (YFP) gene under the control of the PPIR8 promoter. The functionality and suitability of the PipOFF system was evaluated.

2 MATERIALS AND METHODS

2.1 Proteomics study of P301L tau mice

2.1.1 P301L tau mouse generation

2.1.1.1 Transgenic mice

The transgenic mice used in the present study express the human pathogenic mutation P301L of tau together with the longest human brain tau isoform (htau40) under control of the neurone-specific mThy1.2 promoter (Gotz et al., 2001a). This isoform contains exons 2 and 3 as well as four microtubule-binding repeats (2+, 3+, 4R, human tau40). Pronuclear injections were done into C57Bl/6 × DBA/2 F2 oocytes to obtain founder animals that were back-crossed with C57Bl/6 mice to establish transgenic lines. In addition, homozygous P301L tau mice were obtained and confirmed by TaqMan real-time quantitative PCR.

Different age sets of mice were used for different experimental procedures corresponding to various stages in the development of tau pathology. P301L tau mice show tau hyperphosphorylation already at three months (Gotz et al., 2001a). NFT formation starts at six months of age (Gotz et al., 2001b). We used 8.5-10 month old mice for the proteomics analysis to study the consequences of tau pathology at the beginning of NFT formation without the influence of ageing. At a similar age i.e. 12 months old, mitochondrial membrane potential, complex I and IV activity was determined. ATP levels, mitochondrial respiration and ROS levels were analysed in mice at 12 and 24 months of age. 24 month old mice are expected to bear the highest levels of tau pathology. 18 month old mice were used to determine mitochondrial numbers in neurites. This intermediate age allows us to see the full effect of tau pathology on the mitochondrial transport without pronounced ageing effects such as in 24 month old mice. Finally 12 and 24 month old homozygous, hemizygous and wild-type mice were tested for lipid peroxidation.

2.1.1.2 Genotyping of P301L tau mice

Mouse tail lysis

2 mm of tail were cut and incubated in a thermomixer (Vaudaux-Eppendorf AG, Schönenbuch, Switzerland) at 1400 rpm for 30 min at 55°C in 20 µl of digestion buffer (50 mM Tris pH 8.0, 20 mM NaCl, 1 mM EDTA pH 8.0, 1% SDS) supplemented with 2 µl proteinase K (20 mg/ml).

Proteinase K digestion was terminated through denaturation in adding 178 µl double deionised water (ddH_2O) and incubating the tail lysate at 99°C for 5 min at 600 rpm in the thermomixer.

Polymerase chain reaction (PCR)

The polymerase chain reaction technique is a method to amplify DNA sequences of interest (Mullis, 1990), by using two specific primers which are complementary to the two strands and define the sequence to be amplified. Three major steps are involved: First, denaturation of the DNA to single strands at 95°C. Second, annealing of the primers to their complementary sequence on the DNA. Optimal annealing temperatures are ~ 5 to 10°C lower than the T_m values of the primers. The primers should be designed in such a way that an annealing temperature of 55 to 65°C is allowed. Third, elongation of the DNA strand by using a heat stable DNA polymerase adding nucleotides (dNTPs) to the 3'-ends of the primer sequences at 72°C. By repeating these steps several times, the DNA-sequence of interest is amplified exponentially.

Transgenic P301L tau mice were screened with oligonucleotides tau-I (5'-GGAGTTCGAAGTG ATGGAAG-3') and tau-K (5'-GGTTTTTGCTGGAATCCTGG-3'). Briefly, 0.5 µl tail mixture was added to PCR mix (9.5 µl H_2O, 1.25 µl PCR buffer, 0.25 µl 10 mM dNTP, 0.5 µl oligo tau I/K mixture (0.2 µM), 0.5 µl Red Taq genomic DNA polymerase (Sigma, Fluka, Buchs, Switzerland)). Using a GeneAmp PCR system 9700 machine (Applied Biosystem, Rotkreuz, Switzerland), the reaction was heated to 95°C for 2 min before a series of 35 cycles (30 sec at 94°C, 30 sec at 64°C, 1 min at 72°C), then kept at 72°C for 7 min and cooled to 4°C.

Agarose gel electrophoresis

Analysis of PCR products was carried out using agarose gel electrophoresis. PCR mix containing the PCR products were loaded onto a 1% agarose gel in TAE buffer (40 mM Tris-acetate, 1 mM EDTA) supplemented with ethidium bromide (final concentration of 1 µg/ml). An electrical field is used to drag the negatively charged DNA molecules (due to their phosphate groups) through the gel matrix. The migration rate of linear DNA depends mainly on its size and the shorter the DNA molecule the faster it moves through the gel. DNA fragments are then visualised under UV-light by adding ethidium bromide which intercalates between the bases of DNA. The tau PCR yields an amplification product of 500 base pairs.

2.1.2 Brain sample preparation and fractionation

Four pairs of 8.5 month old male hemizygous P301L tau and WT control mice and two pairs of 10 month old male hemizygous P301L tau and WT control mice were sacrificed by cervical

dislocation, brains removed at 4°C, snap-frozen in liquid nitrogen and stored at –80°C until extraction. Brains were sequentially extracted with the ReadyPrep sequential extraction kit (Bio-Rad, Reinach, Switzerland) according to a modified version of the manufacturer's protocol. Only one P301L tau and one WT each were extracted at a time. All steps were carried out at 4°C unless otherwise specified.

Briefly, whole brains were homogenised for 5 min in 3 ml of buffer 1 (40mM Tris pH 7.4, Complete protease inhibitor cocktail (Roche, Rotkreuz, Switzerland), 0.5 mg/ml Pefabloc (Roche), 1 mM Na_3V0_4, 1 mM NaF) and 200 units DNaseI in a glass-teflon potter. After 15 min on ice, the homogenate was transferred into 2 ml Eppendorf tubes and centrifuged at 15,000 x g for 15 min in a bench centrifuge (Centrifuge 5417C, Vaudaux-Eppendorf AG, Schönenbuch, Switzerland). Supernatant E1 was collected for further analysis and frozen in aliquots at –80°C. The pellet was washed twice with buffer 1 using a Pipetman P1000 (Gilson Schweiz AG, Mettmenstetten, Switzerland) and centrifuged for 10 min at 15,000 x g. The washed pellet was resuspended by vortexing and by using a Pipetman P1000, in 750 µl buffer 2 (8 M urea, 4% CHAPS, 40 mM Tris, 0.2% Bio-Lyte 3/10 ampholytes (Bio-Rad, Reinach, Switzerland), 2 mM tributylphosphine (TBP)), incubated for 10 min at room temperature (RT), transferred into Beckmann polycarbonate centrifuge tubes and ultra-centrifuged at 57,000 x g for 30 min with an acceleration 5, deceleration 2, in a Optima TLX ultracentrifuge using a Beckmann TLA 120.2 rotor (Beckmann, Nyon, Switzerland). Supernatant E2 located between the lipid layer surface and the solid pellet was rapidly collected with a Pasteur pipette for further analysis and frozen in aliquots at –80°C. The pellet was washed once with buffer 2 using a 1 ml syringe with a syringe needle (Microlance3 ref 300900, 22 x 1, ¼"-nr.12, 0.7 mm x 30 mm, BD Bioscience, Basel, Switzerland) and centrifuged at 57,000 x g for 30 min. The supernatant was discarded and the pellet was resuspended using a Pipetman P1000, in buffer 3 (5 M urea, 2 M thiourea, 2% CHAPS, 2% caprylyl sulfobetaine (SB) 3-10, 40 mM Tris, 0.2% Bio-Lyte 3/10 ampholytes, 2 mM TBP). The final supernatant E3 was collected after ultra-centrifugation at 89,000 x g for 30 min at 10°C and frozen in aliquots at –80°C.

2.1.3 Protein concentration determination

Protein concentrations of cell or tissue extracts were measured as described by Lowry et al. (Lowry et al., 1951) using the Bio-Rad *DC* Protein Assay Kit (Bio-Rad, Reinach, Switzerland).

Proteins react with an alkaline copper tartrate solution and reduce the folin reagent. The reduced folin species have a characteristic blue colour with an absorption maximum of 750 nm.

2.1.4 Isoelectrical focusing

Isoelectrical focusing (IEF) was carried out using the PROTEAN IEF Cell (Bio-Rad, Reinach, Switzerland). Six P301L tau transgenic and six WT samples were focused simultaneously to avoid variations between IEF runs. Each fraction from the sequential extraction (40 µg E1, 50 µg E2 or 60 µl E3) was mixed by vortex in rehydration buffer (8.5 M urea, 4% CHAPS, 0.5% pharmalytes pH 3-10 (Amersham, Otelfingen, Switzerland) and 1.2% DeStreak reagent (Amersham, Otelfingen, Switzerland)). Samples in rehydration buffer were incubated at RT for 30 min and then centrifuged for 15 min at 21,000 x g in a refrigerated bench centrifuge (Centrifuge 5417R, Vaudaux-Eppendorf AG, Schönenbuch, Switzerland) at respectively 4°C for fractions E1 and E2 and at RT for fraction E3. Samples were then loaded on 17 cm IPG strips (pH 3-10, Bio-Rad) in a rehydration tray. After passive rehydration for 15 h at 20°C, the IPG strips were transferred into a IEF focusing tray and isoelectrically focused following a stepwise increase in voltage from 150 to 10,000 V, finishing with 60,000 Vh (Table 2.). IPG strips were then kept at –80°C until further use.

Table 2.: IEF program using the PROTEAN IEF Cell for sequential extracted brain samples for 2-D gel analysis.

Step	Voltage	Voltage slope	Time
1	150V	linear	30min
2	300V	linear	1h
3	500V	linear	1h
4	1000V	linear	1h
5	10,000V	linear	1h30
6	10,000V	rapid	60,000Vh

Prior to SDS-PAGE, the IPG strips were equilibrated in 2% DTT, 6 M urea, 2% SDS, 0.05 M Tris pH 8.8, 20% glycerol for 30 min and then again in the same buffer with 2.5% iodoacetamide instead of DTT for another 30 min.

For MS analysis, 150 µg E1, 150 µg E2 and 180 µl E3, respectively, were loaded on 24 cm IPG strips (pH 3-10) and isoelectrically focused following a stepwise increase in voltage from 150 to 10,000 V, finishing with 75,000 Vh (Table 3.).

Table 3.: IEF program using the PROTEAN IEF Cell for sequential extracted brain samples for MS analysis.

Step	Voltage	Voltage slope	Time
1	150V	linear	30min
2	300V	linear	1h
3	500V	linear	1h
4	1000V	linear	1h
5	5000V	linear	1h30
6	5000V	rapid	30min
7	10,000V	linear	2h
8	10,000V	rapid	75,000Vh

2.1.5 Two-dimensional electrophoresis

SDS-polyacrylamide gels were prepared twelve at a time in a PROTEAN plus Multi-casting chamber (Bio-Rad, Reinach, Switzerland). PROTEAN plus hinged spacer plates (26.8 x 22.5 (W x L) cm) were used to cast 25 x 20.5 (W x L) cm gels of 1 mm in thickness. After acrylamide degassing, a 12% acrylamide solution was prepared in gel buffer (0.375 mM Tris, pH 8.8, 5% glycerol, 1% SDS). Immediately before gel casting, 0.05% APS and 0.05% TEMED were added to induce polymerisation. Gels were overlaid with 1 ml 50% isopropanol per gel. Gels were left to polymerise for at least one hour at RT.

Equilibrated IPG strips are dipped twice in ddH_2O and loaded onto the gels. Strips are fixed on top of the gels using 0.5% agarose in running buffer (0.025 M Tris, 0.2 M glycine, 0.1% SDS). Second dimension separation was performed in the PROTEAN Plus Dodeca cell electrophoresis system (Bio-Rad, Reinach, Switzerland) filled with 25 litres running buffer. The buffer was constantly cooled to 10°C using a K20 refrigerated circulator bath (Thermo Haake, Bio-Rad, Reinach, Switzerland) and gels were run at 200 V constant and limited to 500 mA with a electrophoresis power supply (Consort E865, Witec AG, Littau, Switzerland). All gels of the six P301L tau transgenic and six WT samples from one fraction were run at the same time.

2.1.6 Two-dimensional gel staining

Silver staining allows the detection of most proteins on polyacrylamide gels. The gel is impregnated with soluble silver ions and developed by treatment with formaldehyde, which reduces silver ions to form an insoluble brown precipitate of metallic silver. This reduction is promoted by proteins. Gels for the Proteomweaver comparison study were stained by Silver staining using a modified version of Blum's Silver staining method (Rabilloud et al., 1988). All

steps were performed on a shaker. Briefly, 2-D gels were removed from gel plates, placed in large plastic boxes (two per box) and fixed overnight in 500 ml 40% ethanol, 10% acetic acid. They were then sequentially washed twice in 30% ethanol and once in ddH_2O for 20 min. Gels were sensitised in 0.02% sodium thiosulfate ($Na_2S_2O_3$) for 1 min and washed 3 x 20 sec in ddH_2O. Gels were then incubated in ice-cold 0.1% silver nitrate ($AgNO_3$) for 20 min at 4°C and washed again 3 x 20 sec in ddH_2O. The gels were developed in 3% sodium carbonate (Na_2CO_3) and 0.05% formalin. As soon as the developer solution became turbid, it was renewed. When the staining was judged sufficient, the reaction was terminated in 1% glycine for 30 min. Finally, the gel was washed 3 x 10 min and stored in ddH_2O at 4°C. Silver stained gels were scanned using an Epson expression 1680 Pro scanner (Epson, Data Quest AG, Dietikon, Switzerland) in greyscale with a resolution of 300 dpi and 8 bits/channel.

For MS analysis, gels were stained with Sypro Ruby (Molecular Probes, Invitrogen, Basel, Switzerland) following manufacturer's instructions. Briefly, gels were fixed twice in 10% methanol, 7% acetic acid for 30 min. Gels were then stained overnight in Sypro Ruby (500 ml per gel) in the dark. Gels were washed twice in 10% methanol, 7% acetic acid for 30 min and stored in ddH_2O at 4°C. Sypro Ruby stained gels were scanned using the fluorescent scanner, Typhoon 9400 PhosphorImager (Amersham, Otelfingen, Switzerland) with an excitation wavelength of 488 nm and an emission wavelength of 610 nm. Gels were scanned with a pixel size of 100 microns.

2.1.7 Two-dimensional gel analysis

Six P301L tau transgenic and six WT 2-D silver stained gels were compared simultaneously with the Proteomweaver imaging software Version 2.1 (Definiens, Munich, Germany). In a first step, the software detects all spots and then performs a matching of every gel with every gel. This means that the spots of each gel are matched with each similar spot in every other gel, creating a group of "superspots". The software then normalises all gels and runs statistics to compare the 2-D spot patterns of every transgenic gel of one fraction with the 2-D spot patterns of every WT gel of the same fraction.

For the statistical analysis, we took only spots present in all 12 gels and with a relative intensity average over 0.05. The spots were manually edited and bad matches were removed. Spots were considered as differentially regulated between P301L tau and WT control samples, if they were

up- or down-regulated by at least 1.5 fold and statistically significant with Student's t-test ($p < 0.05$).

2.1.8 Spot excision

For spot excision, we used 2-D gels loaded with higher amounts of protein and stained with Sypro Ruby which does not affect MS detection. As Sypro Ruby is a fluorescent dye, spots were excised with the GelPix protein spot excision system (Genetix, Hampshire, UK). Briefly the gel was laid on a glass plate, inserted into the apparatus chamber (humidity > 60%) and scanned. Proteomweaver was used to detect the spots and the spots to be excised, were manually selected. The excision parameters were 2 mm pin diameter, 275 µl aspiration volume, 375 µl dispension volume and 525 orbit diameter. Spots were excised and placed in a 96 well plate (round bottom wells).

2.1.9 Trypsin digestion of excised spots

Spots were prepared for in-gel trypsin digestion. All steps were carried out in a sterile clean environment and at RT unless otherwise indicated. Briefly, the excised spots in a 96 well plate were washed twice with ddH_2O and then once with 50 mM NH_4HCO_3/30% ACN for 5 min at 37°C. The solution was removed and residual liquid was evaporated for 10 min at 60°C. The spots were then dehydrated with 80% ACN for 10 min, the solution was removed and residual liquid was evaporated for 10 min at 60°C. Digestion was carried out with 30 ng trypsin per spot in digestion buffer (10 mM Tris pH 8.3, 2 mM $CaCl_2$). Gel pieces were first transferred into 0.5 ml Eppendorfs and 4 µl of trypsin solution was added for 5 min. After rehydration of the gel pieces, an additional 5 µl digestion buffer was added. Digestion was carried out for 3 h at 37°C. Digested gel spots were then sonicated for 5 min in a sonication bath (Transsonic 420, Omnilab AG, Mettmenstetten, Switzerland) and frozen at –80°C.

2.1.10 MALDI-TOF/TOF mass spectrometric analysis of digested spots

0.01% TFA (final concentration) was added to the digested gel pieces. After 5 min sonication, the tryptic digests were desalted and concentrated using µ-C18 ZipTips (Millipore, Volketswil, Switzerland). The bound peptides were eluted directly onto the MALDI target with 0.8 µl of α-cyano-4-hydroxycinnamic acid matrix 5 mg/ml in 65% ACN, 35% ddH_2O containing 0.1% TFA. Digests were analysed by matrix-assisted laser desorption ionisation tandem time-of-flight mass spectrometry (MALDI-TOF/TOF) using a 4700 Proteomics Analyzer MALDI TOF/TOF mass

spectrometer (Applied Biosystems, Foster City, CA, U. S. A.). One mass spectrum and up to five tandem mass spectra of all precursor ions with a minimum signal-to-noise of 80 were recorded for each sample spot. Autoproteolytic fragments of trypsin were used as internal calibrants in the MS mode. The mass and tandem mass spectra were analysed using Mascot (Matrix Science, London, UK, available at http://www.matrixscience.com) as the search engine. A combined MS and MS/MS search with a peptide tolerance of 25 ppm and an MS/MS tolerance of 0.2 Da was carried out against the UniProt complete mouse proteome database (available at ftp://ftp.ebi.ac.uk/pub/databases/integr8). Protein identification was considered significant if the Mascot score was higher than the probability $p < 0.05$ of a random match.

2.2 Proteomics study of P301L tau expressing SH-SY5Y cells treated with ß-amyloid

2.2.1 Aβ preparation

$A\beta_{1-42}$ and reverse $A\beta_{42-1}$ peptides (Bachem, Bubendorf, Switzerland) were reconstituted in PBS to a concentration of 1.1 mM in a sterile environment and frozen at –80°C in aliquots. Before the experiment, aliquots were diluted to 220 µM in PBS and shaken at 1000 rpm for 24 h at 37°C in an Eppendorf thermomixer (Vaudaux-Eppendorf AG, Schönenbuch, Switzerland) to allow aggregation. These fibril preparations contain a mixture of species such as Aβ-monomers and oligomers but also SDS-stable oligomers (Hartley *et al.*, 1999). The Aβ fibrillary preparation is diluted 1:22 in cell culture growth medium to a final concentration of 10 µM.

2.2.2 Cell culture

P301L tau stable transfected SH-SY5Y neuroblastoma cells (DSMZ, Braunschweig, Germany; DSMZ No: ACC 209) were cultivated at 37°C/5% CO_2/95% humidity in growth medium (Dulbecco's modified Eagle's medium F-12 (DMEM F-12) supplemented with 2 mM L-glutamine, 1% penicillin/streptomycin, 10% fetal calf serum (FCS), 5% horse serum (HS)) and 125 µg/ml gentamycin G418 (GIBCO, Basel, Switzerland). Confluent cells were washed with PBS, trypsinized with trypsin/EDTA and passaged by splitting into half. For storage, cells were dissociated with trypsin/EDTA (Invitrogen, Basel, Switzerland), resuspended in medium and pelleted by centrifugation at 1000 x g for 5 min. Then the cells were resuspended in growth medium supplemented with 10% DMSO and 10% FCS and stored in liquid nitrogen. For Aβ treatment, batches of human P301L tau stable transfected SH-SY5Y neuroblastoma cells (DSMZ,

Braunschweig, Germany; DSMZ No: ACC 209) from the same passage number were frozen. Thawed cells separated from freezing medium by centrifugation, were grown in growth medium and 125 µg/ml gentamycin G418 (GIBCO, Basel, Switzerland) for two weeks before Aβ treatment.

For Aβ treatment, cells were plated out into 10 cm Petri dishes at a confluence of 5.5 x 10^5 cells in 10 ml growth medium. 18 h afterwards, medium was removed and 5.5 ml of fresh growth medium was added together with preaggregated $A\beta_{42}$ (final concentration, 10 µM; Bachem, Bubendorf, Switzerland) or PBS. Treated cells were incubated for 5 days without changing the medium before being collected.

2.2.3 Sample preparation and fractionation

All steps were carried out at 4°C unless otherwise indicated.

Cells in 10 cm Petri dishes were washed twice in ice-cold PBS and collected with a rubber scrapper in 70 µl Tris buffer (50 mM Tris pH 7.4, Complete protease inhibitor cocktail (Roche, Rotkreuz, Switzerland), 0.5 mg/ml Pefabloc (Roche)). Samples were stored at –80°C until extraction.

For extraction, cells collected from two plates were pooled together and the total volume was estimated. Samples were supplemented with 5 mM DTT, Complete protease inhibitor cocktail (Roche, Rotkreuz, Switzerland) 1x and phosphatase inhibitors (1 mM Na_3V0_4, 1 mM NaF, 1 µM okadaic acid). DNA was digested with the addition of 200 units DNaseI. Cells were homogenised in a 1 ml glass-teflon potter for 4 min and incubated for 15 min. Cell lysates were centrifuged for 20 min at 21,000 x g in a refrigerated bench centrifuge (Centrifuge 5417R, Vaudaux-Eppendorf AG, Schönenbuch, Switzerland). The supernatant (S1) containing soluble proteins was collected and frozen in aliquots at –80°C until further use. The pellet was washed in 150 µl Tris buffer supplemented with protease and phosphatase inhibitors but without DNaseI. Resuspension of the pellet was carried out first with a Pipetman P200 and then a 1 ml syringe with a syringe needle (Microlance3 ref300900, 22x1, ¼"-nr.12, 0.7mmx30mm, BD Bioscience, Basel, Switzerland). Resuspended pellet was centrifuged at 4°C for 20 min at 21,000 x g and the wash supernatant was discarded. The pellet was resuspended in 100 µl IEF rehydration buffer (8.5 M urea, 4% CHAPS, 0.5% pharmalytes pH 3-10 (Amersham, Otelfingen, Switzerland)) with first a Pipetman P200 and then a 1 ml syringe with a syringe needle (Microlance3 ref300900, 22 x 1, ¼"-nr.12, 0.7mm x 30mm, BD Bioscience, Basel, Switzerland). The resuspended pellet was incubated for

10 min at RT before being centrifuged at 22°C for 20 min at 21,000 x g. The resulting supernatant (S2) containing less soluble proteins was collected and frozen in aliquots at –80°C until further use.

2.2.4 Isoelectrical focusing

S1 and S2 cell fractions were isoelectrically focused on 24 cm IPG strips (pH 3-10). Five replicate supernatant S1 samples treated with Aβ and five treated with reverse Aβ were focused simultaneously. Six replicate supernatant S2 samples treated with Aβ and six treated with reverse Aβ were also isoelectrically focused together.

Briefly respectively 100 µg S1 and 67 µl S2 were added to IEF rehydration buffer (8.5 M urea, 4% CHAPS, 0.5% pharmalytes pH 3-10 (Amersham, Otelfingen, Switzerland) and 1.2% DeStreak reagent (Amersham, Otelfingen, Switzerland)). Samples in rehydration buffer were incubated at RT for 30 min and then centrifuged for 15 min at 21,000 x g in a refrigerated bench centrifuge (Centrifuge 5417R, Vaudaux-Eppendorf AG, Schönenbuch, Switzerland) at respectively 4°C for fractions S1 and at 22°C for fractions S2. Passive rehydration and isoelectrical focusing was carried out as described in 2.1.4 and Table 3.

2.2.5 Two-dimensional gel analysis

IPG strips containing focused S1 or S2 fractions were laid on the top of 12% acrylamide SDS-PAGE gels and separated according to molecular weight in the PROTEAN Plus Dodeca cell electrophoresis system (Bio-Rad, Reinach, Switzerland) as described in 2.1.5. All samples from one same fraction were separated in one same run.

Gels were stained with Sypro Ruby following the protocol described in 2.1.6. and differences between Aβ and reverse Aβ treatment in S1 and S2 fractions were identified by Proteomweaver (2.1.7.). For the statistical analysis, we took only spots present in all gels and we did not set a relative intensity average limit. Spots were considered as differentially regulated between Aβ and reverse Aβ treated samples, if they were up- or down-regulated by at least 1.5 fold and statistically significant with Student's t-test ($p < 0.05$).

2.2.6 MALDI-TOF/TOF mass spectrometric analysis

Differentially regulated spots were excised directly from the gels that were used to perform the gel comparison (as described in 2.1.8). Spots were digested in 20 ng trypsin and analysed by MALDI-TOF/TOF as described respectively in 2.1.9 and 2.1.10.

2.3 Proteomics study of amygdalae from P301L tau mice injected with ß-amyloid

2.3.1 Aβ preparation

$A\beta_{1\text{-}42}$ and reverse $A\beta_{42\text{-}1}$ (Bachem, Bubendorf, Switzerland) were reconstituted in PBS to a concentration of 1.1 mM in a sterile environment and frozen at –80°C in aliquots. Before the experiment, aliquots were diluted to 250 μM in PBS and shaken at 1000 rpm for 84 hours at 37°C in an Eppendorf thermomixer (Vaudaux-Eppendorf AG, Schönenbuch, Switzerland) to allow for aggregation.

2.3.2 Stereotaxic injection of β-amyloid

For stereotaxic injection, we chose 5.5 month old P301L tau hemizygote female mice which do not present NFT at this age and show in general, less pathology variability than male mice. Starting without NFT pathology should allow us to observe a clearer difference when the Aβ treatment induces NFT formation. Female mice were injected one week before the operation with 5 units PMS (Folligon, Veterinaria AG, Zürich, Switzerland) to synchronise hormonal cycles. Seven female P301L tau positive mice were injected with Aβ and seven with reverse Aβ.
Mice were first anaesthetised with a mixture of 0.1 ml/10 g Fentanyl (50 μg/ml) (Sintenyl, Sintetica, Mendrisio, Switzerland), Midazolam (5 mg/ml) (Dormicum, Roche, Reinach, Switzerland), Medetomidin (1 mg/kg) (Domitor, Pfizer, Dr. El Gräub AG, Bern, Switzerland) in NaCl 0.9%.

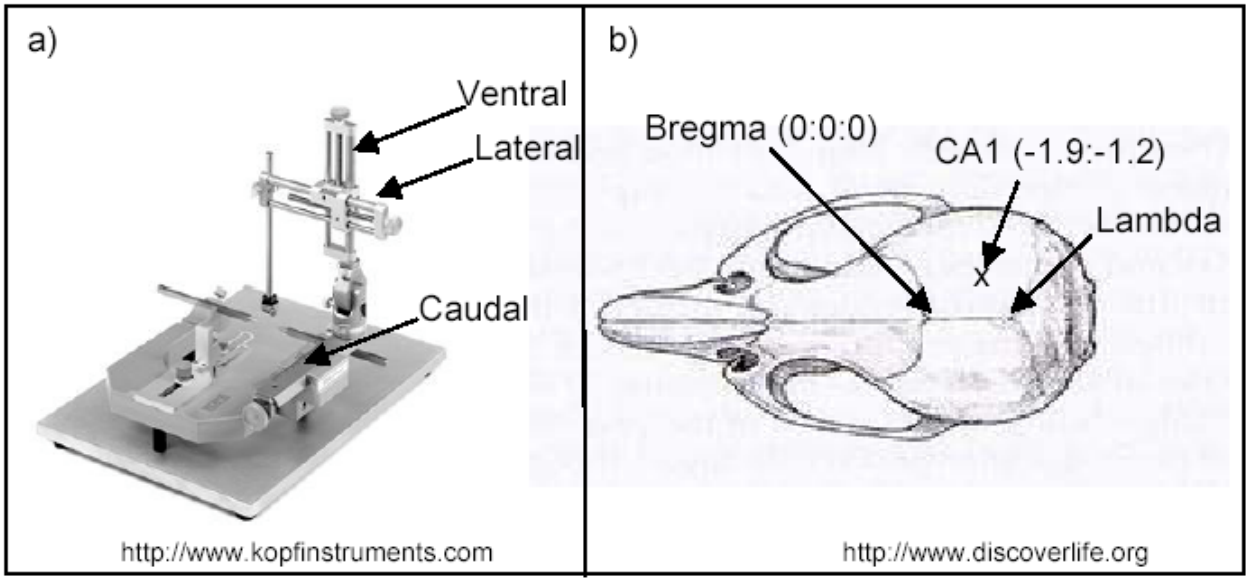

Figure 6.: Stereotaxic injection of Aβ

Mice were then placed in a Stoelting stereotaxic instrument (Stoelting, Illinois, USA) (Fig. 6), and an incision was made along the midline of the head to expose the skull. The co-ordinates for deposition of Aβ were determined according to Bregma co-ordinates, in order to inject into the CA1 region of the hippocampus, in both hemispheres. The calvarium was perforated with a drill (Fine Science Tools, Aichele Medico AG, Aesch BL, Switzerland) at the positions: caudal -1.9 mm, lateral -1.2 mm and caudal -1.9 mm, lateral +1.2 mm. A 10 µl Hamilton syringe was slowly inserted 2.4 mm into the cortex. After 2 min, a total volume of 1.5 µl $A\beta_{1-42}$ or reverse $A\beta_{42-1}$ was injected with an injection speed of 0.15 µl/min using a mini pump. The needle was kept in the injection site for another 2 min before slowly being withdrawn.
After the operation, the mice were given 0.1 ml/10 g antidote (Naloxon (0.4 mg/ml) (Narcan, Bristol-Myers Squibb, Baar, Swizerland), Flumazenil (0.1 mg/ml) (Anexate, Roche, Reinach, Switzerland), Atipamezol (5 mg/ml) (Antisedan, Pfizer, Dr. El Gräub AG, Bern, Swizerland) in NaCl 0.9%) and kept on a heating pad for 3 h.

2.3.3 Amygdala dissection

Three weeks after the Aβ or reverse Aβ injection, the mice were sacrificed by cervical dislocation. The brain was rapidly removed and washed with ice-cold PBS. The cerebellum was removed and then the brain was cut in half between the hippocampus and the amygdala. The hippocampal part was immersed in 4% PFA and further used for immunohistochemistry to determine the site of injection. The part containing the amygdala was cut into coronal slices using a tissue chopper (Bachofer, Reutlinger, Germany) and the amygdalae were dissected under a light microscope. Dissected amygdalae were snap-frozen in liquid nitrogen and stored at –80°C.

2.3.4 Amygdala sample preparation

Amygdalae were extracted in 200 µl IEF rehydration buffer (8.5 M urea, 4% CHAPS, 0.5% pharmalytes pH 3-10 (Amersham, Otelfingen, Switzerland). The amygdalae were first dissolved using a Pipetman P200 and then sonicated for 3 min in a sonication bath (Transsonic 420, Omnilab AG, Mettmenstetten, Switzerland). Homogenates were centrifuged at 89,000 x g for 30 min at 20°C in a Optima TLX ultracentrifuge using a Beckmann TLA 120.2 rotor (Beckmann, Nyon, Switzerland). The supernatant was collected and aliquots were frozen at –80°C.

2.3.5 Isoelectrical focusing

40 µl amygdala homogenate supernatant was mixed with IEF rehydration buffer (8.5 M urea, 4% CHAPS, 0.5% pharmalytes pH 5-8 (Amersham, Otelfingen, Switzerland), 0.25% pharmalytes pH 8-10.5) and 1.2% DeStreak reagent (Amersham, Otelfingen, Switzerland)). Samples in rehydration buffer were incubated at RT for 30 min and then centrifuged for 15 min at 21,000 x g in a refrigerated bench centrifuge (Centrifuge 5417R, Vaudaux-Eppendorf AG, Schönenbuch, Switzerland) at 22°C. Samples were then loaded onto 24 cm IPG strips pH 5-8 (Bio-Rad, Reinach, Switzerland). Amygdala samples from five Aβ and five reverse Aβ injected mice were run together following the IEF program detailed in Table 3.

2.3.6 Two-dimensional gel analysis

Electrophoresis and gel analysis were carried out as described in 2.2.5.

2.3.7 MALDI-TOF/TOF mass spectrometric analysis

Differentially regulated spots were excised directly from the gels that were used to perform the gel comparison (as described in 2.1.8). Spots were digested with 20 ng trypsin and analysed by MALDI-TOF/TOF as described respectively in 2.1.9 and 2.1.10.

2.4 Methods for candidate verification

2.4.1 Gel electrophoresis

The proteins denatured and negatively charged by SDS are separated on 12% SDS-PAGE gels. For more than 10 samples, large gels (W x L, 16 x 20 cm) were run in the PROTEAN II xi apparatus (Bio-Rad, Reinach, Switzerland) and otherwise small gels were used (Mini-PROTEAN, Bio-Rad, Reinach, Switzerland). Gels were cast with two layers, the resolving layer (12% acrylamide solution in 0.375 mM Tris, pH 8.8, 1% SDS) and the stacking layer (5% acrylamide solution in 0.12 M Tris pH 6.8, 0.1% SDS). Immediately before gel casting, 0.05% APS and 0.05% TEMED were added to induce polymerisation. Samples were mixed with loading buffer (33% glycerol, 6.6% SDS, 0.33 M DTT, bromophenol blue, final concentration) and boiled before loading onto the gel. Electrophoresis was carried out at 45 mA with the voltage limited to 250 V.

2.4.2 Western blotting

This method combines very high sensitivity and specific protein visualisation by the use of antibodies. The proteins charged negatively by SDS are transferred towards the positive pole onto a nitrocellulose membrane. This is then probed with a specific primary antibody and followed by a secondary antibody recognising the primary antibody and coupled to HRP (horseradish peroxidase). The luminol-based substrate in the ECL reagent is oxidised by the peroxidase and emits light captured on to the photographic film, revealing the exact position of the specific protein.

Unless otherwise indicated all incubations were carried out for 1h at RT and the blots washed 3 x 10 min in TBS (0.01 M Tris, 0.15 M NaCl, pH 7.5). The SDS-PAGE gel was laid on to a sheet of nitrocellulose (Hybond-C, Amersham Biosciences, Otelfingen, Switzerland) soaked in transfer buffer (0.025 M Tris, 0.2 M glycine, 20% methanol, pH 8.3 (NaOH)). Together they were sandwiched between one layer of Whatman filter paper and foam, inserted into a transfer cell (Amersham Biosciences, Otelfingen, Switzerland) filled with transfer buffer. Blotting was carried out either overnight at 45 mA or for 3 h at 150 mA. General protein levels transferred onto the blot were thereafter determined with the reversible Ponceau S stain, which was washed off in TBS. The blot was then incubated 1 h in blocking buffer (4% milk powder in TBS). After a washing step of 15 min in TBS, the blot was probed with the primary antibody for 1 h at RT or overnight at 4°C. Unbound primary antibodies were removed by washing 3 x 5 min in TBS before the blot was re-probed for 1 h at RT with the appropriate secondary antibody conjugated to HRP (Amersham Biosciences, Otelfingen, Switzerland). Finally after 3 x 5 min washing in TBS, the blot was developed with ECL (Amersham Biosciences, Otelfingen, Switzerland), following manufacturer's instructions and exposed to a film (X-OMAT LS, Kodak/Sigma, Buchs, Switzerland).

Evaluation of complex V levels in human brains (in collaboration with Dr. Rizzu, Amsterdam) Homogenates from temporal cortices of 2 controls and 4 P301L FTDP-17 patients were prepared in 150 mM Tris (pH 6.8), 2.5% SDS, 8 M urea, 20% glycerol, 10% β-mercaptoethanol and 0.1% bromophenol blue and subjected to Western blotting using standard methods. 2.5 µl total brain lysate were loaded. The blots were developed with antibodies directed against the complex V component ATP synthase chain D (Molecular Probes, Invitrogen, Basel, Switzerland, 0.2 µg/ml), and against porin for normalisation (Molecular Probes, Invitrogen, Basel, Switzerland, 0.2

µg/ml). As secondary antibody, a goat-anti-mouse IgG (Amersham, 1:5000) was used. Non overexposed films were used to quantify the bands with the software Image J (available from NIH, http://rsb.info.nih.gov/ij/). Complex V levels were expressed as a percentage of porin levels.

Samples used (as loaded) were (1) control brain, 73 year old female, (2) control brain, 72 year old male, (3) P301L brain, 64 year old female, (4) P301L brain, 52 year old male, (5) P301L brain, 66 year old female and (6) P301L brain, 60 year old male. Three other control samples were used (data not shown) specifically control temporal cortex from 78 year old female, 82 year old female and 78 year old male brains.

2.4.3 Immunohistochemistry

2.4.3.1 Tissue preparation

Mice were perfused transcardially under deep anesthesia with a mixture of 2% xylazine and 10% ketamine (15 µl/g body weight). For that, the thorax was opened to expose the heart and major vessels. A cannula was inserted through the left ventricle into the ascending aorta. Right away, the right atrium was punctured with a scissors, to allow the efflux of return circulation. To remove the blood, mice were initially perfused with PBS (1x) for 5 min until the liver turned beige-yellow, followed by fixation with 4% paraformaldehyde in PBS for 15 min. Brains were then removed, postfixed in the same fixative solution overnight and washed 3x with PBS over 24 h. The brains were then dehydrated respectively in ethanol 70%, 96%, 100% for three hours in each solution and changed every hour. Brains were left overnight in xylol and immersed in liquid paraffin at 60°C for 5 h. Finally the brains were cooled down in paraffin blocks.

2.4.3.2 Immunostaining of paraffin sections

5 µm thin paraffin coronal sections were cut for immunohistochemistry and brain areas were mapped based on the mouse atlas by Paxinos (Paxinos, 1997). To allow antibodies to penetrate fixed tissue embedded in paraffin, sections were dewaxed at 60°C for 2 h, then in xylol and rehydrated in a descending series of ethanol (5 min each, 3 x xylol baths, 2 x ethanol 100%, 96% ethanol, 70% ethanol, 2 x ddH_2O). Sections were then permeabilised with methanol for 10 min at -20 °C. To increase immunoreactivity, depending on the type of antigen, sections were micro-wave treated in citrate-buffer pH 5.8 at 70°C for 15 minutes. Sections were blocked in PBS pH 7.4 containing 4% BSA and 6% goat serum. Sections were incubated with the primary antibody

overnight at 4°C or for 1 h at RT. Sections were washed three times with PBS and incubated with the secondary antibody for 1 h at RT. The immunostained sections were washed again 3 x and then mounted with the anti-fading reagent (Mowiol), and analysed by conventional immunofluorescence.

2.4.4 Crude synaptosome preparation

All steps were performed at 4°C unless otherwise specified.
Five transgene and five WT 12 month old mice were sacrificed by cervical dislocation, the brain was removed and the cerebellum discarded. Brains were washed with ice-cold PBS and weighed. Homogenisation was carried out in 10 volumes per brain weight synaptosome homogenisation buffer (0.32 M sucrose, 4 mM HEPES pH 7.4, Complete protease inhibitor cocktail (Roche, Rotkreuz, Switzerland)) at 900 rpm in a glass-teflon potter. Homogenates were centrifuged for 10 min at 1000 x g in a refrigerated bench centrifuge (Centrifuge 5417R, Vaudaux-Eppendorf AG, Schönenbuch, Switzerland). The supernatant was centrifuged in a second step at 17,000 x g for 15 min. The resulting pellet was resuspended in 1 ml synaptosome homogenisation buffer and further centrifuged at 17,000 x g for 15 min. The washed pellet was then resuspended in 10 mM HEPES, 100 mM NaCl, 1 mM $MgCl_2$, 0.5 mM $CaCl_2$, Complete protease inhibitor cocktail (Roche, Rotkreuz, Switzerland), and frozen at –80°C in aliquots. This resuspension contains a mixture of synaptosomes, endoplasmic reticulum and mitochondria.

2.4.5 Evaluation of lipid peroxidation levels and antioxidant enzyme activity

Preparation of brain hemispheres to determine lipid peroxidation and antioxidant enzyme activities. (in collaboration with Dr. Eckert, Frankfurt/Basel)
Mice were anaesthetised and blood was removed by transcardial perfusion with PBS pH 7.4. One hemisphere was minced in 1 ml of cold 20 mM TBS with ten strokes in a Potter homogeniser at 1200 rpm (the other hemisphere was fixed in PFA). An aliquot of this homogenate was diluted 1:1 with TBS, centrifuged at 3,000 × g for 10 min at 4°C and supernatants were collected and stored at -80°C for lipid peroxidation assays. The remaining homogenate was centrifuged at 8,500 × g for 10 min at 4°C, and supernatants were collected and stored at -80°C until antioxidant enzyme activity determination.

Assay of lipid peroxidation products:

The lipid peroxidation product malondialdehyde (MDA) was determined by a photometrical method using the Lipid Peroxidation Assay Kit (Calbiochem) (Esterbauer and Cheeseman, 1990). The colorimetric reaction is a condensation of the aldehyde with 1-methyl-2-phenylindole yielding a chromophore with an absorption maximum at 586 nm. Basal levels of MDA were assayed after incubation of samples for 30 min at 37°C, and stimulated MDA levels were determined under the same conditions in the presence of 50 µM $FeCl_3$ in the sample homogenate.

Cu/Zn-SOD activity:

Cu/Zn-SOD (EC 1.15.1.1) activity was measured with the Superoxide Dismutase Assay Kit (Calbiochem) (Nebot et al., 1993). To remove interfering substances and rule out Mn-SOD activity, Cu/Zn-SOD enzyme activity was assayed after an extraction procedure with chloroform and ethanol according to the supplier's manual. SOD activity was calculated based on the V_s/V_c ratio of the autoxidation rates of the chromophore BXT-01050 measured at 37°C in the presence (V_s) and absence (V_c) of sample. The chromophore was measured in a Genesys 5 photometer (Spectronic Instruments, Rochester, USA) at 525 nm. One Cu/Zn-SOD activity unit is defined as the activity that doubles the auto-oxidation background ($V_s/V_c = 2$).

GPx activity:

GPx (cytosolic GPx, EC 1.11.1.9) activity was measured using the Cellular Glutathione Peroxidase Assay Kit (Calbiochem) (Paglia and Valentine, 1967) and tert-butylhydroperoxide as substrate. This reaction is based on the enzymatic reduction of hydroperoxide by GPx under consumption of reduced glutathione GSH which is restored from oxidised glutathione GSSG in a coupled enzymatic reaction by GR. GR reduces GSSG to GSH under consumption of NADPH as reducing equivalents. The decrease in absorbance at 340 nm due to NADPH consumption was measured in a Victor2 multiplate reader using a 355 nm filter with 40 nm bandpass. One unit of GPx is defined as the activity that converts 2 µmol of reduced glutathione per minute at 25°C.

GR activity:

The GR (EC 1.8.1.7.) activity was determined using the Glutathione Reductase Assay Kit (Calbiochem) (Mizuno and Ohta, 1986). The enzymatic activity was assayed photometrically by measuring NADPH consumption during the enzymatic reaction. In the presence of GSSG and

NADPH, GR reduces GSSG and oxidises NADPH to yield NADP resulting in a decrease of absorbance at 340 nm, which was measured in a Victor2 plate reader. One unit of GR is defined as the activity that reduces 1 µmol of GSSG (corresponding to 1 µmol of NADPH) per minute at 25°C.

2.4.6 Mitochondrial assays

Brain tissue preparation for mitochondrial analysis. (in collaboration with Dr. Eckert, Frankfurt/Basel)

Mice (8 pairs of 12 month and 8 pairs of 24 month old hemizygous P301L tau and WT control mice) were sacrificed by decapitation and brains were quickly dissected on ice (modified after (Stoll et al., 1992)). After removing the cerebellum, one hemisphere (the other hemisphere was directly used for preparation of isolated mitochondria) was minced into 1 ml of medium I (138 mM NaCl, 5.4 mM KCl, 0.17 mM Na_2HPO_4, 0.22 mM K_2PO_4, 5.5 mM glucose, 58.4 mM sucrose, pH 7.35) with a scalpel and further dissociated by trituration through a nylon mesh (pore diameter 1 mm) with a Pasteur pipette. The resulting suspension was filtered by gravity through a fresh nylon mesh with a pore diameter of 102 µm, and the dissociated cell aggregates were washed twice with medium II (110 mM NaCl, 5.3 mM KCl, 1.8 mM $CaCl_2*H_2O$, 1 mM $MgCl_2*6\ H_2O$, 25 mM glucose, 70 mM sucrose, 20 mM HEPES, pH 7.4) by centrifugation (400 x g for 3 min at 4°C). 100 µl of the suspension were used for protein determination. After centrifugation, cells were resuspended in 3 ml DMEM, then aliquots of 100 µl were distributed per well in a white 96 well plate for measurement of ATP levels and aliquots of 250 µl were distributed per well in a 48 well plate for measurement of the mitochondrial membrane potential and ROS levels. The latter were maintained at 37°C in a humidified atmosphere of 5% CO_2/95% air for the staining period with the appropriate dye or incubated with Aβ for 4 hours. The preparations of cortical cells from P301L tau transgenic mice and WT littermate controls (cross-over design) were made within 2 hours under the same conditions and in parallel. Data are expressed as fluorescence unit per mg/ml protein. The total protein content was determined (Lowry et al., 1951).

Determination of the mitochondrial membrane potential ψm:

The membrane potential of the inner mitochondrial membrane was measured using the Rhodamine 123 (R123) dye added to the cell culture medium at a final concentration of 0.4 µM

for 15 min. Cells were washed twice with HBSS (Hank's Balanced Salt Solution, Sigma, Germany), and fluorescence was determined with a Victor2 multiplate reader (Perkin Elmer, Rodgau-Jügesheim, Germany) at 490 nm/535 nm (Ex/Em). Loading capacity of the dye within the membrane decreases when the mitochondrial membrane potential declines after damage, e.g. exposure to $A\beta_{1-42}$. For the secondary insult with $A\beta_{1-42}$, cells were incubated for 4 hours with 50 nmol/l pre-aggregated $A\beta_{1-42}$.

To test acute and fast changes in ψm, the fluorescent dye Tetramethylrhodamine-ethylester (TMRE) was used at 0.4 µM for 15 min. TMRE exhibits a characteristic increase in fluorescence at 490 nm/590 nm (Ex/Em) after challenging mitochondria with drugs which decrease the membrane potential. The mitochondrial membrane potential was recorded with the respiratory inhibitors rotenone (2 µM), thenoyltrifluoroacetone (TTFA, 10 µM), antimycin (2 µM), oligomycin (10 µM) and sodium azide (10 mM) (Collins et al., 2002; Krohn et al., 1999).

ATP levels:

ATP levels were determined with a bioluminescence assay (ViaLight HT, Cambrex Bio Science). The enzyme luciferase is utilised which catalyses the formation of light from ATP and luciferin. The emitted light is linearly related to the ATP concentration and is measured using a luminometer (Crouch et al., 1993).

ROS levels:

Levels of cytosolic ROS were measured using the fluorescent probe 2',7'-dichlorodihydrofluorescein diacetate (H_2DCF-DA) and levels of superoxide anion radical by using dihydroethidium (DHE), respectively. Brain cells were loaded for 15 minutes with 10 µM H_2DCF-DA or 10 µM DHE. After washing twice with HBSS, formation of the fluorescent product DCF was detected with Victor2 multiplate reader (Perkin Elmer) at 485 nm/535 nm (Ex/Em). DCF is trapped mainly in the cytoplasm and is oxidised by several ROS, most notably hydrogen peroxide (Kenney and Kocsis, 1998). DHE which is oxidised to the fluorescent ethidium cation by $O_2^{\cdot -}$ was detected with Victor2 multiplate reader at 490 nm/590 nm (Ex/Em) (Budd et al., 1997).

Amount of mitochondria:

The total amount of mitochondria was measured using the cell-permeable mitochondrion-selective dye MitoTracker Green FM (100 nM, 15 min) which is essentially nonfluorescent in aqueous solutions and only becomes fluorescent once it accumulates in the lipid environment of mitochondria (490 nm/516 nm Ex/Em). To determine numbers of mitochondria, in addition, four pairs of 18 month old P301L tau transgenic and WT mice were perfused transcardially with 4% paraformaldehyde in microtubule stabilisation buffer (65 mM PIPES, 25 mM HEPES, 10 mM EGTA, 3 mM $MgCl_2$, pH 6.9). 5 µm paraffin brain sections were co-immunostained with anti-porin (A31855, Molecular Probes, Invitrogen, Basel, Switzerland; diluted 1:2000) and anti-tubulin antibodies (YOL 1/34, Abcam Limited, Cambridge, UK; 1:600) followed by incubation with Cy3- and Cy2-conjugated secondary antibodies (Jackson Immunoresearch, Milan Analytic, Fribourg, Switzerland). Numbers of mitochondria in neurites of CA1 hippocampal neurones were counted both proximal and distal to the cell body.

Preparation of isolated mitochondria:

Mice were sacrificed by decapitation and one brain hemisphere was rapidly dissected on ice and washed in an ice-cold buffer (210 mM mannitol, 70 mM sucrose, 10 mM HEPES, 1 mM EDTA, 0.45% BSA, 0.5 mM DTT, protease inhibitor cocktail Complete tablets, Roche Diagnostics). After removing the cerebellum, the tissue sample was homogenised in 2 ml buffer with a glass homogeniser (10 to 15 strokes, 400 rpm) and the resulting homogenate was centrifuged at 1400 x g for 7 min at 4°C, to remove nuclei and tissue particles. The low speed centrifugation step was repeated once with the supernatant. Then, the supernatant fraction was centrifuged at 10,000 x g for 5 min at 4°C to pellet mitochondria. The resulting pellet was resuspended in 1 ml ice-cold buffer and centrifuged again at 800 x g for 3 min at 4°C. Finally, the mitochondria-enriched supernatant was centrifuged at 10,000 x g for 5 min at 4°C to obtain a mitochondrial fraction. This fraction was resuspended in 100 µl of ice-cold buffer and stored at 4°C until use, followed by determination of protein content (Lowry et al., 1951).

Mitochondrial respiration:

The rate of mitochondrial respiration was monitored at 25°C using an Oxygraph-2k system (Oroboros, Innsbruck, Austria) equipped with two chambers and DatLab software. Mitochondria (0.5 mg) were added to 2 ml of a buffer containing 65 mM sucrose, 10 mM potassium phosphate,

10 mM Tris-HCl, 10 mM $MgSO_4$ and 2 mM EDTA (pH 7.0). State 4 respiration was measured after adding 40 µl malate/glutamate (240 mM/ 280 mM; assay concentration 4.8/5.6 mM). Then, 10 µl ADP (100 mM; assay concentration 0.5 mM) were added to measure state 3 respiration. After determining coupled respiration, 1 µl carbonyl cyanide 4-(trifluoromethoxy)phenylhydrazone (FCCP, 0.1 mM; assay concentration 0.05 nM) was added to the reaction chamber, and respiration was measured in the absence of a proton gradient. To inhibit complex I activity, a total volume of 3 µl (2 + 1 µl) rotenone (0.1 mM; final concentration 0.15 nM) was added. Then, 10 µl succinate (1 M; final concentration 5 mM) was added and respiration was measured. Finally, 8 µl KCN (0.5 M; assay concentration 2 nM) was added to inhibit complex IV activity. P301L tau mice and WT mitochondria were measured in parallel pairs using the same conditions (cross-over design).

Complex I activity:

Isolated mitochondria were solubilised in n-dodecyl β-D-maltoside (20%) (Sigma-Aldrich, Taufkirchen, Germany). NADH: hexaammineruthenium(III)-chloride (HAR) activity was measured at 30°C in a buffer containing 2 mM Na^+/MOPS, 50 mM NaCl and 2 mM KCN (pH 7.2) using 2 mM HAR and 200µM NADH as substrates to estimate the complex I content. To determine NADH:ubiquinone oxidoreductase activity, 100 µM n-decylubiquinone (DBQ) and 100 µM NADH were used as substrates, as described previously (Djafarzadeh et al., 2000). Oxidation rates of NADH were recorded with a Shimadzu Multi Spec-1501 diode array spectrophotometer ($\varepsilon_{340-400\ nm}$ = 6.1 mM^{-1} cm^{-1}). Complex I activity was normalised to the complex I content of the mitochondrial preparation and is given as DBQ/HAR ratio.

Complex IV activity:

Cytochrome c oxidase activity was determined in intact isolated mitochondria using the Cytochrome c Oxidase Assay Kit. The colorimetric assay is based on the observation that a decrease in absorbance at 550 nm of ferrocytochrome c is caused by its oxidation to ferricytochrome c by cytochrome c oxidase. The Cytochrome c Oxidase Assay was performed as described previously (Rasmussen and Rasmussen, 2000).

2.5 Study of tau insolubility after proteasome inhibition in P301L tau overexpressing SH-SY5Y cells treated with ß-amyloid

We wanted to test potential consequences on tau insolubility that could be mediated by proteasome inhibition with and without Aβ.

2.5.1 Neuroblastoma SH-SY5Y cell differentiation and Aβ treatment

To induce neuronal differentiation, P301L tau stable expressing cells were seeded on collagen type I-coated 10 cm Petri dishes at a confluency of 8 x 10^5 cells per dish and sequentially treated for 5 days with retinoic acid (20 µM; Sigma, Buchs, Switzerland) in growth medium ((Dulbecco's modified Eagle's medium F-12 (DMEM F-12) supplemented with 2 mM L-glutamine, 1% penicillin/streptomycin, 10% FCS, 5% HS) and 125 µg/ml gentamycin G418 (GIBCO, Basel, Switzerland)), followed by 5 days with brain-derived neurotrophic factor (BDNF; 50 ng/ml; Peprotech, Lucerne, Switzerland) in serum-free medium (Encinas *et al.*, 2000). These neuronal differentiated cells were then further cultured in serum-free medium. Suspensions of fibrillar $A\beta_{1-42}$ preparations (see 2.2.1) corresponding to 10 µM soluble peptide were added to the cultures for five days (see 2.2.2). Once $A\beta_{1-42}$ had been added to the cells, the medium was not changed anymore.

2.5.2 Proteasome inhibition in cell culture

We used three different proteasome inhibitors in cell culture. SH-SY5Y cells were differentiated and treated with Aβ or PBS as described in 2.5.1. Low concentrations of proteasome inhibitors (Affiniti, Exeter, UK) were added at the same time as Aβ and again 48 h afterwards. We used lactacystin (final concentration in cell growth medium, 1 µM) and epoxomicin (0.01 µM), both shown to strongly inhibit chymotrypsin-like proteasome activity (Kim et al., 1999; Vigouroux et al., 2003) and MG132 (0.005 µM), shown to inhibit all three peptidase activities of the proteasome (Vigouroux et al., 2003). We tested the cells with PBS, Aβ, each proteasome inhibitor or each proteasome inhibitor together with Aβ. At least two replicates for each condition were performed.

2.5.3 Sequential extraction of insoluble tau protein

The level of insoluble tau protein was determined by sequentially extracting Aβ-treated and reverse Aβ control cells using buffers with increasing ionic strength. All steps were carried out at 4°C unless otherwise indicated.

Cells in 10 cm Petri dishes were washed twice in ice-cold PBS and collected with a rubber scrapper in 100 µl RAB buffer (0.1 M MES, 1 mM EGTA, 0.5 mM MgSO4, 0.75 M NaCl, 0.02 M NaF, 1 mM PMSF, 0.1 mM EDTA), supplemented with Complete EDTA-free protease inhibitor cocktail (Roche, Basel, Switzerland) and 0.5 mg/ml Pefabloc (Roche). Cells were homogenised on ice with a Microlance 25 GA1 tip and then incubated for 20 min, followed by centrifugation for 20 min at 10,000 x g. The supernatant containing mostly soluble proteins was carefully removed (RAB fraction) and the RAB-insoluble pellet was extracted in 100 µl RIPA buffer (50 mM Tris pH 8.0, 150 mM NaCl, 5 mM EDTA, 0.1% SDS, 0.5% sodium deoxycholate, 1% NP40) with a Microlance 26 GA5/8 tip. After incubation for 20 min and centrifugation for 20 min at 10,000 x g, the supernatant containing mostly membrane proteins was recovered (RIPA fraction). The RIPA insoluble pellet was transferred with a pipette tip to a Beckman centrifuge tube. The pellet was extracted in 100 µl 70% formic acid (FA) with a Microlance 26 GA5/8 tip and incubated for 20 min. The FA-solution was centrifuged for 30 min at 50,000 x g in an Optima TLX ultracentrifuge using a Beckmann TLA 120.2 rotor (Beckmann, Nyon, Switzerland). The supernatant containing insoluble tau protein was transferred onto a Millipore dialyze membrane (Millipore, Volketswil, Switzerland) and dialyzed against 50 mM Tris pH 7.4, 1 mM DTT, and 0.1 mM PMSF for 1 h at RT (FA fraction). All fractions were stored in aliquots at -80°C.

Tau insolubility was evaluated by Western blotting of the FA samples probed with the human specific tau antibody, HT7 (Innogenetics Inc, Belgium).

2.6 Study of tau phosphorylation in P301L tau mouse brains

To characterise pathological related tau phosphorylation in the P301L tau mice, we carried out a sequential tau extraction to isolate "AD-P tau" adapted from Alonso et al. and Köpke et al. (Alonso et al., 1994; Kopke et al., 1993).

2.6.1 Tau extraction

All steps were carried out at 4°C unless otherwise indicated.

Mice were sacrificed by cervical dislocation, the brain was removed and washed in ice-cold PBS. The cerebellum was removed and the remaining brain was snap-frozen in liquid nitrogen. Homogenisation was performed in 4.5 ml homogenisation buffer (20 mM Tris pH 8.0, 0.32 M sucrose, 5 mM EGTA, 5 mM $MgSO_4$, 5 mM DTT, Complete protease inhibitor cocktail (Roche,

Basel, Switzerland), 50 mM NaF, 1 mM Na_3V0_4, 1 µM Okadaic acid, 0.1 mM PMSF) in a glass-teflon potter for 5 min. Homogenates were incubated for 10 min and centrifuged at 27,000 x g for 30 min with an acceleration 5, deceleration 2, in a Optima TLX ultracentrifuge using a Beckmann TLA 120.2 rotor (Beckmann, Nyon, Switzerland). Supernatant was removed and ultra-centrifuged at 200,000 x g for 1 h. The resulting pellet was resuspended in 100 µl 8 M urea with a Pipetman P200 and incubated at RT for 1 h, before a final centrifugation at 334,000 x g for 45 min at 22°C. The supernatant obtained should contain hyperphosphorylated AD-P tau and was stored at –80°C in aliquots until analysis.

2.6.2 Proteomics

AD-P tau fraction was mixed with IEF rehydration buffer (8.5 M urea, 4% CHAPS, 0.5% pharmalytes pH 5-8, 0.25% pharmalytes pH 8-10.5 (Amersham, Otelfingen, Switzerland)) and 1.2% DeStreak reagent (Amersham, Otelfingen, Switzerland)). Samples in rehydration buffer were incubated at RT for 30 min and then centrifuged for 15 min at 21,000 x g in a refrigerated bench centrifuge (Centrifuge 5417R, Vaudaux-Eppendorf AG, Schönenbuch, Switzerland) at 22°C. The samples were then loaded onto 17 cm IPG strips pH 5-8 (Bio-Rad, Reinach, Switzerland) and isoelectrically focused following the program detailed in Table 2. Focused IPG strips were loaded on 10% SDS-PAGE gels and 2-D patterns were revealed by Silver staining. We also probed for tau protein using the anti-human tau HT7 antibody by Western blotting after transferring the 2-D gel onto a nitrocellulose membrane.

2.7 PipOFF system

2.7.1 PipOFF constructs

Original constructs were obtained from Prof. Fussenegger (ETH, Zürich, Switzerland). All cloning was done by Daniel Schuppli.

Two PIT constructs:

EF1α-PIT: pMF255 vector containing the EF1α promoter and PIT gene.

CMV/β-actin-PIT: PIT gene was cloned into the pCAGGS vector containig the CMV-IE enhancer and the chicken beta-actin promoter.

Three reporter constructs:

PPIR8-YFP: YFP (from the pd2EYFP-N1 vector) was inserted into the pBP33 vector containing the PPIR8 promoter.

PPIR8-GFP: pMF164 containing the PPIR8 promoter and GFP gene.
PPIR8-LacZ: LacZ gene was inserted into the pBP33 vector containing the PPIR8 promoter.

2.7.2 Transgenic mouse generation

Pronuclear injections were done into C57Bl/6 × DBA/2 F2 oocytes to obtain founder animals. We generated EF1α-PIT and PPIR8-YFP co-injected mouse founders as well as CMV/β-actin-PIT and PPIR8-LacZ coinjected mouse founders. We also generated single transgenic EF1α-PIT; single transgenic PPIR8-YFP and single transgenic PPIR8-GFP. Single transgenics were crossed to generate double transgenics.

2.7.3 PCR

DNA was extracted from tail biopsies using the Genelute mammalian genomic DNA kit (Sigma, Buchs, Switzerland). PCR was carried out using a GeneAmp PCR system 9700 machine (Applied Biosystem, Rotkreuz, Switzerland). For EF1α-PIT, PPIR8-YFP and PPIR8-GFP PCRs, 0.5 µl tail mixture was added to PCR mix (15.9 µl H_2O, 2.05 µl PCR buffer, 0.41 µl 10 mM dNTP, 0.41 µl oligo mixture (20 pmol/µl), 0.82 µl Red Taq genomic DNA polymerase (Sigma, Fluka, Buchs, Switzerland)).
PIT PCR for EF1α-PIT: Screened with PIT fv (5'-CCCCACGACTCCGCCGGGTACG-3') and PIT rv (5'-CCTCCCACACCTCCCCCTGAACCTGA-3'). The reaction was heated to 95°C for 2 min before a series of 35 cycles (30 sec at 94°C, 30 sec at 64°C, 50 sec at 72°C), then kept at 72°C for 7 min and cooled to 4°C.
YFP PCR for PPIR8-YFP: Screened with YFP fv (5'-CATGGTGAGCAAGGGCGAGGAG-3') and YFP rv (5'-TGTCGCCCTCGAACTTCACCTC-3'). The reaction was heated to 95°C for 2 min before a series of 35 cycles (30 sec at 94°C, 30 sec at 56°C, 50 sec at 72°C), then kept at 72°C for 7 min and cooled to 4°C.
GFP PCR for PPIR8-GFP: Screened with OMF34 (5'-GATCGAATTCGATCCAAGCTTG CCTCGAG-3') and OMF37 (5'-GATCCTGCAGCCCGGGTTATTTGTAGAGCTCATC-3'). The reaction was heated to 95°C for 2 min before a series of 35 cycles (30 sec at 94°C, 30 sec at 55°C, 1 min at 72°C), then kept at 72°C for 7 min and cooled to 4°C.
PIT PCR for CMV/β-actin-PIT: Screened with first star PIT up (5'-CCATCTCGGCCGTCTTCC AGTTCGTCT-3') and star PIT low (5'-ACTCGTCAATTCCAAGGGCATCGGTAAA-3') and in a second step, the products of the PCR were screened using PIT nestup (5'-CCATCTCGGCC

GTCTTCCAGTTCGTCTAC-3') and PIT nestlow (5'-AGCCGCCAGCCCCGCCTCTTC-3'). For both reactions, 1 µl tail mixture or PCR reaction was added to PCR mix (38.5 µl H_2O, 5 µl PCR buffer, 1 µl 2 mM dNTP, 1 µl oligo mixture (20 pmol/µl), 2.5 µl Red Taq genomic DNA polymerase (Sigma, Fluka, Buchs, Switzerland)). For the first PCR, the reaction was heated to 95°C for 2 min before a series of 35 cycles (30 sec at 94°C, 30 sec at 56°C, 1 min at 72°C), then kept at 72°C for 7 min and cooled to 4°C. For the second PCR, the reaction was heated to 95°C for 2 min before a series of 35 cycles (30 sec at 94°C, 30 sec at 61°C, 50 sec at 72°C), then kept at 72°C for 7 min and cooled to 4°C.

LacZ PCR of PPIR8-LacZ: Screened with CAGGS1691-1718 (5'-GGTTATTGTGCTGTCTCA TCATTTTGGC-3') and lacZ322-295 (5'-TGGGATAGGTTACGTTGGTGTAGATGGG-3'). 0.5 µl tail mixture was added to PCR mix (15.5 µl H_2O, 2 µl PCR buffer, 0.4 µl 10 mM dNTP, 0.8 µl oligo mixture (20 pmol/µl), 0.8 µl Red Taq genomic DNA polymerase (Sigma, Fluka, Buchs, Switzerland)). The reaction was heated to 95°C for 2 min before a series of 35 cycles (30 sec at 94°C, 30 sec at 55°C, 50 sec at 72°C), then kept at 72°C for 7 min and cooled to 4°C.

2.7.4 Cell culture

Mouse 3T3 fibroblasts were grown as described in 2.2.2.and plated at 0.4 x 10^6 cells/well in 6 well plates 24 h before transfection. EF1α-PIT and PPIR8-YFP plasmids were introduced using a gene gun (Bio-Rad, Reinach, Switzerland). After transfection, cells were treated with and without 20 µg/ml Pristinamycin (PI) from Pyostacin tablets (Aventis, Paris, France) solubilised in DMSO. After 24 h PI treatment, the cells were observed under the fluorescence microscope.

2.7.5 Tail staining

To check for YFP expression in double transgenic EF1α-PIT and PPIR8-YFP founders, we performed immunostaining on tail biopsies. As control, the tail from a constitutive GFP expressing mouse was taken. Tails were embedded in paraffin, sectioned and immunostained with the anti-GFP antibody ab290 (Abcam, Cambridge, UK) at the dilution 1:200 (as described in 2.4.3).

2.7.6 Western blotting

Organs were homogenised 5 min in a glass-teflon potter in RIPA buffer (50 mM Tris pH 8.0, 150 mM NaCl, 5 mM EDTA, 0.1% SDS, 0.5% sodium deoxycholate, 1% NP40) supplemented with Complete EDTA-free protease inhibitor cocktail (Roche, Basel, Switzerland) and 0.5 mg/ml

Pefabloc (Roche). Homogenates were centrifuged at 21,000 x g for 10 min at 4°C and supernatant was frozen in aliquots at –80°C. Transfected cells with both EF1α -PIT and PPIR8-YFP plasmids were used as the positive control. 50 µg was loaded on a 12% SDS-PAGE and subsequently blotted (as described in 2.4.2.). To detect the PIT protein, we used the antibody sc-7545 (Santa Cruz Biotechnology, Labforce, Nunningen, Switzerland) against the VP16 transactivator domain of PIT at the dilution 1:100. To detect YFP or GFP, we used the anti-GFP antibody ab290 (Abcam, Cambridge, UK) at the dilution 1:2000.

2.7.7 LacZ staining

2.7.7.1 LacZ staining of mouse ears

Ear punches were washed in PBS and fixed for 15 min in 0.2% glutaraldehyde in PBS. After three time washing for 5 min in PBS, they were stained in X-gal stain (1 mg/ml X-gal, 5 mM $C_6FeK_3N_6$, 5 mM $C_6FeK_4N_6$, 0.01% sodium deoxycholate, 0.02% Nonidet-P40, 2 mM $MgCl_2$, PBS pH 7.3) overnight at 37°C.

2.7.7.2 LacZ staining of cryostat sections

LacZ staining of cryostat sections was used to check for beta-galactosidase expression in the LacZ ear positive mouse. The mouse was perfused with PBS, organs were removed and directly embedded in Tissue freezing medium (Jung, Leica, Glattbrugg, Switzerland) in isopentane cooled on dry ice. Organs were cut into 10 µm thick sections and dried. For LacZ staining, sections were fixed in cold PBS containing 0.2% glutaraldehyde for 10 min and then washed 3 x 5 min in lacZ wash buffer (2 mM $MgCl_2$, 0.01% sodium deoxycholate, 0.02% Nonidet-P40, PBS pH 7.3). Sections were then stained in X-gal stain solution (1 mg/ml X-gal, 5 mM $C_6FeK_3N_6$, 5 mM $C_6FeK_4N_6$, 0.01% sodium deoxycholate, 0.02% Nonidet-P40, 2 mM $MgCl_2$, PBS pH 7.3) overnight at 37°C. Finally sections were washed 3 x 5 min in PBS.

2.8 Antibodies used

Table 4.: Antibody list.

Antibody	Specificity	Source	IC	WB
HT7	Monoclonal phosphorylation-independent human tau antibody, epitope corresponding to aa 159-163	Innogenetics Inc, Belgium	1:200	1:500-1:1000
α-Synaptophysin	Polyclonal anti-synaptophysin	Dako, Zug, Switzerland	1:200	
α-Synaptophysin	Monoclonal anti-synaptophysin	Sigma, Buchs, Switzerland		1:2000
α-Synapsin	Polyclonal anti-synapsin	Molecular Probes, Invitrogen, Basel, Switzerland		1:600
α-DRP	Monoclonal anti- dihydropyrimidinase related protein	Supplied by: Maho Morishima and Yasuo Ihara, Department of Neuropathology, Faculty of Medicine, University of Tokyo, Japan		1:7000
α-CDCrel-1	Monoclonal anti-CDCrel-1 (septin 5)	Supplied by: Hansruedi Büeler, Institute of Molecular Biology, University of Zurich, Switzerland		1:400
α-GFP	Anti green fluorescent protein, ab290	Abcam, Cambridge, UK	1:200	1:2000
α-porin	Monoclonal anti-porin	Molecular Probes, Invitrogen, Basel, Switzerland	1:2000	1:5000
α-complex V	Monoclonal anti-OxPhos Complex V	Molecular Probes, Invitrogen, Basel, Switzerland		1:5000
α-tubulin	Monoclonal anti-tubulin, epitope corresponding to aa 414-422, YOL 1/34	Abcam Limited, Cambridge, UK	1:600	
α-PIT (VP16)	Anti VP16(sc-7545), epitope corresponding to aa 456-490 of VP16	Santa Cruz Biotechnology, Labforce, Nunningen, Switzerland		1:100
α-GFAP	Polyclonal anti-glial fibrillary acidic protein	Sigma, Buchs, Switzerland	1:100	
α-actin	Monoclonal anti-actin, ab6276	Abcam, Cambridge, UK		1:5000

3 RESULTS

3.1 Proteomics optimisation for the analysis of P301L tau mouse brains

3.1.1 Optimisation of the sequential extraction for whole brain samples

Most studies published until recently have performed 2-DE analysis without carrying out any prefractionation. However as there is no amplification method like PCR for nucleic acid, it is essential to carry out fractionation of the sample to improve detection of less abundant proteins especially from highly complex tissues such as brain. Indeed without prefractionation, 2-D gels of whole brain samples contain mostly structural protein such as tubulin and actin, and metabolic related proteins such as enolase, glyceraldehyde-3-phosphate dehydrogenase (GAPDH), pyruvate kinase, triosephosphate isomerase, phosphoglycerate mutase which form large groups of protein spots covering up less abundant proteins. We chose to carry out a sequential extraction according to protein solubility.

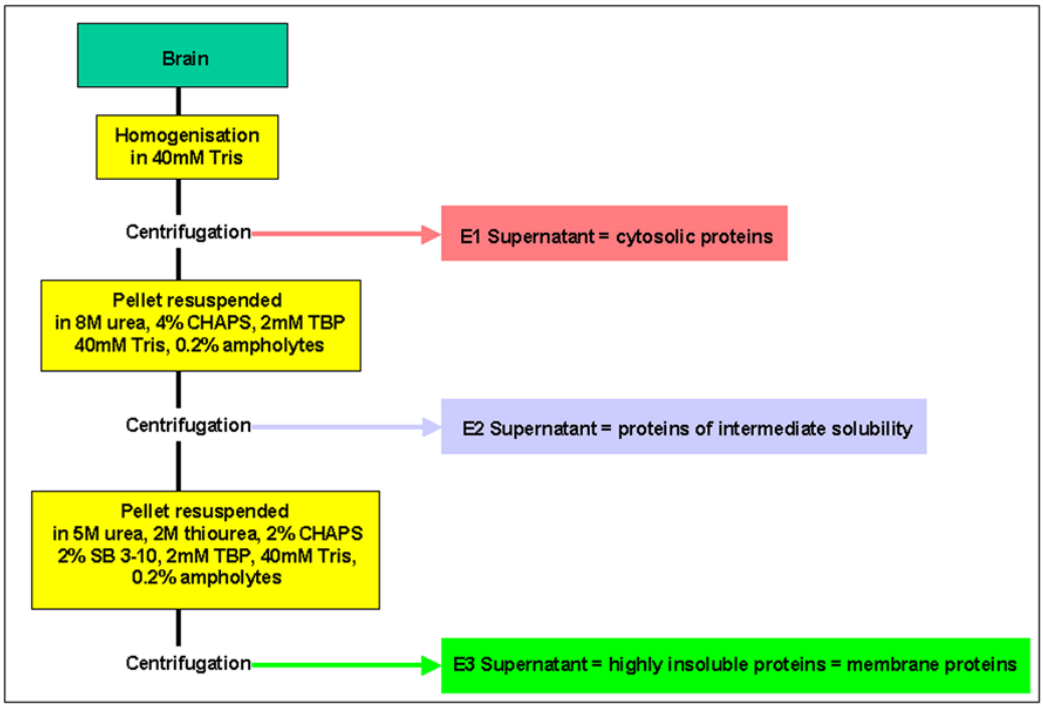

Figure 7.: Sequential extraction according to protein solubility.

To extract mouse brain samples, we have adapted a sequential extraction established by Molloy et al. (Molloy et al., 1998) for *Escherichia coli* proteins. Using this method, brain proteins were sequentially extracted into three fractions according to their solubility, namely E1 (soluble proteins), E2 (intermediate soluble) and E3 (less soluble) (Fig. 7). We optimised the starting homogenisation volume by increasing it to 3 ml, which improved extraction quality. Centrifugation steps were also optimised to improve separation especially of E2 and E3 fractions. DNaseI was added to the homogenate to remove DNA which causes vertical streaking in 2-DE.

3.1.2 Optimisation of two-dimensional gel quality and spot resolution

3.1.2.1 Isoelectrical focusing and two-dimensional electrophoresis

The three main optimisations in isoelectrical focusing concerned the amount of sample loaded, the IEF program and the reduction of sample oxidation. We could show that increasing the protein load on the IPG strip did not necessarily increase the amount of spots detected on the 2-D gel. On the contrary, decreasing the amount of proteins down to 40 µg E1, 50 µg E2 and 60 µl E3 significantly increased the number of spots distinguished on the 2-D gels. This suggests that high amounts of certain proteins impair isoelectrical focusing. In order to improve horizontal streaking in 2-D gel patterns, we introduced a stepwise increase in voltage during IEF (see material and methods, 2.1.4) to enhance protein focusing and we also increased the total focusing time as compared to most IEF programs. The most significant improvement of 2-D gel quality and spot resolution came with the use of the Destreak reagent. Oxidation is a major problem during the IEF runs and causes horizontal streaking. The Destreak reagent contains several reductants and when added to the protein sample in IEF rehydration buffer, it transforms the thiol groups into stable disulphide groups thus preventing unspecific oxidation. The use of Destreak greatly improved the resolution and allowed us for the first time to perform gel comparison between samples with significant matching between gels (Fig. 8).

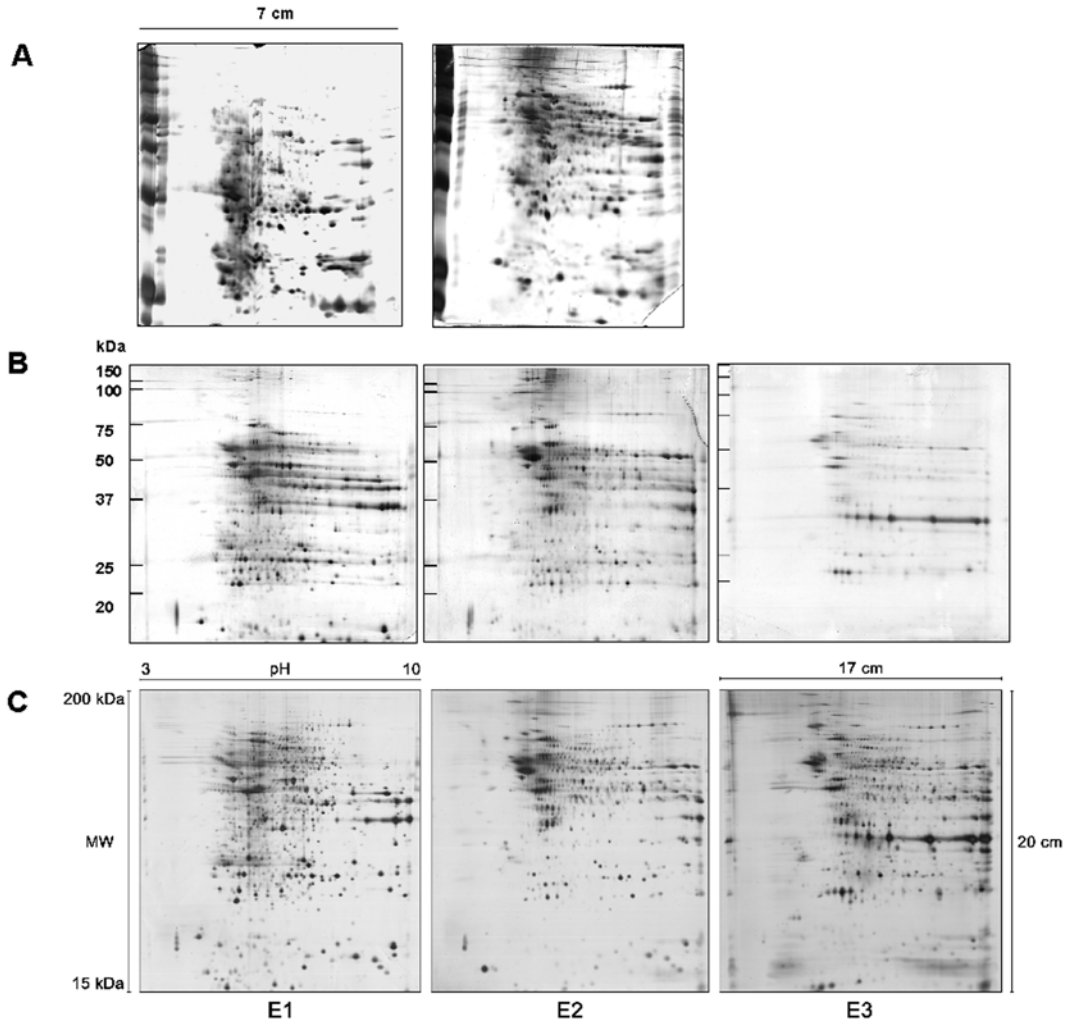

Figure 8.: Representative 2-D gels. A, Example of early gels. 80 µg of E1 (left) and E2 (right) were loaded onto 7 cm IPG (pH 3-10) strips in rehydration buffer (8 M Urea, 2% CHAPS, 7.5 mM DTT, 0.5% pharmalytes pH 3-10). B, Horizontal streaking and poor resolution without Destreak. 250 µg were loaded on 17 cm IPG strips in rehydration buffer (8 M urea, 4% CHAPS, 0.5% pharmalytes pH 3-10 supplemented with 2 mM TBP). C, Representative gels with Destreak reagent, used for Proteomweaver comparison. 40 µg E1, 50 µg E2 and 60 µl E3 were loaded in rehydration buffer (8.5 M urea, 4% CHAPS, 0.5% pharmalytes pH 3-10 and 1.2% DeStreak reagent).

Minor optimisations concerned the IEF rehydration, the IPG strip size, IPG equilibration times and gel thickness. We tried various IEF rehydration buffers, with different concentrations of urea, with or without thiourea, with either pharmalytes from Amersham or bio-lytes from Bio-rad, with different reductants such as TCEP or TBP. The final and optimal rehydration buffer contained 8.5 M urea, 4% CHAPS, 0.5% pharmalytes pH 3-10 and 1.2% DeStreak. In order to improve resolution and number of spots resolved, we switched from 7 cm IPG strips to 17 cm. The IPG strip equilibration step is an essential step needed to allow the IEF focused proteins to fully interact with SDS and in order to reduce and alkylate sulfhydryl groups with respectively DTT

and then iodoacetamide thus preventing their reoxidation. We optimised the equilibration incubation times to 30 min for each step as too short or too long times diminished the quality of the gels both in resolution and in numbers of spots observed. We also improved resolution by decreasing the thickness of the SDS-PAGE gels from 1.5 mm to 1 mm.

3.1.2.2 Gel staining

The most important proprieties of protein detection methods are high sensitivity, high linear dynamic range, reproducibility and compatibility with MS. We chose to use MS compatible Silver staining which is far more sensitive than Coomassie Blue and can detect as low as 1 ng protein/spot. However it is important to note that Silver staining has a limited dynamic range and is rapidly saturated. We evaluated four different MS-compatible Silver staining methods to select for the protocol with the best reproducibility and sensitivity. Silver staining kits from both Bio-Rad (Silver Stain Plus Kit) and Amersham Biosciences (PlusOne Protein Silver Staining Kit) lacked in sensitivity. The Silver staining protocol according to Shevchenko et al. (Shevchenko et al., 1996) produced uneven staining. A modified version of Blum's Silver staining was judged to be the most reproducible and sensitive Silver staining from among those tested.

3.1.3 Two-dimensional electrophoresis gel comparison

We tested two different software to compare differences between gels. The Melanie software was developed by the Swiss Institute of Bioinformatics and is distributed by GeneBio. This software has the advantage that the user can modify a great number of parameters during the analysis. However to perform a comparison between groups of samples, it is necessary to select a reference gel for each group, to which all gels of one group will be matched and similarly a reference gel must be chosen before matching between groups. This means that spots not present in the reference gel will not be taken into consideration in the comparison process. After testing the Melanie software on the E1 fractions, we tried the Proteomweaver software. This software offers a more powerful algorithm than the Melanie software as it allows the matching of 2-D patterns of every gel with every gel without the use of reference gels. Therefore the multi-matching performed by Proteomweaver provides a consistent spot identification in the whole experiment and avoids unnecessary elimination of protein spots not present in a specific gel. Proteomweaver also provides a replicate quality test which we used to test the minimum trustable

regulation factor that could be used for each fraction. This was less than 1.5 for gels from each fraction.

3.1.4 Optimisation of protein identification

3.1.4.1 Trypsin digestion

We tried out various trypsin digestion protocols with Silver stained spots. We evaluated the use of Silver destaining, protein reduction and alkylation, peptide extraction after digestion and the amounts of trypsin needed for digestion. As several aspects of the sample preparation for trypsin digestion and MS analysis parameters were sometimes modified in parallel, it is not always possible to evaluate which steps brought a significant improvement or not. In general, we found that removing silver ions by destaining with 30 mM $K_3(Fe(CN)_6)$ in 100 mM $Na_2S_2O_3$ for 10 min helped protein identification. An additional protein reduction and alkylation step during spot preparation does not improve MS analysis. Peptide extraction from gel pieces after digestion using several acetonitrile steps, also does not help MS analysis. Overall we can conclude that it is best to keep to a minimum the number of steps during spot preparation. Furthermore it is also important to reduce trypsin amounts to 20-30 ng per spot, as too high levels of trypsin peptides prevent the detection of other peptides by the MALDI MS. Analysis of both Silver stained and Sypro Ruby stained spots revealed that Silver staining significantly impairs MS detection as compared to Sypro Ruby. Most of the spots shown to be regulated in our samples were weakly stained spots and the identification of these spots was only possible after Sypro Ruby staining. To improve detection, we also increased protein load up to 150 µg on 2-D gels by employing 24 cm IPG strips rather than 17 cm.

3.1.4.2 Mass spectrometric identification

We evaluated both ESI and MALDI-TOF MS. However we obtained very poor results with ESI MS for digested protein spots. ESI MS analysis has also a major disadvantage compared to MALDI-TOF MS as the analysis of one spot takes in total three hours together with a wash run, whereas MALDI-TOF MS followed by MS/MS needs only a few minutes per spot. The accuracy of MALDI-TOF/TOF MS was continually improved by Dr. Peter Gehrig at the FGCZ centre with the most important improvement being the internal calibration of MS according to trypsin peptide m/z instead of solely an external calibration.

3.2 Proteomic analysis of P301L tau mouse brains

We performed a proteomic study to carry out an unbiased characterisation of the consequences of the expression of the human P301L mutant tau in a transgenic mouse model (David et al., 2005). To favour the visualisation of a relatively large proportion of different proteins on 2-D gels, the brain proteins were sequentially extracted in three fractions according to their solubility, namely E1 (soluble proteins), E2 (intermediate soluble) and E3 (less soluble). The proteins of each fraction from six pairs of hemizygous P301L tau and WT control mice were first focused in 17 cm IPG strips depending on their pI and then resolved in the second dimension by their molecular weight on SDS-PAGE gels. Silver staining revealed reproducible 2-D protein patterns for each sequentially extracted fraction. Differences between transgenic and WT mice were highlighted by the Proteomweaver software which normalises the overall spot intensities and then performs a comparison of every gel with every other gel. Protein spots that differed by more than 1.5-fold and statistically significant by Student's t-test ($p < 0.05$), were considered for further investigation. Overall, we found 15 up-regulated and 22 down-regulated protein spots in P301L tau transgenic mice as compared to WT controls, including four up- and four down-regulated in fraction E1, ten up- and seventeen down-regulated in fraction E2 and one up- and one down-regulated in the last fraction E3. After trypsinization, all but three of these differentially regulated protein spots were identified by MALDI-TOF/TOF mass spectrometry (Table 5). Several spots contained more than one protein and some were identified as the same protein.

The greater part of the regulated spots identified are related to either metabolism and mitochondrial respiration, oxidative stress or synapse function. In the first category, we identified one spot as the 30 kDa subunit of the NADH-ubiquinone oxidoreductase (electron transport chain complex I) and two spots as the ATP synthase D chain (complex V). All three spots were down-regulated as well as the metabolic related spots, triosephosphate isomerase (TPI), a glycolytic enzyme, and the cytoplasmic malate dehydrogenase involved in the malate-aspartate shuttle providing a metabolic co-ordination between cytosol and mitochondria. In contrast, a spot identified as inorganic pyrophosphatase was up-regulated. Associated with oxidative stress, spots representing the antioxidant enzymes peroxiredoxin 6, perioredoxin 3 (thioredoxin-dependent peroxide reductase), glutathione S-transferase (GST) P2 and Mu1, and phospholipid hydroperoxide glutathione peroxidase (PHGPx) were all down-regulated. In the last functional category, we found up-regulated spots related to synaptic function, such as the synaptic vesicle associated proteins, synapsin I, CDCrel 1 and septin 11, the axonal growth related protein,

dihydropyrimidinase related protein 2 (DRP-2) and another member of the dihydropyrimidinase family, DRP-3. Further differentially regulated spots (Table 5) included stathmin, a microtubule destabilising protein; MSTI1, the murine homologue of hop (heat-shock protein 70/heat-shock protein 90 (HSP70/HSP90) organising protein); γ-SNAP, involved in vesicle trafficking; the β-alanine oxoglutarate aminotransferase homologue, a GABA transaminase; the probable D-tyrosyl-tRNA deacylase and the growth factor receptor-bound protein 2 (GRB2), an adapter protein in signalling pathways. Therefore, P301L tau expression results in distinct modifications of the brain proteome suggesting alterations in the mitochondrial electron transport chain, in cellular antioxidant capacities and in synaptic properties.

Table 5.: Protein alterations in P301L tau mice.

Protein	Accession number[a]	Fraction[b]	Spot number	Fold difference	Student's t test	Mascot score[c]
Proteins involved in mitochondrial respiration and metabolism:						
NADH-ubiquinone oxidoreductase 30kDa subunit	Q9DCT2	E2	375	-1.62	0.0089	101
ATP synthase D chain	Q9DCX2	E2	455	-1.90	0.0124	134
ATP synthase D chain	Q9DCX2	E2	1457	-1.66	0.0026	62
Triosephosphate isomerase	P17751	E2	750	-1.79	0.0139	71
Inorganic pyrophosphatase (2010317E03Rik protein)	Q9D819	E1	576	1.56	0.0007	218
Malate dehydrogenase, cytoplasmic	P14152	E1	323	-1.58	0.0096	63
Proteins involved in oxidative stress:						
Peroxiredoxin 6	O08709	E2	38	-1.90	0.0076	287
Thioredoxin-dependent peroxide reductase (perioredoxin 3)	P20108	E2	978	-1.76	0.0007	91
Glutathione S-transferase P2	P19157	E2	443	-1.68	0.0104	158
Glutathione S-transferase Mu 1	P10649	E2	622	-1.61	0.0145	182
Phospholipid hydroperoxide glutathione peroxidase	O70325	E1	1605	-1.57	0.0168	98
Synaptic related proteins:						
Dihydropyrimidinase related protein-2	O08553	E1	311	1.50	0.0074	305
Dihydropyrimidinase related protein-2	O08553	E1	1983	1.53	0.0136	103
Dihydropyrimidinase related protein-2	O08553	E2	1853	1.62	0.0001	222
Dihydropyrimidinase related protein-2	O08553	E2	140	1.59	0.0000	133
Dihydropyrimidinase related protein-2	O08553	E2	1289	1.51	0.0001	105
Dihydropyrimidinase related protein-3	Q62188	E1	1307	1.64	0.0217	81
Synapsin I	O88935	E2	1597	1.91	0.0069	172
Synapsin I	O88935	E2	2160	1.83	0.0077	140
Septin 11	Q8C1B7	E2	1589	1.70	0.0152	122
Septin 5 (CDCrel-1)	Q9Z2Q6	E2	2112	1.59	0.0002	341
Other proteins:						
Stathmin[d]	P54227	E1	2156	-1.66	0.0081	55[d]
MSTI1 (stress-induced phosphoprotein 1)	Q60864	E2	1741	1.53	0.0064	113
Stress-induced phosphoprotein 1	Q99L66	E2	1741	1.53	0.0064	101
Gamma-soluble NSF attachment protein (γ-SNAP)	Q9CWZ7	E3	337	-1.52	0.0048	491
Endoplasmic reticulum protein Erp29 precursor	P57759	E2	778	-2.08	0.0058	134
Endoplasmic reticulum protein Erp29 precursor	P57759	E2	582	-1.72	0.0112	100

Lipoamide acyltransferase component of branched-chain alpha-keto acid dehydrogenase complex	P53395	E2	1893	1.50	0.0126	87
Beta-alanine oxoglutarate aminotransferase homologue (GABA transaminase)	Q8BZA3	E2	240	-1.71	0.0107	74
mus musculus adult male kidney cDNA; gene name: ethe1, synonym: hsco	Q9DCM0	E2	782	-1.56	0.0137	71
Probable D-tyrosyl-tRNA deacylase	Q9DD18	E1	251	-1.71	0.0004	131
GRB2 adapter protein	Q60631	E2	1213	-1.57	0.0100	122
Lamin C and C2	P11516	E2	1207	1.86	0.0075	203
Lamin A	P48678	E2	1207	1.86	0.0075	203
Paraspeckle protein 1	Q8R326	E2	1207	1.86	0.0075	196
Myeloid leukemia factor 2	Q99KX1	E2	1609	-1.56	0.0190	83
UPF0082	Q8K0Z7	E3	178	1.58	0.0086	135

[a] SWISS-PROT/TrEMBL accession number.
[b] Sequential extraction fraction where the protein was identified.
[c] Mascot protein identification score is –10*Log (P) where P is the probability that the observed match is a random event. Protein scores greater than 57 are significant ($p<0.05$) as based on the mouse database used here.
[d] This spot was independently identified twice as stathmin with a Mascot score near to significance. Tandem mass spectra were manually validated and the identification was considered correct.

Human P301L FTDP-17 brains show decreased complex V levels. As the proteomics comparison of the P301L tau and WT control mice revealed a significant decrease of two spots identified as the ATP synthase D chain, we looked at complex V levels in human FTDP-17 patient brains carrying the P301L tau mutation. Four P301L FTDP-17 brain and two control brain homogenates were examined by Western blotting (Fig. 9A).

We used the mitochondrial protein marker, porin to control for variations in mitochondrial amounts. Normalisation of complex V levels with porin levels showed a significant decrease in complex V levels in all P301L brain samples compared to control brains (Fig. 9B). Similar control complex V/porin percentages were found in three other control brain samples (data not shown). In average, we measured a 62.3% reduction of complex V levels in P301L FTDP-17 brains compared to control brains. The decreased levels of complex V in human P301L FTDP-17 brains confirms the proteomics observation made in the P301L tau transgenic mice and suggests that the P301L mutant tau pathology causes potentially a specific mitochondrial dysfunction in humans as well as in mice.

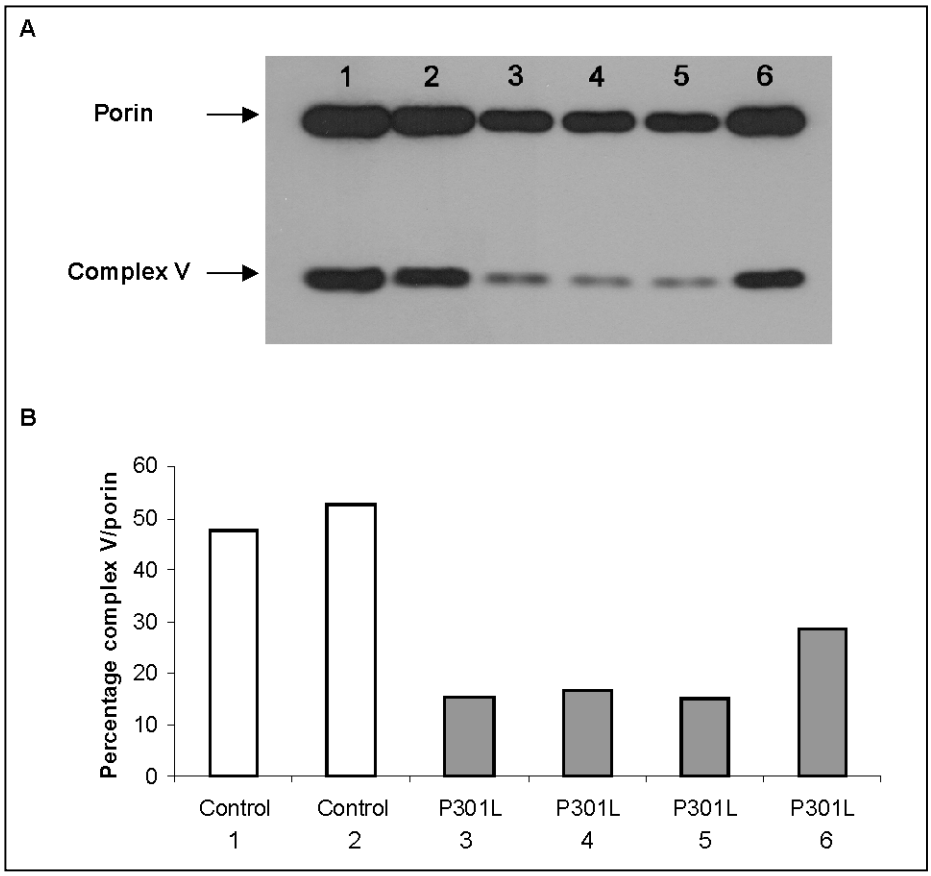

Figure 9.: Reduced complex V levels in human P301L FTDP-17 brains. A, Western blot of human temporal cortex brain homogenates. Complex V (ATP synthase) is recognized as the lower band using an anti-ATP synthase D chain antibody and the mitochondrial protein marker, porin as the upper band using an anti-porin antibody. Control brain homogenates were loaded in lanes 1 and 2 and P301L FTDP-17 brain homogenates in lanes 3 to 6. B, Complex V/porin percentages for control and P301L brains after Western blot band quantification. Sample percentages are represented in the same order as on the Western blot above.

3.3 Functional analysis of P301L tau mouse brains

3.3.1 Synaptic deficit

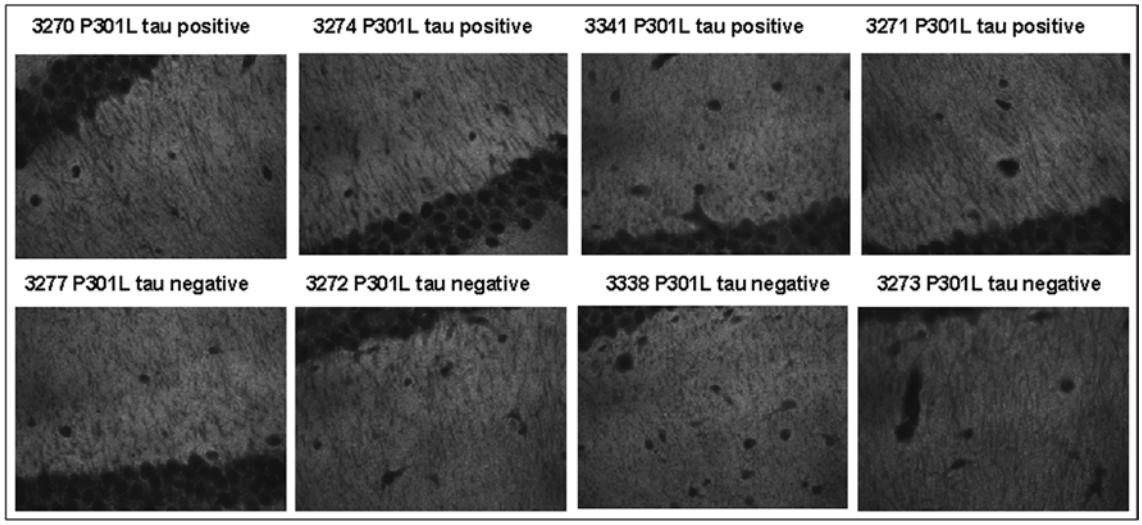

Figure 10.: Synaptophysin staining of 18 month old P301L tau transgenic and WT hippocampi. Synaptophysin (Dako) used at 1:200 followed by Cy3 conjugated anti-rabbit. No significant difference can be observed between synaptic staining of transgenic and WT mice.

The proteomic data obtained from comparing P301L tau transgenic and WT mice suggest a potential synaptic dysfunction. To evaluate this, we performed both immunostaining of coronal brain slices with synaptophysin and synapsin and Western blotting of homogenates and crude synaptosome preparations with synapse specific antibodies. We could not observe any significant difference in general synapse staining as evaluated by anti-synaptophysin (Dako, Zug, Switzerland) (Fig. 10). Immunostaining with anti-synapsin (Molecular Probes, Invitrogen, Basel, Switzerland) did not show specific synaptic staining.

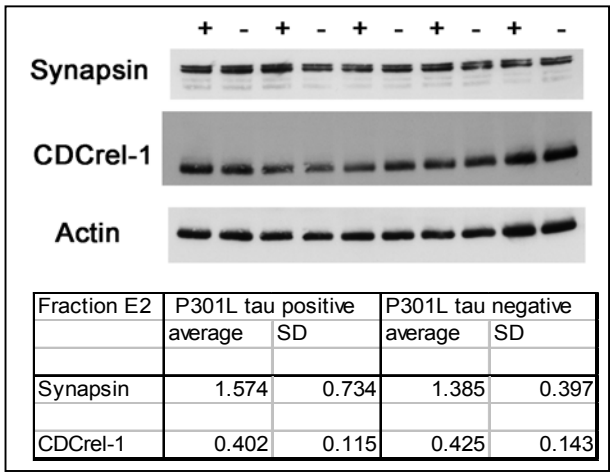

Fraction E2	P301L tau positive		P301L tau negative	
	average	SD	average	SD
Synapsin	1.574	0.734	1.385	0.397
CDCrel-1	0.402	0.115	0.425	0.143

Figure 11.: E2 fractions probed with synapsin and CDCrel-1. 10 µg of E2 fractions were loaded per well. Synapsin and CDCrel-1 bands were normalised with actin bands. No significant differences in levels of synapsin or CDCrel-1 can be observed between P301L tau and WT mice.

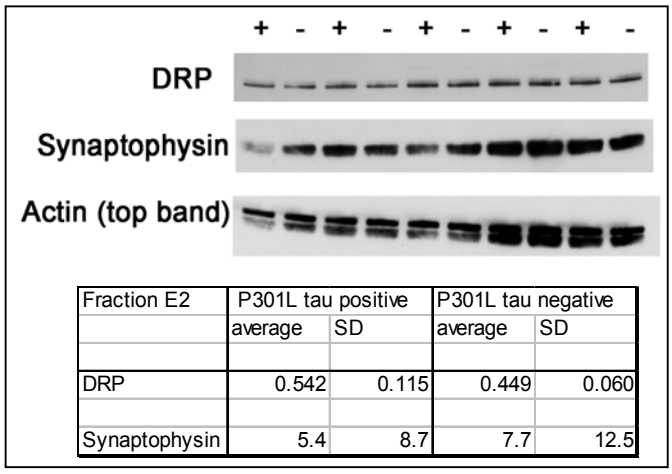

Fraction E2	P301L tau positive		P301L tau negative	
	average	SD	average	SD
DRP	0.542	0.115	0.449	0.060
Synaptophysin	5.4	8.7	7.7	12.5

Figure 12.: E2 fractions probed with DRP and Synaptophysin. 10 µg of E2 fractions were loaded per well. DRP and synaptophysin bands were normalised with actin bands. No significant differences in levels of DRP or synaptophysin can be observed between P301L tau and WT mice.

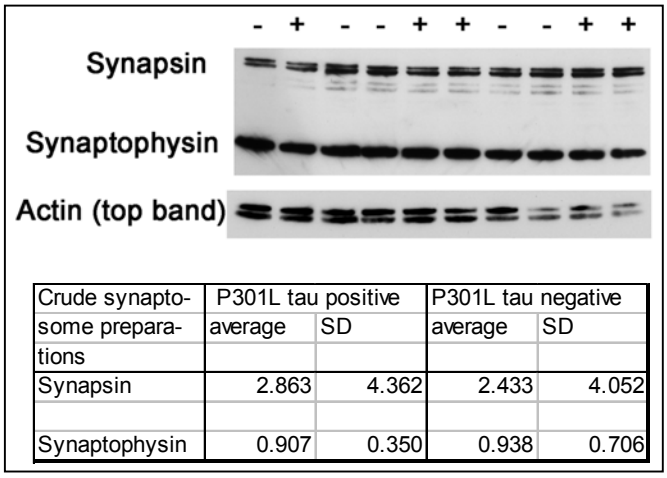

Crude synapto-some prepara-tions	P301L tau positive		P301L tau negative	
	average	SD	average	SD
Synapsin	2.863	4.362	2.433	4.052
Synaptophysin	0.907	0.350	0.938	0.706

Figure 13.: Crude synaptosome preparations probed with synapsin and synaptophysin. 5 µg of crude synaptosomes were loaded per well. Synapsin and synaptophysin bands were normalised with actin bands. No significant differences in levels of synapsin or synaptophysin can be observed between P301L tau and WT mice.

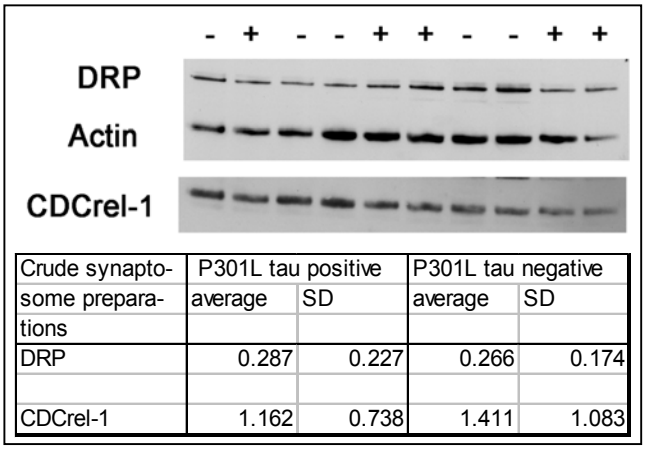

Crude synapto-some prepara-tions	P301L tau positive		P301L tau negative	
	average	SD	average	SD
DRP	0.287	0.227	0.266	0.174
CDCrel-1	1.162	0.738	1.411	1.083

Figure 14.: Crude synaptosome preparations probed with DRP and CDCrel-1. 5 µg of crude synaptosomes were loaded per well. DRP and CDCrel-1 bands were normalised with actin bands. No significant differences in levels of DRP or CDCrel-1can be observed between P301L tau and WT mice.

To better quantify any potential synaptic deficit, we carried out Western blotting with first E2 fractions and then crude synaptosome preparations. We probed against synapsin, DRP and CDCrel-1, all found by proteomics as up-regulated in the P301L tau mice and against synaptophysin. After normalisation of these proteins with actin, the average intensity for both P301L tau mouse and WT control bands was calculated. We found no statistical difference between transgenic and WT mice, for any of these synaptic proteins (Fig. 11, 12, 13, 14). However it is important to note that we observed a great variability in levels of all these synaptic related proteins both in E2 fraction and in crude synaptosome preparations (see standard deviations (SD) in Fig. 11, 12, 13, 14). Therefore these results do not preclude that a potential synaptic dysfunction could be present.

3.3.2 Mitochondrial deficit

P301L tau mice exhibit mitochondrial respiratory defects. We examined the metabolic capacity and function of cerebral mitochondria from P301L tau transgenic mice. Consistent with the down-regulation of subunits of mitochondrial electron transport chain complexes I and V, treatment with specific complex inhibitors showed a general reduction in mitochondrial depolarisation of P301L tau brain cells compared to WT and specifically a significantly reduced depolarisation after inhibition of complexes I and V (Fig. 15A).
Using a direct measurement of complex I activity, we observed a significant reduction of NADH-ubiquinone oxidoreductase (NADH:DBQ) activity in mitochondria of 12 month old P301L tau mice (Fig. 15B), whereas NADH:HAR activity (Fig. 15C) was not different indicating that complex I content is similar in P301L tau and WT control mice. Thus, P301L tau mitochondria present a functional defect of complex I activity with a reduction of 30.75% as revealed after normalising complex I activity with complex I content (Fig. 15D). In contrast, complex IV showed no differences in the cytochrome c oxidase activity between WT and P301L tau transgenic mice (Fig. 15E).

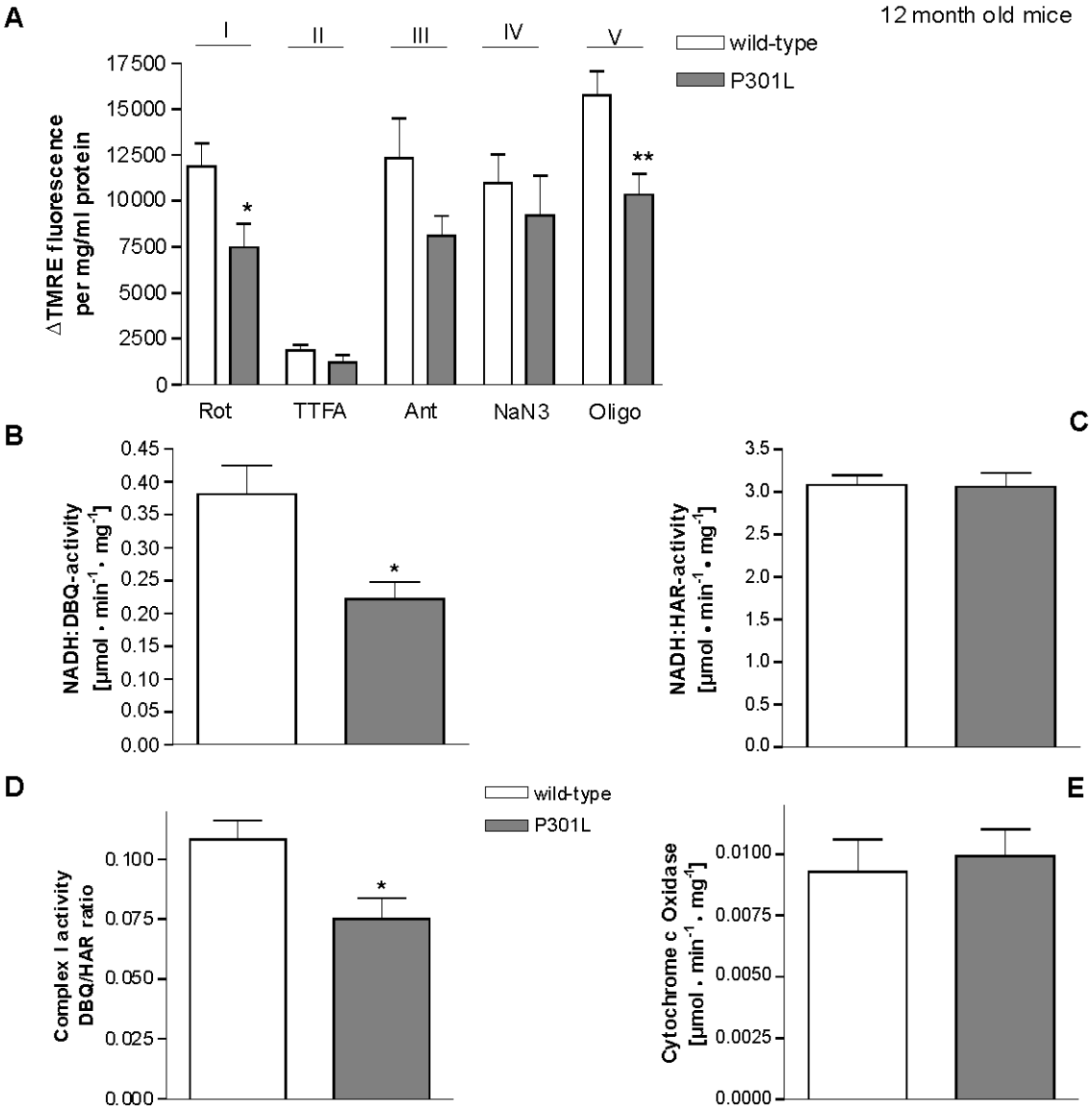

Figure 15.: Impaired depolarization and reduced mitochondrial complex I activity in P301L tau mice. A, Use of specific complex inhibitors reveals a significantly reduced depolarization of mitochondria from 12 month old P301L tau mice after treatment with the complex I inhibitor rotenone (Rot) and the complex V inhibitor oligomycin (Oligo) (*p<0.05, **p<0.01 vs. corresponding WT control mice, Student's t-test). A similar tendency was also found by inhibition of complex II with TTFA, complex III with antimycin (Ant) and complex IV with NaN_3. Two-way ANOVA reveals a significant effect of the transgene (p<0.01) and individual complexes (p<0.001) with no interaction between the two parameters. B-D, Complex I activity in cerebral mitochondria from 12 month old P301L tau mice and age-matched WT control mice. B, Reduced NADH-ubiquinone oxidoreductase (NADH:DBQ) activity in mitochondria of P301L tau mice (*p<0.05 vs. WT control mice, Student's t-test). C, Unaltered NADH:HAR activity. D, Complex I activity was normalized to the complex I content of the mitochondrial preparation and is given as DBQ/HAR ratio (*p<0.05 vs. WT control mice, Student's t-test). E, Unaltered complex IV activity. All values represent ± S.E. from n=6-8 animals per group.

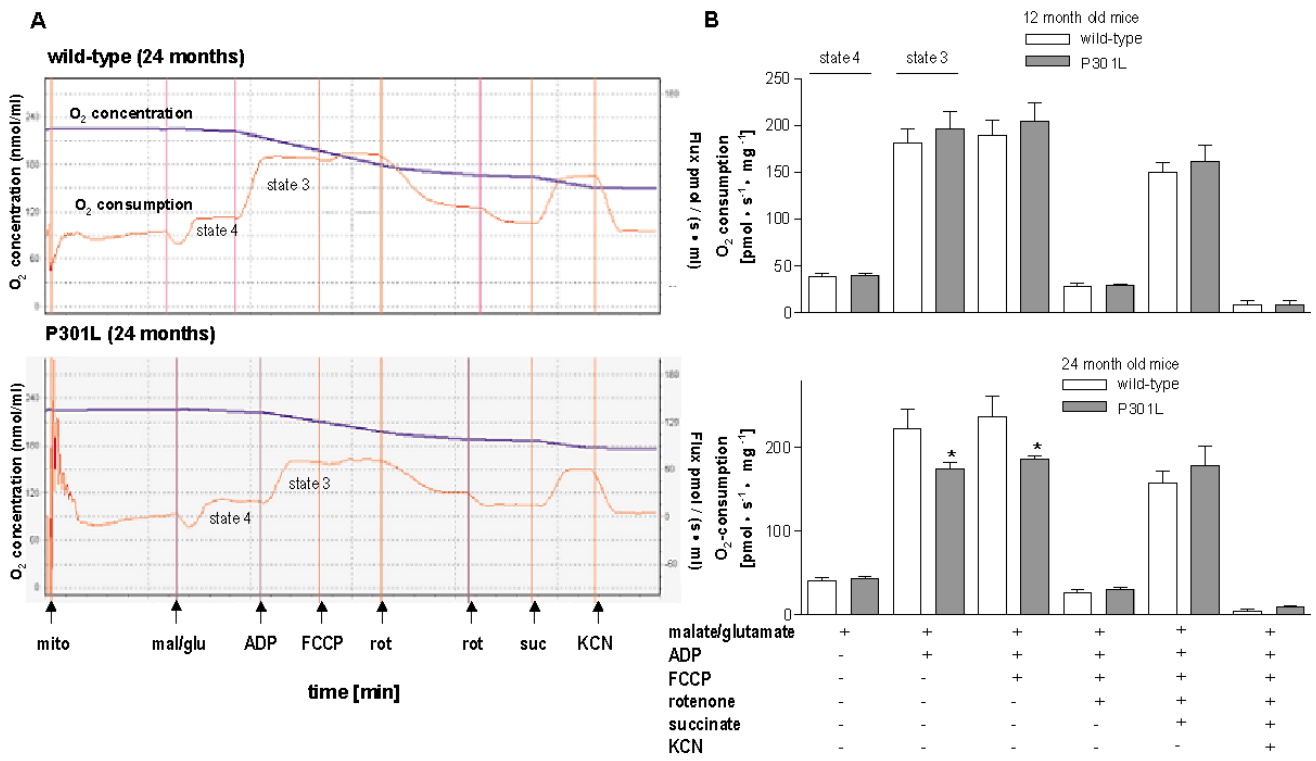

Figure 16.: Oxygen electrode reveals a reduction of O_2 consumption of P301L tau mitochondria during aging. A, Representative diagrams of measurement of oxygen (O_2) consumption in mitochondria from a 24 month old WT control (upper panel) and from an age-matched P301L tau mouse (lower panel) demonstrating a decrease in the total O_2 concentration with time. O_2 flux and consumption by mitochondria (mito) was measured after addition of different agents (marked by arrows): malate/glutamate (mal/glu; state 4), ADP (state 3), FCCP, rotenone (rot), succinate (suc), and KCN. B, O_2 consumption in freshly isolated cerebral mitochondria from 12 month (upper panel) and 24 month old mice (lower panel), respectively. State 4 was measured after adding malate/glutamate. Then, ADP was added to measure state 3 respiration. After determining coupled respiration, FCCP was added and respiration was measured in the absence of a proton gradient. To inhibit complex I activity, rotenone was added. Then, respiration was measured after adding succinate. Finally, complex IV activity and O_2 consumption was inhibited by treatment with KCN. Two-way ANOVA reveals a significant effect of the transgene ($p<0.05$) on coupled (state 3 and 4) and FCCP-induced uncoupled respiratory rates of mitochondria from 24 month old P301L tau mice compared to age-matched WT controls by using the specific complex I substrates malate/glutamate. Thus, aged, but not 12 month old, P301L tau mice exhibit a significant impairment of complex I related respiration (*$p<0.05$ vs. corresponding WT control, Student's t-test), while respiratory rates after addition of the complex II substrate succinate are unchanged. Values represent means ± S.E. from n=4 animals per group (measurement of WT control and P301L tau in parallel). All experiments were performed in duplicate

In addition, we determined the state 3 and state 4 respiration using substrates for complex I (glutamate/malate) (Fig. 16A, B). State 3 respiration measures the capacity of mitochondria to metabolise oxygen and the selected substrate in the presence of a limited quantity of ADP, which is a substrate for the ATP synthase (complex V). State 4 respiration measures respiration when all ADP is exhausted and is associated with proton leakage across the inner mitochondrial membrane. Therefore, it represents a "basal-coupled" rate of respiration. Whereas state 3 and state 4 respiration remained unchanged with complex I substrates in 12 month old P301L tau mice (Fig. 16B, upper panel), a significantly reduced state 3 respiration could be observed in 24

month old P301L tau mice (Fig. 16A, B, lower panels each), leading to a markedly reduced respiratory control ratio compared to age-matched WT mice (Fig. 17A). The respiratory control ratio provides a measure for the efficiency of coupling of the mitochondrial respiratory chain, indicating that the relative efficiency of metabolic coupling of the electron chain complexes is impaired during ageing in P301L tau mice. In addition, after uncoupling with FCCP, the respiratory rate in the absence of a proton gradient was significantly diminished in 24 month old P301L tau mice (Fig. 16B, lower panel), indicating a reduced maximum capacity of the electron transport chain. After complete inhibition of complex I with rotenone, succinate was added as a substrate for complex II. No difference in respiratory rate could be observed between transgenic and WT mice showing that complex II is not impaired by P301L tau.

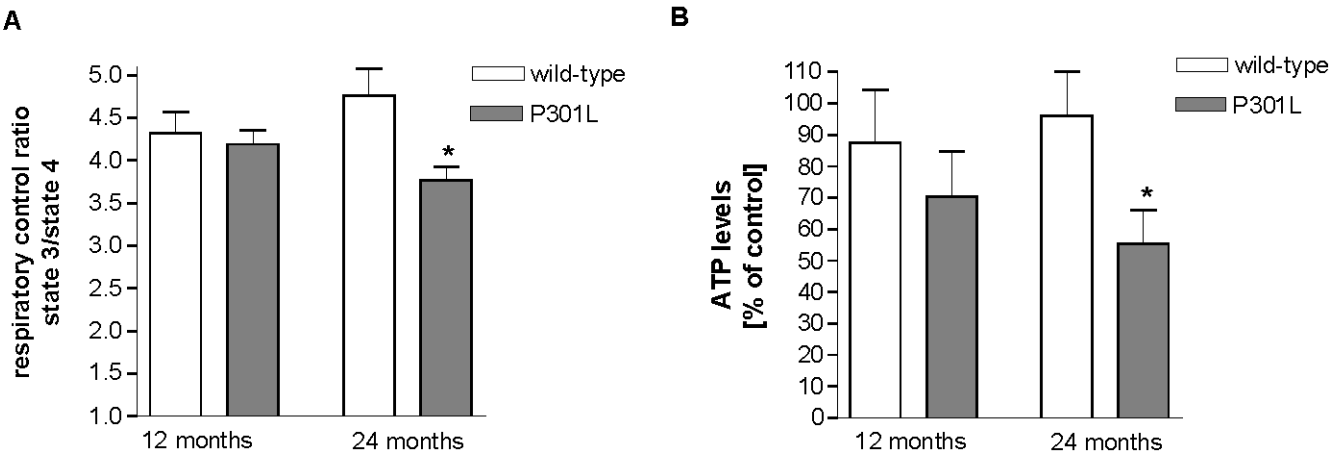

Figure 17.: Reduced respiratory control ratio and impaired ATP synthesis in P301L tau mice with aging. A, Reduced respiratory control ratio in 24 month old P301L tau mitochondria (*p<0.05 vs. age-matched WT control mice, Student's t-test), indicating an impaired efficiency of electron transport in aging. Values represent means ± S.E. from n=4 animals per group. All experiments were done in duplicates. B, In accordance, cerebral ATP levels are significantly reduced in 24 month old P301L tau mice (*p<0.05 vs. age-matched WT control mice, Student's t-test). Two-way ANOVA reveals a significant effect of the transgene (p<0.05) on ATP levels. Values represent means ± S.E. from n=6-7 animals per group.

In accordance with the respiratory control ratio, ATP levels of cerebral cells were unchanged in 12 month old P301L tau transgenic mice, but significantly reduced with ageing (Fig. 17B). Together these results suggest that P301L tau mice exhibit an initial defect in mitochondrial function with reduced complex I activity, which with age is translated into a mitochondrial respiration deficiency with diminished ATP synthesis corresponding to reduced complex V activity.

Mitochondrial dysfunction is not coupled to alterations in the number of mitochondria in P301L tau mice. Evaluation of the amount of mitochondria in cerebral brain cells revealed no difference between P301L tau and WT mice either in the cerebrum (Fig. 18A) or in the cerebellum (data not shown). In addition, co-immunostaining of mitochondria and microtubules and subsequent counting of the mitochondria in proximal and distal parts of neurites in the CA1 region of the hippocampus also showed no variation between P301L tau and WT mice (Fig. 18B). These data suggest that mitochondrial dysfunction is not associated with reduced mitochondrial numbers or significant changes in transport of mitochondria along neurites.

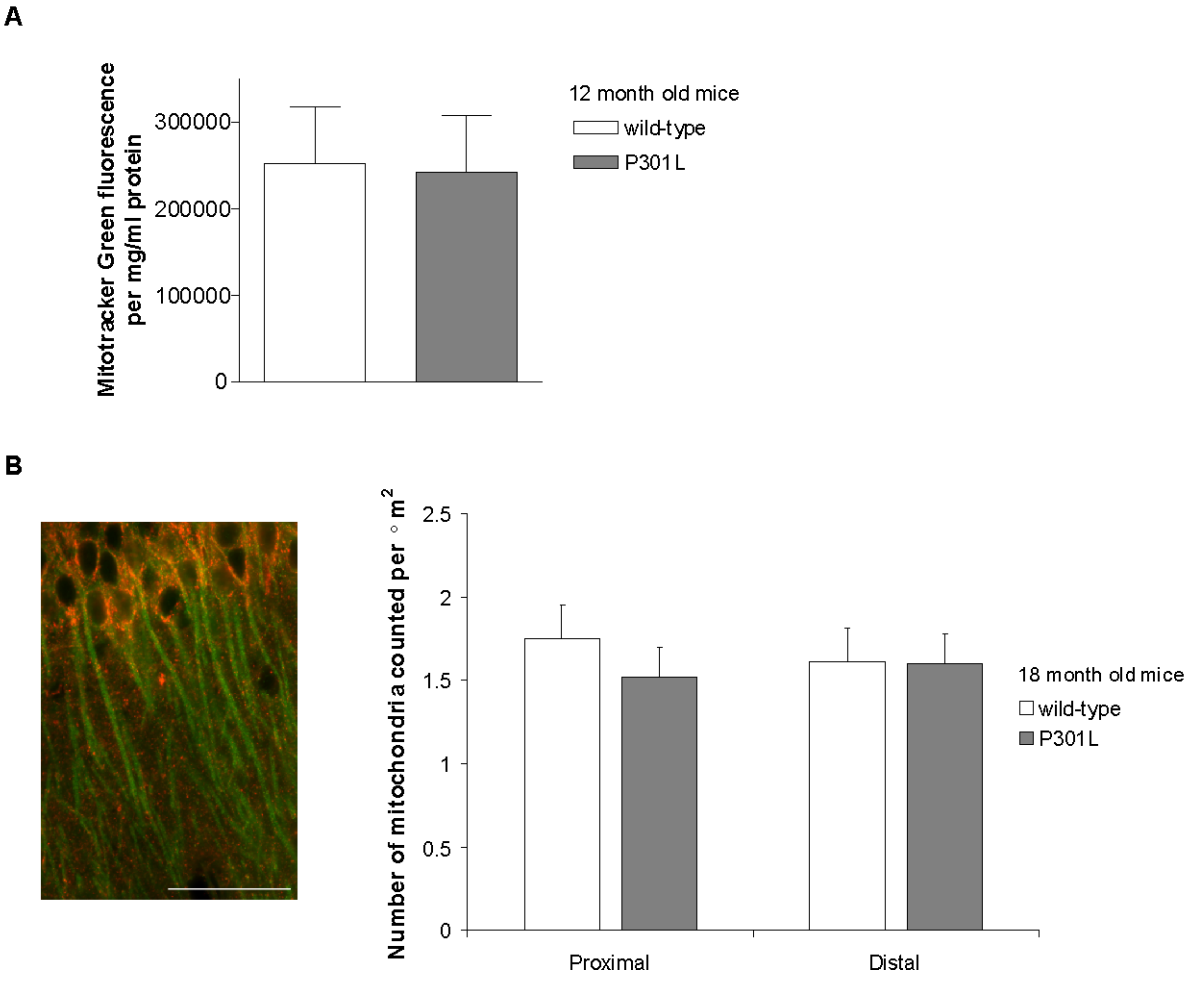

Figure 18.: Unchanged number of mitochondria. A, Measuring the amount of mitochondria using the cell-permanent mitochondrion-selective dye Mitotracker Green reveals no differences between P301L tau and WT mice in cerebrum. Values represent means ± S.E. from n=8 animals per group. B, immunostaining of mitochondria and microtubules in CA1 hippocampal brain sections with anti-porin (Cy3, in red) and anti-tubulin antibodies (Cy2, in green) again reveals no statistical difference in mitochondrial neuritic numbers at proximity or distally to the cell body between 18 month old P301L tau and WT mice. Values represent means ± S.D. from n=4 animals per group where mitochondria were counted in four different neurites per animal. Scale bar represents 50 µm.

Aβ insult causes increased membrane potential reduction in P301L tau mitochondria.
Extracellular Aβ treatment of PC12 cells has been shown to lead to a significant decrease in mitochondrial membrane potential (Keil et al., 2004). In order to investigate whether brain cells from P301L tau mice are more susceptible to Aβ, we measured the mitochondrial membrane potential of isolated cortical brain cells with and without Aβ treatment. Interestingly, the basal mitochondrial membrane potential was still conserved in cerebral cells from P301L tau mice. However secondary insult with $A\beta_{1-42}$ resulted in a higher reduction in membrane potential in P301L tau mitochondria than in WT (Fig. 19A). Importantly, this effect is brain region-specific and therefore probably dependent on the presence of P301L tau since cells from cerebellum with very low P301L tau expression levels were not vulnerable to this damage (Fig. 19B). This data suggests a synergistic action of Aβ and tau pathology on mitochondrial function.

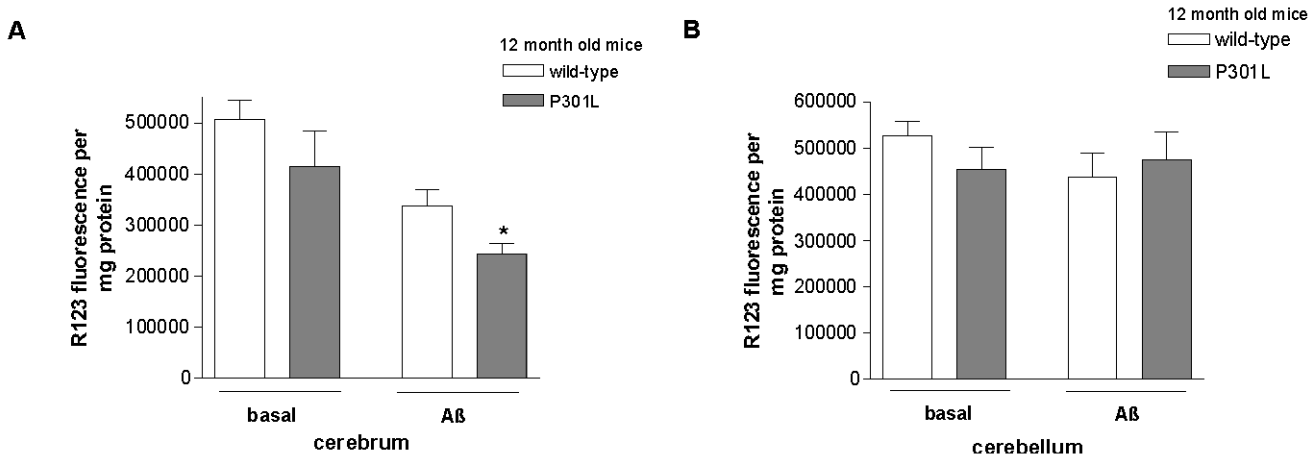

Figure 19.: Brain region-specific decrease of membrane potential after secondary insult with 50 nM Aβ. Aged, aggregated preparations of $A\beta_{1-42}$ were given to brain cells as secondary insult. An increased reduction of $\Delta\psi m$ was observed with the addition of Aβ to cerebral cells (A) (*$p<0.05$ vs. WT control mice, Student's t-test), but not with cerebellar cells (B) from 12 month old P301L tau mice. Two-way ANOVA reveals a significant effect of the transgene ($p<0.05$) on changes of mitochondrial membrane potential in cerebral cells. Values represent means ± S.E. from n=6-7 animals.

3.3.3 Oxidative stress

Increased tau pathology causes higher oxidative stress, modified lipid peroxidation levels and up-regulation of antioxidant enzyme activities in P301L tau mice. In P301L tau mice, these mitochondrial defects are associated with increased ROS formation, as both staining with DHE for detection of superoxide anions as well as staining with H_2DCF-DA for detection of cytosolic peroxides were increased (Fig. 20A, B).

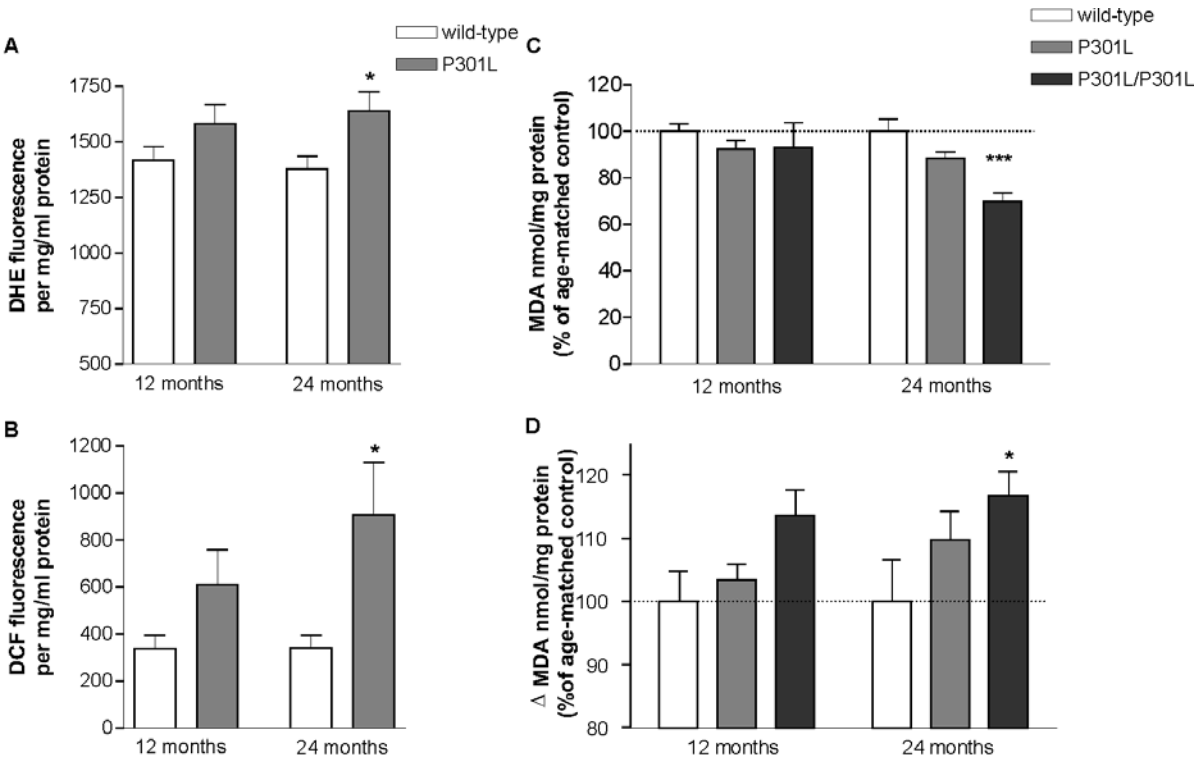

Figure 20.: Increased ROS production. A, Increases in superoxide anion radicals determined by DHE oxidation. Fluorescence (arbitrary units) normalized for protein content in brain cells from hemizygous P301L tau mice was measured after incubation of samples with DHE for 15 min. Two-way ANOVA: $p < 0.01$ effect of transgene, age and interaction n.s. Bonferroni post test: * $p < 0.05$ WT versus hemizygous P301L tau mice. B, Increases in cytosolic H_2O_2 determined by H_2-DCF oxidation. Fluorescence in brain cells from hemizygous P301L tau mice was measured after incubation of samples with H_2-DCF-DA for 15 min. Two-way ANOVA: $p < 0.01$ effect of transgene, age and interaction n.s. Bonferroni post test: * $p < 0.05$ WT versus hemizygous P301L tau mice. C, Reduced lipid peroxidation in P301L tau brains under basal conditions determined by MDA levels (nmol/mg protein). Two-way ANOVA: $p < 0.01$ effect of transgene, $p < 0.05$ age group, $p < 0.05$ interaction. Bonferroni post test: *** $p < 0.001$ WT versus homozygous P301L tau mice (P301L/P301L). D, Increased lipid peroxidation under stimulated conditions in 24 month old homozygous P301L tau mice. Formation of MDA (nmol/mg protein) in brain homogenates after 30 min incubation with $FeCl_3$ is increased in samples from P301L tau mice. Two-way ANOVA: $p < 0.05$ effect of transgene, age and interaction n.s. Bonferroni post test: * $p < 0.05$ controls versus homozygous P301L tau mice. All values represent means ± S.E. from n = 6-9 animals per group (except for 12 month old homozygous, n = 3).

Increased ROS levels could be detected already in 12 month old P301L tau mice but were more pronounced and statistically significant in 24 month old mice correlating with the age-specific increase in tau pathology. As a measure of free radical damage to critical cellular components, levels of malondialdehyde (MDA) as lipid peroxidation end product were determined. Despite increased ROS levels, basal levels of MDA were decreased in 24 month old hemizygous P301L tau mice and more pronounced in homozygous mice indicating that ROS levels are met by adequate antioxidant defences in these mice (Fig. 20C). However, upon stimulation with ferric iron, increased MDA levels were formed in P301L tau mice (Fig. 20D). This effect was already observed in 12 month old mice, but was more pronounced and statistically significant in 24 month old homozygous mice. Furthermore, basal and stimulated MDA levels remained unchanged in the cerebellum of 24 month old hemi- and homozygous P301L tau and WT mice (data not shown). As P301L tau is expressed at very low levels in the cerebellum (Gotz et al., 2001a), we can conclude that modifications in lipid peroxidation are specifically caused by the presence of the P301L tau protein. Hence, the presence of mutant tau impairs antioxidant defence under conditions of increased oxidative stress.

As a direct measure of antioxidant defence, activities of antioxidant enzymes were determined. While no significant changes were observed in 12 month old mice, 24 month old homozygous P301L tau mice displayed increased activities of Cu/Zn-superoxide dismutase (Cu/Zn-SOD) and glutathione reductase (GR) (Fig. 21A, C), while the activity of glutathione peroxidase (GPx) was not significantly increased (Fig. 21B). The increased enzyme activities may provide protection against ROS damage under basal conditions, but are obviously not sufficient to eliminate lipid peroxidation damage caused by the *in vitro* stimulation of brain homogenates with ferric iron. It is important to note that modified lipid peroxidation levels and increased antioxidant enzyme activities are dependent on the levels of P301L tau pathology as these changes were only detected as significant in old homozygous P301L tau mice.

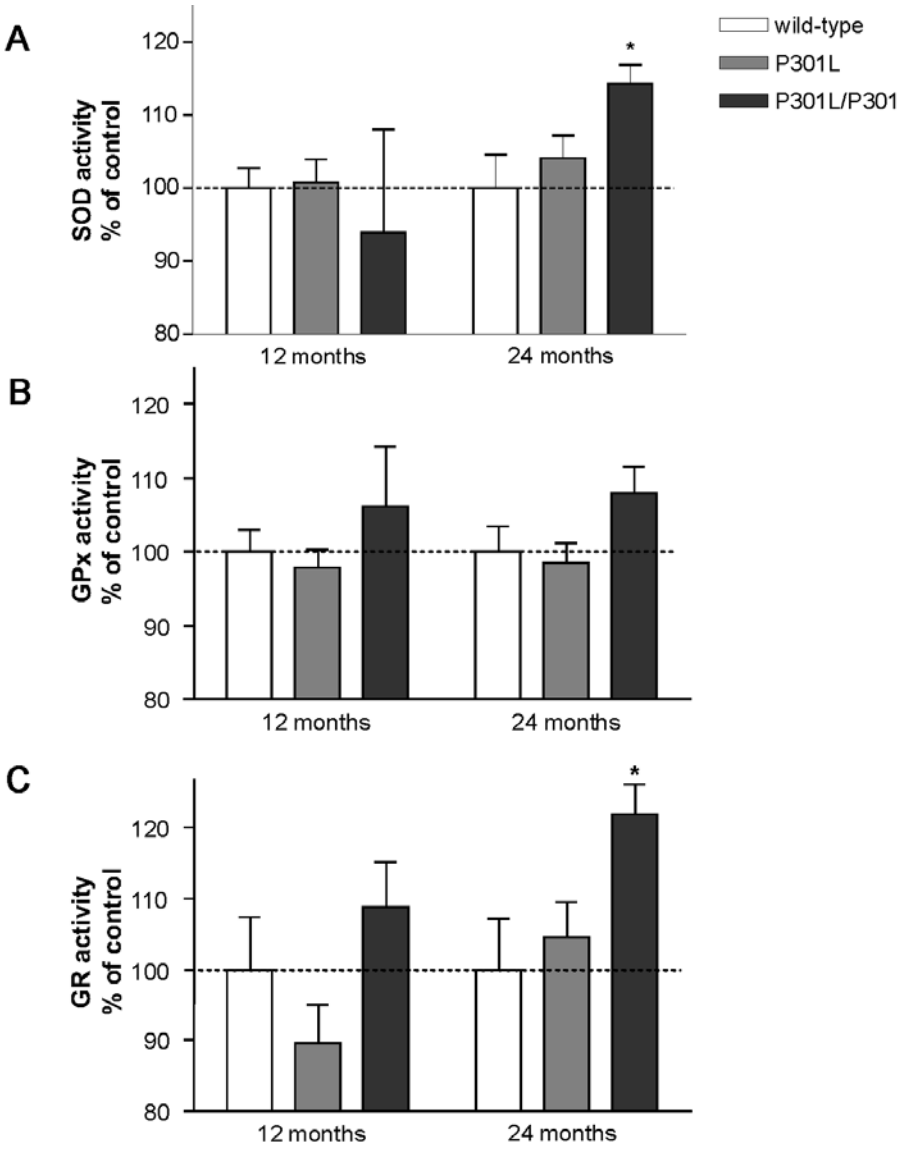

Figure 21.: Altered levels in detoxifying enzymes. A, Increased Cu/Zn-SOD activity in 24 month old homozygous P301L tau mice. Two-way ANOVA: effect of transgene n.s., $p < 0.05$ age group, $p < 0.05$ interaction. Bonferroni post test: * $p < 0.05$ controls versus homozygous P301L tau mice. B, GPx activity. Two-way ANOVA: $p < 0.05$ effect of transgene, age group and interaction n.s. C, Increased GR activity in 24 month old homozygous P301L tau mice. Two-way ANOVA: $p < 0.05$ effect of transgene, age group and interaction n.s. Bonferroni post test: * $p < 0.05$ controls versus homozygous P301L tau mice. Values represent means ± S.E. from n = 6-9 animals per group (except for 12 month old homozygous, n = 3).

3.4 Proteomic analysis of P301L tau overexpressing SH-SY5Y cells treated with ß-amyloid

To assess the effects of Aβ on the proteome of SH-SY5Y cells overexpressing tau protein, we homogenised five samples treated with Aβ and five samples treated with reverse Aβ, and sequentially extracted them into two fractions. In order to directly identify protein spots from the

gels used for the Proteomweaver analysis, Aβ and reverse Aβ treated fractions were isoelectrical focused on 24 cm IPG pH 3-10 strips, which allowed us to load 100 µg S1 and 67 µl S2.
We have proved that Silver staining can be compatible with a 2-DE proteomic approach and differences found between transgenics and WT mice can be confirmed by functional assays. However Silver staining presents some major drawbacks mainly concerning the linear range of staining and reproducibility. In comparison, Sypro Ruby, a ruthenium complex-based stain, offers significant advantages over Silver staining by combining staining reproducibility, a linear dynamic range of quantitation over three orders of magnitude and a detection limit of approximately 1-2 ng protein/spot. This staining is also compatible with MS. Therefore we used Sypro Ruby to detect protein spots in the fractions from Aβ treated SH-SY5Y cells.

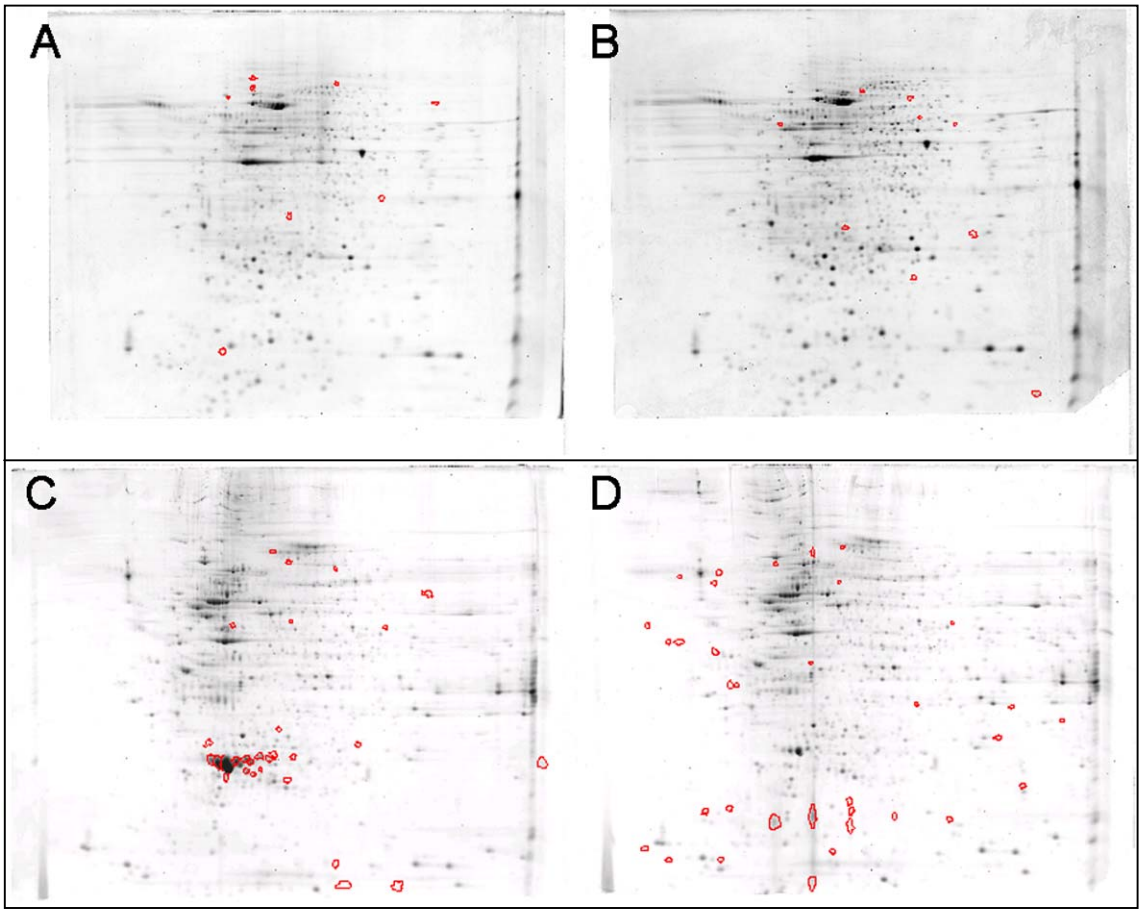

Figure 22.: Proteomweaver analysis of supernatant S1 and S2 from SH-SY5Y cells treated with Aβ. A, Spots up-regulated with Aβ reverse treatment in S1 fraction; B, Spots up-regulated with Aβ treatment in S1 fraction; C, Spots up-regulated with Aβ reverse treatment in S2 fraction; D, Spots up-regulated with Aβ treatment in S2 fraction.

The software Proteomweaver was used to normalise all gels and to compare each 2-D spot pattern of every gel from Aβ treated cells of one fraction with each 2-D spot pattern of every gel from reverse Aβ treated cells of the same fraction. Only spots present in all 12 gels and differentially regulated by at least 1.5 fold were considered for statistical analysis with Student's t-test ($p < 0.05$) (Fig. 22). We found in the supernatant S1 fraction, 9 spots up-regulated with Aβ, of which two are only found in the Aβ treated samples; and 8 spots up-regulated with reverse Aβ. In the supernatant S2 fraction, we found 34 spots up-regulated with Aβ and 28 spots up-regulated with reverse Aβ. Regulated S1 and S2 spots await identification by MALDI-TOF/TOF MS.

3.5 Proteomic analysis of amygdalae from P301L tau mice injected with ß-amyloid

P301L tau transgenic mice were intracranially injected with either Aβ or reverse Aβ. After three weeks, the mice were sacrificed, the amygdalae were dissected and the hippocampus was fixed in PFA. For each mouse, we checked the site of injection in the hippocampus by GFAP immunostaining with detects the reactive astrocytes around the injection tract. For all mice, the site of injection could be located to the CA1 region of the hippocampus although some injections were slightly deeper.

As we have discussed in 3.1.1., prefractionation of samples before proteomic analysis is essential to distinguish medium to low abundant proteins. Therefore we tried to adapt the sequential extraction following protein solubility that was used for whole brains (see 3.1.1 and 3.2), to our dissected amygdala samples. However we could not optimise the protocol to obtain distinct fractions as a high level of overlap between fractions was observed (Fig. 23). It is important to note that we used throughout the trials and for the final comparison, a small pH range of 5-8 for IEF separation instead of pH 3-10. This should allow us to zoom in on lower abundant proteins without loosing too many significant hits as indeed most proteins are concentrated in this pH range on 2-D gels.

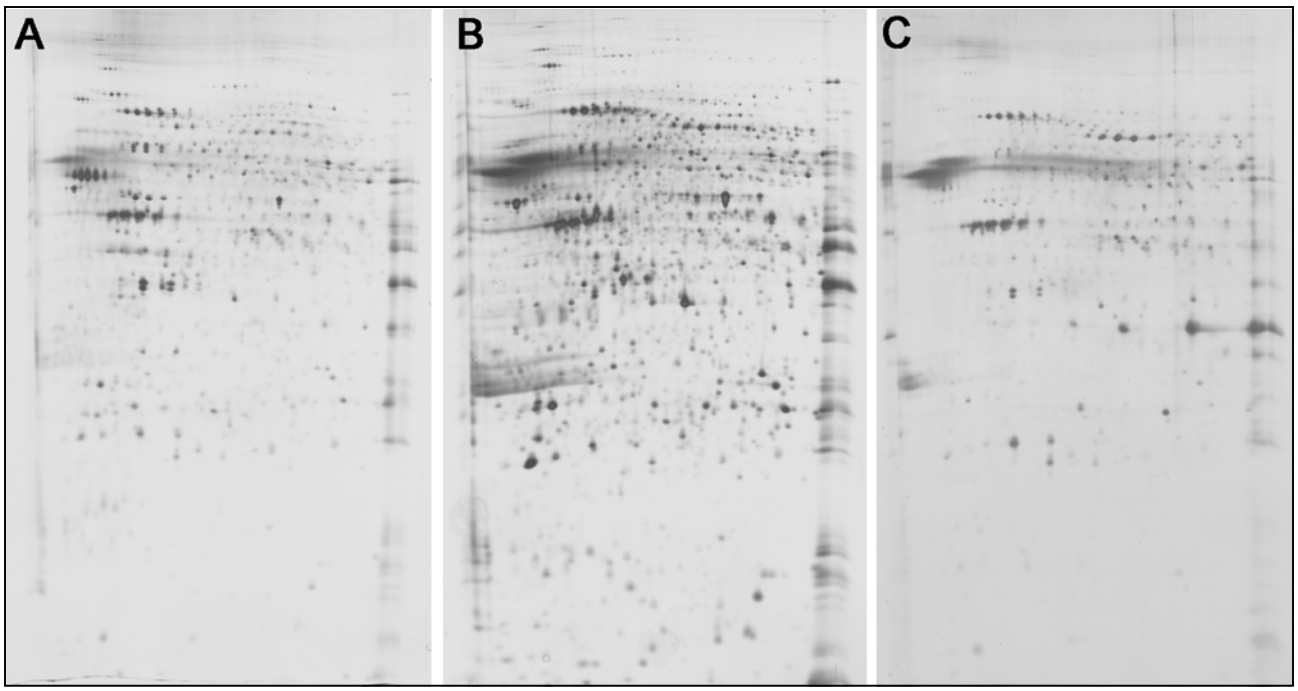

Figure 23.: Amygdala extraction trial into E1, E2 and E3 following the protocol used for P301L tau whole brain samples. All fractions were isoelectrically focused on 11 cm IPG strips pH 5-8. A, E1 fraction. B, E2 fraction. C, E3 fraction. All fractions show a high level of overlap in protein spots.

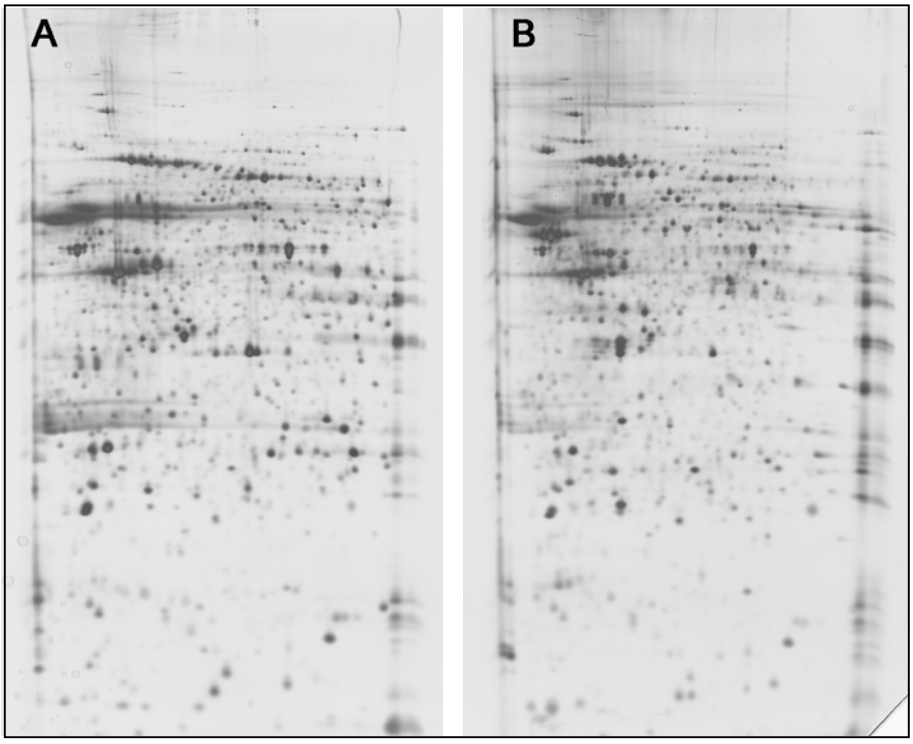

Figure 24.: Amygdala extraction trial into S1 and S2 following the protocol used for Aβ treated SH-SY5Y cells. Both S1 and S2 fractions were isoelectrically focused on 11 cm IPG strips pH 5-8. A, S1 fraction. B, S2 fraction. Both fractions show a high level of overlap in protein spots.

In a second step, we separated the amygdalae into two fractions, S1 and S2 following the protocol that we established for Aβ treated SH-SY5Y cells. Again the 2-D patterns of S1 and S2 showed a high degree of spot overlapping (Fig. 24). Therefore we decided to extract amygdala samples directly in IEF rehydration buffer without prefractionation. To improve protein extraction and recovery, we tried three different homogenisation methods, 3 min sonication, homogenisation using a syringe or homogenisation in a glass-teflon potter. Sonication gave the best results.

After centrifugation of sonicated samples, the supernatant was collected and loaded on 24 cm IPG pH 5-8 strips. Amygdala samples from five Aβ and five reverse Aβ injected mice were isoelectrically focused simultaneously, separated on 12% SDS-PAGE gels and stained with Sypro Ruby.

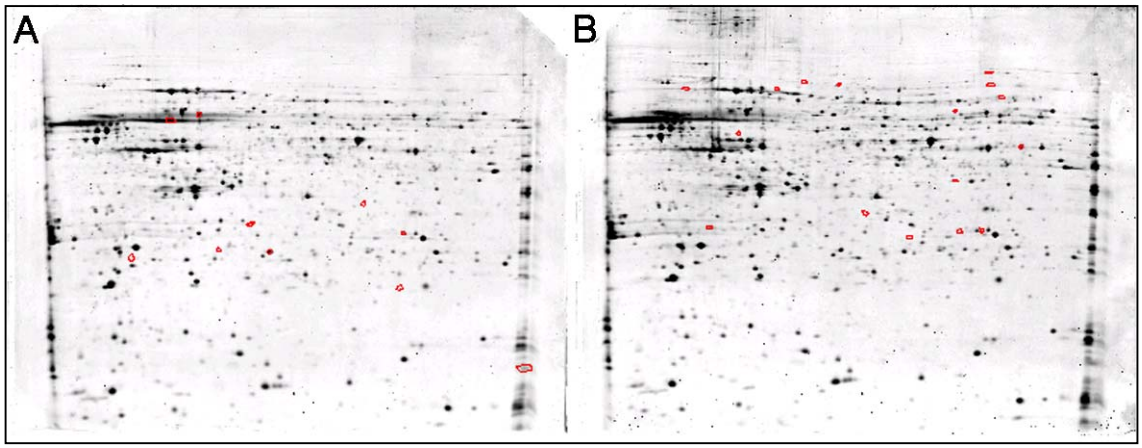

Figure 25.: Proteomweaver analysis of amygdala from P301L tau transgenic mice injected with Aβ. A, Spots up-regulated with Aβ reverse injection; B, Spots up-regulated with Aβ injection.

The 2-D patterns showed a high degree of similarity and were quantified with Proteomweaver. Only spots present in all 10 gels and differentially regulated by at least 1.5 fold were considered for statistical analysis with Student's t-test ($p < 0.05$). We found 16 spots up-regulated with Aβ and 10 spots up-regulated with reverse Aβ (Fig. 25). Regulated spots were directly picked out of the gels used for the comparative study, digested and are in the process of being analysed by MALDI-TOF/TOF MS.

3.6 Study of tau insolubility after proteasome inhibition in P301L tau overexpressing SH-SY5Y cells treated with ß-amyloid

To evaluate potential consequences of proteasome inhibition on Aβ mediated tau insolubility, we treated differentiated P301L tau expressing SH-SY5Y cells with various proteasome inhibitors. We choose differentiated cells to minimise the effect of proteasome inhibitors on cell cycle and apoptosis. First we tested different concentrations of proteasome inhibitors on differentiated SH-SY5Y cells to determine which concentration does not induce significant cell death over 5 days. We treated differentiated cells either with Aβ or PBS for 5 days together with or without different proteasome inhibitors. The whole experiment with epoxomicin and lactacystin was carried out three times.

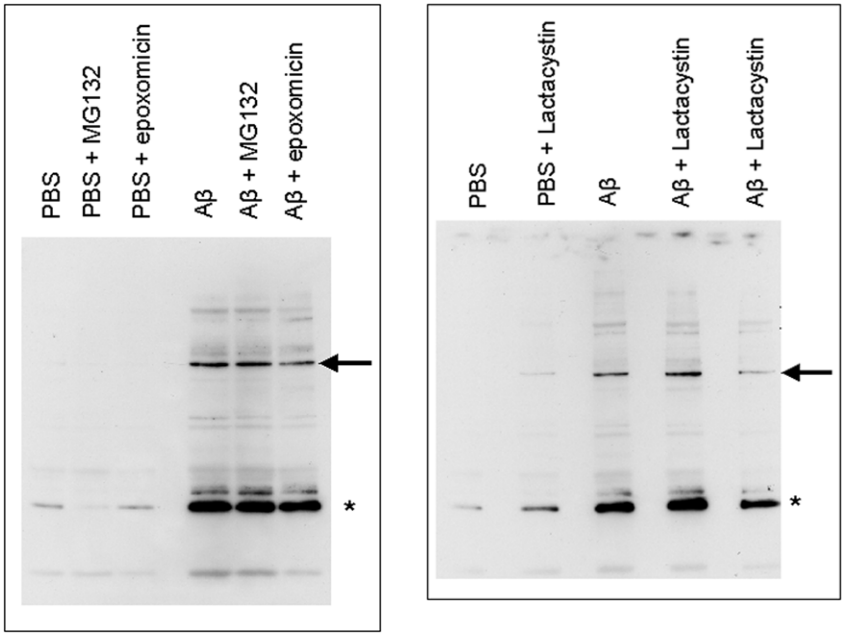

Figure 26.: Formic acid fractions from differentiated P301L tau expressing SH-SY5Y cells treated with Aβ and proteasome inhibitors. Blot were probed with the human specific tau antibody HT7. Full-length tau is indicated by an arrow and an asterisks marks the position of a 25 kDa truncated species possibly also tau.

Tau insolubility was evaluated by Western blotting of formic acid fractions obtained after a sequential extraction of the collected cells. Fig. 26 shows representative blots. Although we confirmed again that Aβ induces tau insolubility, results were too variable to show a significant effect of proteasome inhibitors on tau insolubility together with Aβ. Indeed in Figure 26, Western blotting of formic acid fractions from cells treated with lactacysin and Aβ, shows both an

increase and a decrease in levels of insoluble tau. This variability is probably due to a certain amount of variability in the sequential extraction of tau which has been observed by several members of the laboratory.

3.7 Study of tau phosphorylation in P301L tau mouse brains

Soluble tau is generally extracted by perchloric acid, based on tau's acid stability. However, this method is not compatible with MS analysis of tau phosphorylation as it oxidises tau amino acids. Therefore we adapted a milder extraction method published by Köpke et al. (Kopke et al., 1993) which separates the AD hyperphosphorylated tau (AD-P tau) from the cytosolic non-phosphorylated tau and insoluble NFT tau.

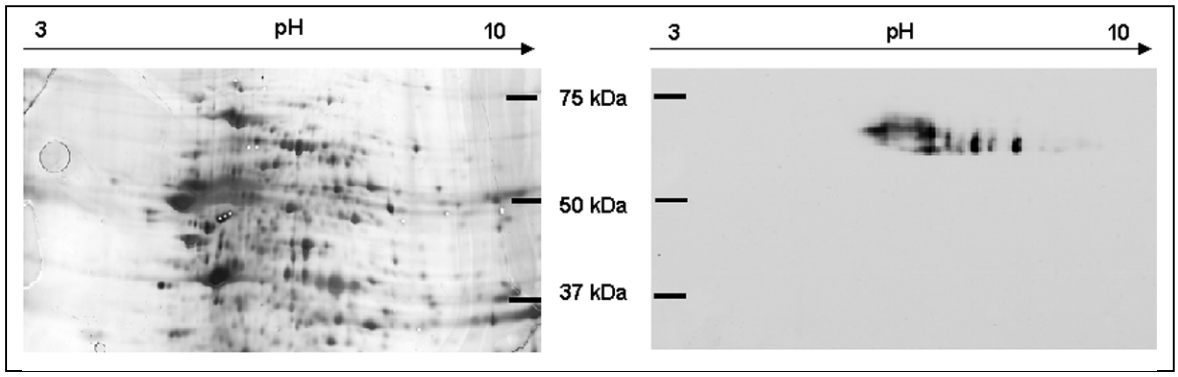

Figure 27.: Extraction for AD-P tau. P301L tau transgenic brain pellet from the 200,000 x g ultracentrifugation step was resuspended in 8 M urea. 300 µg was loaded on a 17cm IPG strip pH 3-10. Left.: 2-D gel of sample. Right.: Western blotting of 2-D gel probed with tau specific antibody, HT7. Tau was identified in a spot picked from this 2-D gel.

First we evaluated the presence and level of tau in the urea soluble pellet obtained after 200,000 x g centrifugation (Fig. 27). Western blotting showed us that indeed tau is present and one spot picked from the 2-D gel was identified as tau protein by MS. However the 2-D pattern reveals that a significant amount of other proteins are still present in this AD-P tau fraction. To remove these, we performed a final 334,000 x g ultracentrifugation step with the urea solublised fraction. We also isoelectrically focused the sample on IPG strips with a smaller pH range from 5 to 8, where tau proteins should be present.

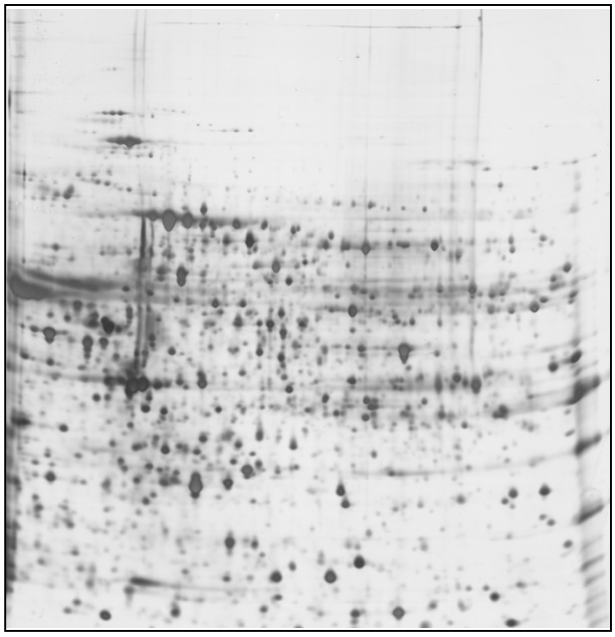

Figure 28.: Extraction of AD-P tau. 200,000 x g pellet was resuspended and centrifuged at 334,000 x g. The supernatant (80 µl) was loaded on a 17 cm IPG strips pH 5-8. 2-D gel shows that the tau extract still contains a wide variety of other proteins.

The 2-D pattern shows that this last centrifugation step is still not sufficient to remove most contaminants (Fig. 28). We also did not observe a significant amount of protein spots in the pI and molecular weight region for tau, which differed between P301L tau transgenic and WT samples. We therefore conclude that this extraction method is not sufficient in its present form, to provide an AD-P tau separation pure enough to dissociate most of the tau species present for MS analysis of phosphorylation.

3.8 PipOFF system

Our goal in this study was to assess whether the PipOFF transactivation system developed by Prof. Fussenegger for mammalian cell culture, would also work in the mouse model. We generated several double transgenic mice with the PIT gene under the control of either the EF1α or the CMV/β-actin promoter and the PPIR8 promoter controlling expression of either the reporter gene YFP, GFP or LacZ.

First we tested the PipOFF transactivation in cell culture with the EF1α-PIT and PPIR8-YFP constructs. After transfecting cells with both plasmids using the Gene Gun, we observed about 10% of cells expressing YFP (Fig. 29). YFP expression was turned off only after treatment with 20 times more PI as originally published (Fussenegger et al. (2000) *Nature Biotechnology* 18,

1203-1208). This could be due to differences in the dissolution protocol of the PI. All together this proves that the PipOFF system functions in cell culture with these constructs.

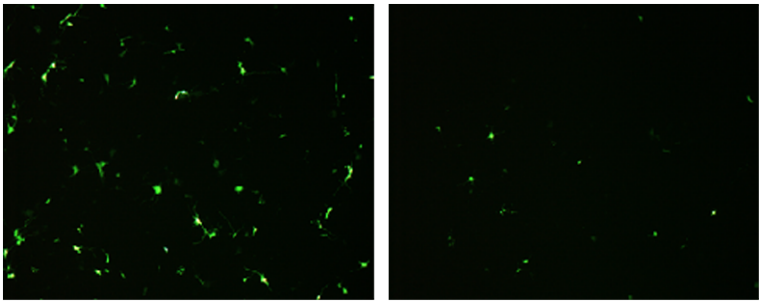

Figure 29.: 3T3 cells transfected with EF1α-PIT and PPIR8-YFP constructs using a GeneGun. Left, non-treated cells expressing both constructs. Right, cells treated with 20 µg/ml PI from Pyostacin tablets (Aventis). YFP is expressed in the absence of PI and knocked down by the treatment with PI demonstrating that the PipOFF transactivation system works with these constructs and can be turned off.

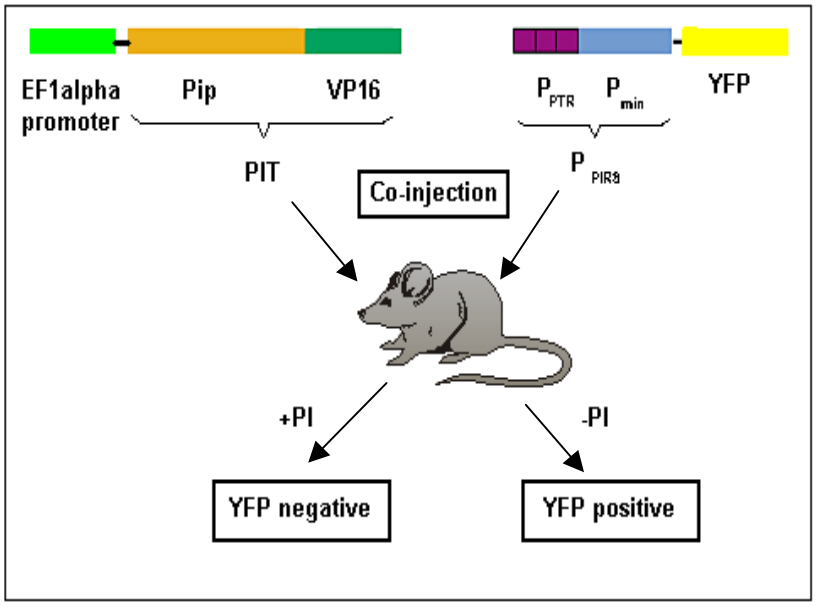

Figure 30.: Generation of double transgenic EF1α-PIT and PPIR8-YFP mice. In the absence of pristinamycin PI, PIT protein should bind to the PPIR8 promoter and induce transcription of YFP. In the presence of PI, PIT should no longer promote YFP expression.

To generate transgenic mice with the PipOFF system, we co-injected both EF1α-PIT and PPIR8-YFP constructs to produce double transgenic mice (Fig. 30). Transmission from the founders to the F1 generation was unusually low with only one of the six positive double transgenic founders that gave double positive pups. We also obtained two single PIT transgenic founders from co-injections. We tried feeding the female double transgenic founders in mating with dry food pellets containing PI to inhibit YFP expression during the embryonic period. However this did not result in transmission of the transgenes to the offspring, suggesting that a least YFP expression is not lethal during development.

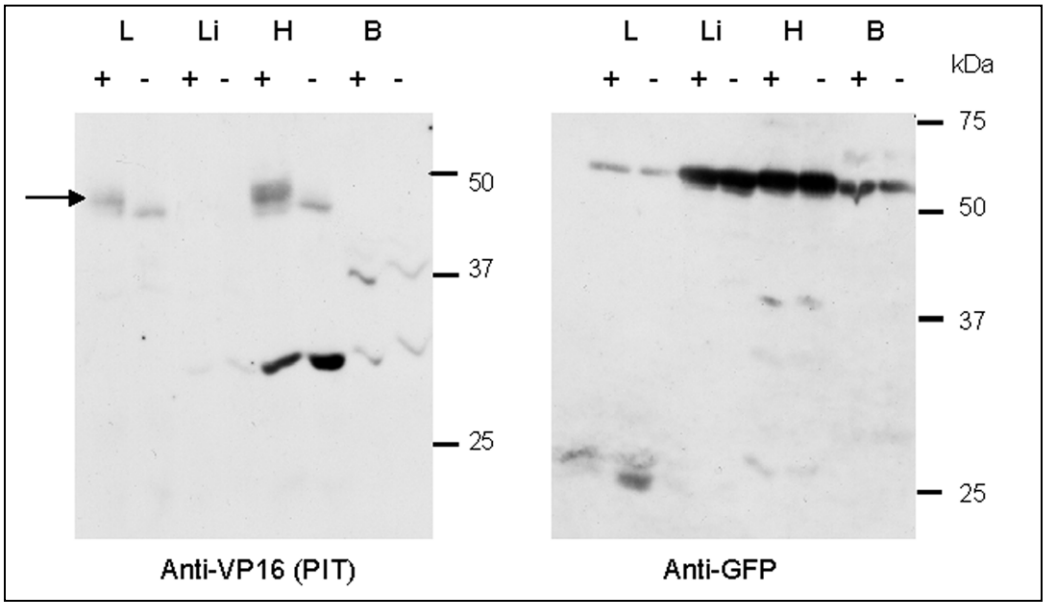

Figure 31.: Western blot of double transgenic EF1α-PIT and PPIR8-YFP offspring (co-injected of both constructs). Left: probed with an anti-VP16 antibody. Arrow indicates the potential PIT band. Right: probed with an anti-GFP antibody. L: lung, Li: liver, H: heart, B: brain.

In the positive founders, we could not observe any YFP fluorescence in ear cuttings under the microscope. Therefore we carried out immunohistochemistry on tail cuttings. However, we also could not detect any YFP expression in the tails of any of the double transgenic EF1α-PIT and PPIR8-YFP founders. In order to detect low quantities of YFP, we did a Western blot with different organs from a double transgenic mouse (Fig. 31). However we could not detect a band at 28 kDa or any higher bands specifically expressed in the PCR positive animal. We also probed for PIT protein with an antibody against the transactivation part VP16. Fig. 31 shows a band in

the lung and heart of the PCR positive animal but this band is slightly higher than the theoretical 47 kDa molecular weight for PIT. Subsequently, we produced single transgenics PPIR8-YFP and crossed these with single PIT transgenics which had only integrated the PIT construct from the EF1α-PIT and PPIR8-YFP co-injection. Here a normal transmission rate of the transgenes was observed. However, we could not detect the expression of PIT or YFP by Western blotting (data not shown).

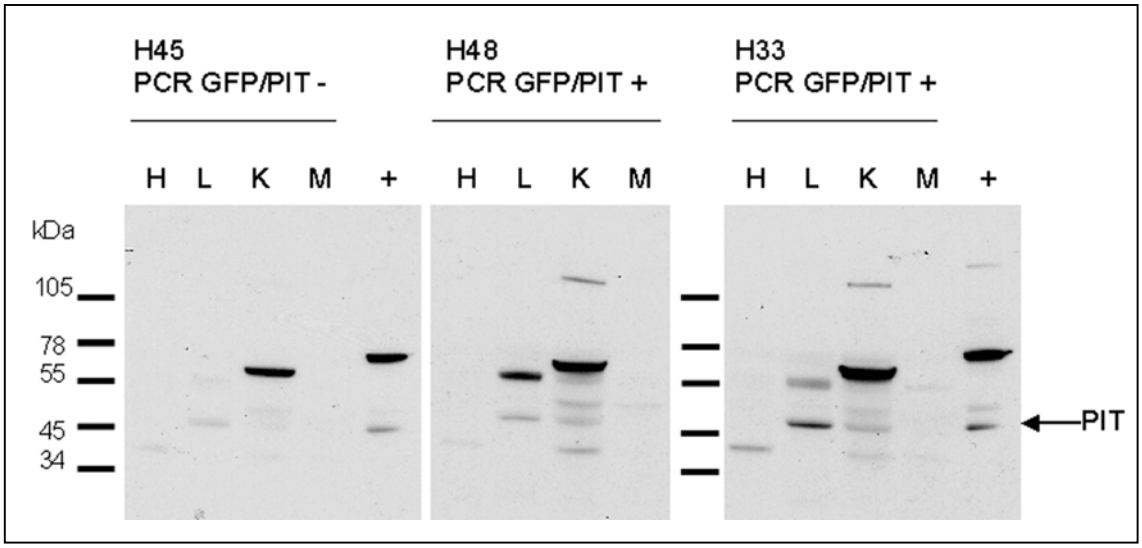

Figure 32.: Western blots of double transgenic EF1α-PIT and PPIR8-GFP mice with the VP16 antibody to detect PIT protein. PIT protein (47 kDa) is detect in the positive control from cells transfected with EF1α-PIT as the second strongest band. A similar MW band can be detected in lung and kidney tissue but is present in both PCR positive and negative animals.
H: heart, L: lung, K: kidney, M: muscle, +: positive cell lysate control.

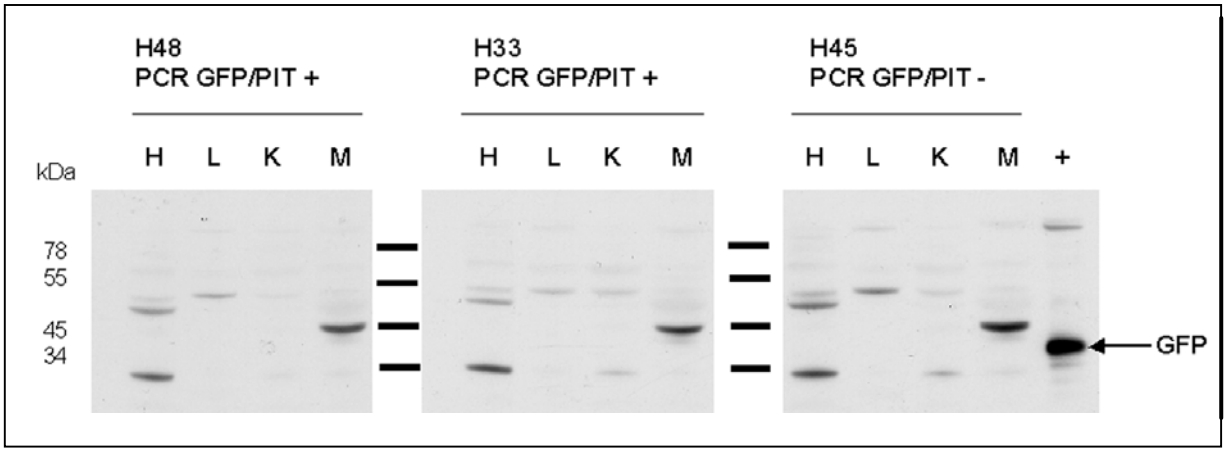

Figure 33.: Western blots of double transgenic EF1α-PIT and PPIR8-GFP mice with the GFP antibody. YFP protein (28 kDa) is detect in the positive control from cells transfected with EF1α-PIT and PPIR8-YFP. No similar MW band can be detected the PCR positive animal tissues (both GFP and YFP are of similar MW). H: heart, L: lung, K: kidney, M: muscle, +: positive cell lysate control.

Background fluorescence *in vivo* has been shown to be decreased using the longer wavelength needed to detect YFP compared to that used for GFP. However, GFP expression is easier to detect in the mice as a simple UV light is needed. Therefore, we also produced in parallel single PPIR8-GFP transgenic mice. These mice were crossed with the EF1α -PIT single transgenic line. But again we did not detect expression of GFP or PIT on Western blots of various organs from the double transgenic mice. The positive control in Fig. 32 shows a band at the right size for PIT (47 kDa). A similar band is present in lung and kidney from both PIT positive animals but also in the negative control animal. Furthermore we can distinguish various higher molecular weight and stronger bands, suggesting that the VP16 antibody is cross reacting with other proteins present. Western blotting with the GFP antibody (Fig. 33) presents a strong band at about 40 kDa in the positive cell lysate control, whereas the calculated molecular weight of GFP and YFP is around 28 kDa. We have demonstrated that the cells double transfected with EF1α-PIT and PPIR8-YFP express YFP. Therefore this slightly higher band detected in the positive control is most probably YFP. Both PCR positive animals do not show any GFP bands at this height or any other bands that are different from the PCR negative animal.

Following the failure to produce double transgenic mice expressing YFP or GFP with the PipOFF system, we decided to change both the promoter controlling PIT expression and the reporter gene. We chose the more ubiquitous and strong promoter, CMV/β-actin promoter to control PIT expression and we changed the reporter gene to LacZ. The CMV/β-actin-PIT and PPIR8-LacZ constructs were co-injected to produce double transgenic mice. 106 double CMV/β-actin-PIT and PPIR8-LacZ co-injected founders were generated. LacZ ear staining was first carried out, showing positive staining of certain founders. However repetition of the staining revealed a high variability. Furthermore, LacZ staining of cryostat sections from different organs of mice identified as positive by ear staining was negative. PCR for PIT and LacZ demonstrated that only two founders were LacZ positive and only one was transgenic for both LacZ and PIT. However LacZ staining of ear tissue from the double positive was negative. Furthermore the mouse died before giving offspring.

We also tried to generate single CMV/β-actin-PIT transgenic mice. Mice implanted with embryos gave very low numbers of offspring. Despite a generally impressive track record with other DNA constructs, we could only obtain 16 offspring of which none were PIT positive. As the generation of double EF1α-PIT and PPIR8-YFP transgenic mice unexpectedly also gave very few double

positive mice, we can conclude that the PIT construct in itself is probably not integrating into the genome and disturbs the integration of the other construct.

4 DISCUSSION

4.1 Analysis of P301L tau mouse brains

The P301L mutation of tau is one in a set of mutations implicated in FTDP-17 (Spillantini et al., 2000). This mutation reduces the ability of tau to interact with microtubules and promotes the assembly of tau into filaments *in vitro*. In our P301L tau transgenic mice, tau filaments start to accumulate at about six months of age preceded by distinct hyperphosphorylation of tau (Gotz et al., 2001a; Gotz et al., 2001b). Furthermore, the tau pathology causes specific behavioural deficits in the mice related to the amygdala, an area with prominent NFT formation (Pennanen et al., 2004).

Proteomics is becoming more and more widely used to study brain changes under physiological and pathological conditions such as in AD (Butterfield et al., 2003; Schonberger et al., 2001). Considering the complexity of brain tissue, we adapted a sequential extraction method to separate the brain proteins according to solubility before proteomic analysis (Molloy et al., 1998). This approach followed by functional analysis of the P301L tau mice suggests that tau accumulation, in the absence of massive NFT formation, induces a mitochondrial dysfunction. The down-regulation of nuclear encoded subunits of electron transport chain complexes I and V was accompanied by a reduced depolarisation of mitochondria from 12 month old P301L tau mice after treatment with the complex I inhibitor rotenone and the complex V inhibitor oligomycin. We could also demonstrate a direct decrease in complex I activity. At this age, the other mitochondrial respiratory chain complexes seemed to be able to compensate since the respiratory control ratio and mitochondrial membrane potential remained unchanged. However following the increase of tau pathology with ageing, this compensation is no longer sufficient and mitochondria from 24 month old P301L tau mice exhibited an impaired efficiency of coupling between the mitochondrial respiratory chain complexes, diminished capacity in electron transport and a significant reduction in ATP levels. In particular, the reduction in state 3 respiration reflects a reduced capacity of mitochondria to metabolise oxygen and the complex I substrate in the presence of a limited quantity of ADP. Thus, there is also a clear complex I deficiency in the mitochondrial respiration at 24 months of age.

Our results correlate with previous studies on AD, suggesting partial mitochondrial uncoupling (Sims et al., 1987), modifications of mitochondrial encoded complex I subunit mRNA (Aksenov

et al., 1999; Li et al., 2003) and reduction in protein levels of the 24 and 75 kDa subunits of complex I (Kim et al., 2001) as well as diminished ATP synthase (complex V) levels (Schagger and Ohm, 1995). As demonstrated in primates, complex I activity has been shown to be reduced with ageing which could potentially intensify complex I activity defects in the P301L tau mice (Bowling et al., 1993). Furthermore, we could show a clear-cut reduction in levels of complex V in human P301L FTDP-17 brains compared to control human brains. This important finding confirming the decrease in complex V identified twice in our proteomics analysis of the P301L tau mouse argues in favour of a potential mitochondrial dysfunction in human FTDP-17 patients. This result also emphasises the relevance of our P301L tau mouse as a model of the human tau pathology.

Our proteomic analysis revealed also modifications in levels of TPI, cytoplasmic malate dehydrogenase and inorganic pyrophosphatase implying a broader metabolic disorder possibly encompassing the glycolysis cycle. The glycolytic enzyme TPI can bind to microtubules (Orosz et al., 2000), and higher levels of nitrated TPI have been found in AD brains (Castegna et al., 2003). Consistent with an overall metabolic failure, several reports using positron emission tomography (PET) revealed reduced glucose metabolism in AD and frontotemporal dementia (FTD) brains (Diehl et al., 2004; Grimmer et al., 2004; Jagust et al., 1991; Mielke et al., 1996; Santens et al., 2001). Notably, high levels of phosphorylated tau have been linked to glucose hypometabolism in mild cognitively impaired patients (Fellgiebel et al., 2004).

Together, this evidence supports a role of tau pathology in mitochondrial and metabolic dysfunction. However, it remains unclear how tau accumulation mediates these changes. Overexpression of WT tau in cell culture caused impairment of plus-end-directed transport resulting in a reduction of mitochondria levels in the neurites (Ebneth et al., 1998). Although we can not exclude this occurring in the P301L tau mice, mitochondrial neuritic numbers counted at proximity or distally to the cell body, did not vary significantly compared to WT numbers. Furthermore, the total amount of mitochondria remained unchanged as measured in brain cells of transgenic compared to control mice. This suggests that either P301L tau induces a different pathological mechanism than overexpressed WT tau or that tau action on mitochondria transport in cell culture cannot be extrapolated over to the mouse model. Consistent with these findings, similar numbers of mitochondria were reported between NFT and non-NFT bearing cells in AD (Sumpter et al., 1986). Alternatively, tau accumulation could have direct repercussions on the mitochondria as the accumulation of increasingly insoluble ATP synthase α-chain together with

NFT has been shown in AD brains whereas detergent soluble levels were reduced (Sergeant et al., 2003). Overall it is important to note that the mitochondrial pathology in the P301L tau mice observed in this study is unlikely to be a direct consequence of tau hyperphosphorylation. Indeed the transgene levels of expression in these mice are relatively low (Gotz et al., 2001a) and depletion of ATP solely due to tau hyperphosphorylation would be improbable.

We furthermore demonstrate that accumulation of P301L tau causes significant modifications in the oxidative state of the brain. ROS measurements revealed increased levels of cytosolic H_2O_2 and superoxide anion radicals in two year old P301L tau mice. These increased ROS levels may be a direct consequence of reduced complex I activity in P301L tau mice, as inhibition of complex I can lead to increased superoxide formation (Turrens and Boveris, 1980). The increased activity of Cu/Zn-SOD measured in P301L tau mice should ameliorate the accumulation of superoxide but also gives rise to H_2O_2, which is then insufficiently processed by GPx leading to accumulation of peroxides. Accordingly, the relative increase in H_2O_2 in P301L tau mice was much more pronounced than the increase in superoxide radicals. Somewhat unexpectedly, along with increased tau pathology we observed decreased levels of the lipid peroxidation product MDA as a marker for ROS damage to cellular membranes, in old homozygous P301L tau mice despite increased levels of ROS. One potential explanation for this discrepancy could be that the cells affected by lipid peroxidation are removed by apoptosis, although we could not detect major differences in levels of apoptotic cells detected by TUNEL staining (data not shown). As several steps lead from ROS accumulation to lipid peroxidation damage, another possibility would be that the up-regulation of antioxidant activities of Cu/Zn-SOD and glutathione reductase (GR) in P301L tau mice may intercept ROS before they can critically damage membranes. As previously reported, rising Cu/Zn-SOD and GR activities in aged mouse brains can protect against lipid peroxidation (Schuessel et al., 2005). Furthermore, SOD can prevent lipid peroxidation both *in vitro* and *in vivo* (Bonnes-Taourel et al., 1993; Gutteridge, 1984; Gutteridge et al., 1983; Liu et al., 2003; Tien et al., 1981). Similarly, increased GR activity in P301L tau mice may protect against accumulation of MDA by increasing levels of the antioxidant reduced glutathione. In several experimental models, increased levels of reduced glutathione were associated with lower levels of lipid peroxidation products and *vice versa* (Comporti, 1987; Younes and Siegers, 1980). Upon *in vitro* stimulation, however, higher levels of MDA were formed in homozygous P301L tau brain homogenates. Obviously, the increased activities of Cu/Zn-SOD and GR were not sufficiently protective under these conditions. This

may be explained by a relative lack in GPx activity, as the accumulation of H_2O_2 observed in brains from P301L tau mice combined with the exogenously added ferric iron can lead to increased formation of hydroxyl radicals via Haber-Weiss and Fenton reactions. Reports on lipid peroxidation in brains from patients with tauopathies are inconsistent. Although increased levels of the lipid peroxidation product HNE were found in patients with progressive supranuclear palsy (Odetti et al., 2000) and tau was colocalised with MDA immunoreactivity in AD patients (Dei et al., 2002), another study reported increased lipid peroxidation products specifically in AD patients, but not in patients with FTD (Yao et al., 2003). Therefore, tau pathology may not be associated inevitably with lipid peroxidation processes in human brain tissue, consistent with our observations in P301L tau mice. Most studies have reported an up-regulation of antioxidant enzyme activities in AD (Lovell et al., 1995). These changes were most pronounced in brain regions that are severely affected by AD pathology (Karelson et al., 2001; Lovell et al., 1995; Schuessel et al., 2004).

Our proteomic analysis also suggests changes in cellular antioxidant mechanisms as shown by variations in spots representing the antioxidant enzymes perioredoxin 3, peroxiredoxin 6, GST P2 and Mu1, and PHGPx. Peroxiredoxin reduces peroxides including H_2O_2, GST catalyses the conjugation of reduced glutathione to a wide number of molecules and PHGPx directly reduces peroxidized phospholipids in membranes (Ursini et al., 1985). Although all these protein spots were down-regulated in the P301L tau mouse, this does not necessarily reflect enzyme activities. Besides, under oxidative conditions, these antioxidant enzymes are prone to oxidative modifications represented by a set of distinct spots on 2-D gels as suggested for peroxiredoxin which undergoes overoxidation (Chevallet et al., 2003; Wagner et al., 2002). The thioredoxin/thioredoxin reductase system mediates the regeneration of oxidised peroxiredoxins and to some extent glutathione peroxidases (Nordberg and Arner, 2001). However AD brains show decreased thioredoxin levels and increased thioredoxin reductase levels (Lovell et al., 2000). Therefore the dysfunction of this system could cause an accumulation of oxidative modification in peroxiredoxins. Interestingly, AD brains also show decreased GST activity (Lovell et al., 1998) and GST omega-1 mRNA levels in AD (Li et al., 2003), and single nucleotide polymorphisms (SNPs) in GST omega-1 are associated with age-at-onset in AD (Li et al., 2003).

Hence both our functional and proteomic data indicate a complex regulation and potential malfunction of the cellular antioxidant defence mechanisms in response to increased ROS levels

in this mouse model. As mitochondrial dysfunction appears prior to oxidative stress, this suggests that it is probably the initiating factor. However we can speculate that both mitochondrial dysfunction and oxidative stress act in synergy creating a vicious cycle. Indeed increases in ROS and antioxidant enzyme dysfunction could affect the integrity of the mitochondria and in particular, the electron transport chain (Keil et al., 2004). Furthermore glutathionylation of complex I in oxidative conditions leads to increased superoxide production (Taylor et al., 2003). Another possible consequence of higher oxidative stress levels could be an acceleration of tau pathology (Hartzler et al., 2002; Perez et al., 2000). Moreover, tau can be readily oxidised by H_2O_2 to form disulfide linked species which manifest reduced propensity to promote microtubule assembly (Landino et al., 2004b). Oxidised tau then becomes a substrate of the thioredoxin reductase and glutathione/glutaredoxin reductase systems (Landino et al., 2004a; Landino et al., 2004b). Thereby we can speculate that the accumulation of oxidised P301L tau might overload these antioxidant regenerating systems causing further oxidative stress.

Results from our proteomic study further suggest a potential synaptic dysfunction as we found an up-regulation of a series of synaptic related proteins. The identified DRP-2 is known to promote axonal growth by interaction with the tubulin heterodimer and has also been shown to induce neurite formation (Fukata et al., 2002; Inagaki et al., 2001). Synapsin I is thought to regulate the reserve pool of synaptic vesicles (Gitler et al., 2004). The septin member, CDCrel-1 is found mainly in inhibitory presynaptic terminals and inhibits exocytosis (Beites et al., 1999; Kinoshita et al., 2000). Interestingly, both DRP-2 and septin associate with NFT in AD (Kinoshita et al., 1998; Yoshida et al., 1998). Therefore in response to tau pathology, the transgenic mouse neurones may be attempting a compensatory mechanism by increasing synaptic vesicle control proteins and potentially aberrant synaptic sprouting. Indeed, although advanced stages of AD are associated with synaptic loss, an initial increase in synaptic protein levels in AD brains was observed which was correlated with the appearance of the tau pathology but not with Aβ plaques (Mukaetova-Ladinska et al., 2000). On the contrary, a decrease of synaptic proteins occurred only after the appearance of the full spectrum of tau and Aβ pathology. Although it is uncertain exactly how tau mechanistically affects synapses, we can postulate that either the mutant tau acts by modifying microtubule stability and axonal transport or by inhibiting energy production through complex I in the synapses. Indeed a reduction in activity of complex I by only 25% has been shown to impair energy metabolism in synaptic mitochondria (Davey et al., 1998), whereas at least 72% is needed in non-synaptic mitochondria (Davey and Clark, 1996). In this

study, our mitochondrial isolation does not include synaptic mitochondria. It would be interesting to measure complex I activity and mitochondrial respiration in a pure synaptosomal mitochondrial preparation.

We were not able to show by either Western blotting or immunostaining a significant up-regulation of DRP, CDCrel-1, synapsin or synaptophysin due to high levels of variability between individual mice. Observation of the number of synapses using Golgi staining might allow a quantification between P301L tau and WT mice. It would also be worthwhile to carry out electrophysiology as this should show whether the P301L tau mice have dysfunctional synapses due to aberrant synapse sprouting.

In addition to the three major categories, mitochondrial proteins, antioxidant enzymes and synaptic proteins, we could identify by proteomics, several other proteins modified by the presence of the P301L tau and potentially linked to AD pathology. The up-regulated MSTI1 mediates assembly of HSP70/HSP90 (Scheufler et al., 2000). A proteomic study has shown modifications in various chaperone levels in AD brain (Yoo et al., 2001b). In addition, levels of HSP αB-crystallin, HSP27 and HSP60 were found to be increased in tauopathies with glial pathology (Dabir et al., 2004). Decreased in the P301L tau mouse brain proteome pattern is GRB2, an adapter protein which is involved in the activation of the MAPK signalling pathway, through interaction with son-of-sevenless (SOS). Interestingly, AD brains show higher amounts of GRB2 than control (McShea et al., 1999; Russo et al., 2002) and a differential cellular distribution of GRB2 was observed as being more confined to the cell body (McShea et al., 1999). Levels of the microtubule destabilising protein stathmin have been found to be negatively correlated with NFT numbers in AD neocortex (Jin et al., 1996) and were also down-regulated in the P301L tau mice. Another interesting down-regulated candidate is the probable D-tyrosyl-tRNA deacylase, which removes D-tyrosine and other D-amino acids from charged tRNAs (Yang et al., 2003). This enzyme carries out an essential role in protein synthesis proof-reading by protecting against the incorporation of D-amino acids into proteins and could be relevant to AD. Indeed studies have shown increased D-aspartate in AD grey matter compared to control, higher levels of D-aspartate in PHF-tau, and the presence of D-aspartate in Aβ isolated from AD brains (Fisher et al., 1992; Kenessey et al., 1995; Roher et al., 1993). Moreover, we could identify two other proteins down-regulated and potentially related to synapse function. The β-alanine oxoglutarate aminotransferase homologue (GABA transaminase) is involved in the metabolism of GABA (Jeon et al., 2000) and γ-SNAP (γ-soluble N-ethylmaleimide-sensitive factor (NSF)

attachment protein) is implicated in vesicle trafficking through its interaction with NSF and Gaf-1/Rip11 (Tani et al., 2003). However, a proteomic study with AD brain samples did not reveal a significant modification in γ-SNAP levels (Yoo et al., 2001a).

Finally, our data from the proteomic and functional study of the P301L tau transgenic mouse should help to better distinguish between the respective pathological actions of Aβ and tau protein. Numerous studies indicate that Aβ also causes oxidative stress and mitochondrial malfunction (Anandatheerthavarada et al., 2003; Blanchard et al., 2003; Keil et al., 2004; Keller et al., 1997). In particular, Aβ has been shown to generate free radicals *in vitro* (Hensley et al., 1994) and reduces mitochondrial respiration through inhibition of cytochrome c oxidase activity (Casley et al., 2002; Keil et al., 2004). We show here that Aβ causes increased reduction of mitochondrial membrane potential in P301L tau mouse cerebrum compared to wild-type. Importantly, this is not observed in the cerebellum of P301L tau mice, a brain area with very low levels of transgenic tau. This could partially explain that injection of fibrillar Aβ peptide into the hippocampus of P301L tau mice accelerated NFT formation in the amygdala, in line with the amyloid cascade hypothesis (Gotz et al., 2001b). Therefore both tau and Aβ accumulation probably act in synergy on oxidative stress and mitochondrial dysfunction.

In conclusion, our study helps understand the pathological consequences of tau alone, suggesting that not only Aβ but also tau accumulation acts on the metabolism of the brain and the oxidative conditions in AD. This implies that it will be important to address the treatment and/or removal of both Aβ and tau pathology to efficiently treat AD patients.

4.2 Proteomic analysis of the action of ß-amyloid on P301L tau overexpressing SH-SY5Y cells and P301L tau transgenic mouse amygdalae

Aβ causes the specific phosphorylation of certain epitopes on the tau protein, in both amygdalae of P301L tau transgenic mice injected intracranially with Aβ and cells overexpressing P301L tau treated with Aβ (Ferrari et al., 2003; Gotz et al., 2001b). In the cellular system, Ferrari et al. (Ferrari et al., 2003) could also demonstrate that Aβ induces tau insolubility, which was estimated by Western blotting after sequential extraction of the samples. Finally in both systems, our group could show that Aβ induces tau filament formation.

In another cellular system, DeTure et al. showed increases in tau insolubility and the formation of tau filaments in H4 neuroglioma cell overexpressing the mutant tau V337M

compared to expressing the R406W mutation or wild-type tau (DeTure et al., 2002). In this system and in the tau mutant transgenic mice, tau filament formation (15-25 nm in diameter) is induced in the absence of Aβ and is probably due to a combination of high levels of tau and the potentiation of fibrillogenesis caused by the presence of the mutation. However no other group has been able to demonstrate until now, an induction of tau insolubility caused by Aβ in cell culture. This may be due to difficulties in obtaining the right amount of tau expression in cell culture as especially high levels of tau protein causes on its own, an increase in tau insolubility as has been observed by other members of our group. On the other hand, Aβ induced tau filament formation by intracranial Aβ injection in the mouse model has been reproduced by Walzer et al. (Walzer et al., 2003) also using a transgenic mouse expressing P301L tau. This study showed that the total phosphorylated sarcosyl insoluble tau protein levels were increased by Aβ injection. In both the cell culture and mouse model, we did not observe significant high levels of cell death induced by Aβ. Therefore the analysis of both systems should bring insight into the consequences of exposure to Aβ without strong unspecific effects due to cell death.

Aβ has been shown to cause a wide array of specific effects in the cell (see 1.2.2.). Whereas we should observe direct effects of Aβ in the cell culture system, it still remains unclear whether the injection of Aβ in the P301L tau mouse hippocampi, mediates a direct or indirect effect to the amygdala as no immunoreactivity of Aβ was detected in the amygdala. It is however possible that small non-detectable quantities of Aβ are either transported by diffusion or by the hippocampal projections into the amygdala.

In the cellular system, we show that Aβ causes relatively few significant differences in the cytoplasmic proteins although we could detect two spots only in the Aβ treated fraction. This is however two times more differentially regulated spots than in the proteomic study of the cytoplasmic fraction from untreated P301L tau mice, although we used five pairs of replicates instead of six pairs as in the mouse model. On the contrary, the pellet showed a large number of differentially regulated spots. This could be due to the presence of Aβ which is observed as a vertical streak (see Fig. 22, D). Indeed although we centrifuged the sample, it is possible that some Aβ solubilises in the urea, CHAPS solution. Relatively large quantities of Aβ compared to other proteins, could be modifying the isoelectrical focusing in the neighbouring pH range. Indeed most significant up and down-regulated proteins are located in the pH region around the Aβ vertical streak. The identity of the proteins should help us decide whether these are unspecific

differences or not. If so, it would be probably best to only consider protein spots away from this pH range.

Comparison of amygdala samples from Aβ or reverse Aβ injected P301L tau mice, show relatively few statistical differentially regulated spots compared to the cellular system, although we used a small pH range (pH 5-8) to focus on lower abundant protein changes. This could be due to the fact that differences are hidden by the relatively large amount of proteins concentrated in this sample as we did not perform a fractionation of the sample. This further underlines the importance of sample fractionation before proteomic analysis. However in this study, we were unable to optimise a fractionation protocol following protein solubility to obtain distinct 2-D patterns for each fraction. This is probably due to the low amount of material available and differences in the ratio of material and solution volumes.

The relatively few differences in the amygdala compared to the cellular system, suggest also that the cells in the amygdala are probably not in direct contact with the Aβ injected or in contact with only very small amounts. This would argue in favour of the action of Aβ through neuronal projections from the hippocampal site of injection to the amygdala which could be possibly activity or stress dependent. It would be worthwhile tracing the distribution of Aβ after injection by radioactive labelling of Aβ.

Outlook: We hope that the identification of Aβ mediated changes in both the cellular and animal system will highlight specific pathways as in the proteomics study of the P301L tau mice, and that we will be able to further investigate the action of Aβ on these pathways by functional tests.

4.3 Study of tau insolubility after proteasome inhibition in P301L tau overexpressing SH-SY5Y cells treated with ß-amyloid

A wide variety of studies have examined the relationship between Aβ and the proteasome. Aβ has been shown to be degraded by the proteasome (Lopez Salon et al., 2003) but also to inhibit proteasome activity (Gregori et al., 1995; Song et al., 2003). Furthermore the proteasome activity was found to be impaired in AD patient brains (Keller et al., 2000). Aβ causes the up-regulation of mRNA of several components of the ubiquitin proteasome system in cortical neurones in culture (Song et al., 2003). In particular, they found an induction of E2-25K/Hip-2 with Aβ which they correlated with the inhibition of the proteasome activity. Other studies have

demonstrated that *in vitro*, Aβ can directly bind to the proteasome and inhibit its chymotrypsin-like activity. On the other hand, tau protein has been shown to be degraded by the proteasome (David et al., 2002) and tau inclusions in oligodendroglial cells are stabilised through the inhibition of the proteasome (Goldbaum et al., 2003).

Considering the precedent evidence, we speculated that the general inhibition of the proteasome by MG132 in P301L tau overexpressing neuroblastoma cells and treatment with Aβ would increase levels of insoluble tau protein. In addition we extrapolated that proteasome inhibition without Aβ should also cause an increase in insoluble tau. The 20S proteasome possesses three peptidase activities, cleaving substrates after large hydrophobic, basic or acidic residues, designated as chymotrypsin-like, trypsin-like, and peptidylglutamyl-peptide hydrolysing (PGPH) activities, respectively (Orlowski, 1990). We also used in this study, two other proteasome inhibitors, lactacystin and epoxomicin. Both inhibitors affect all three activities of the proteasome but inhibit most potently the chymotrypsin-like activity, although epoxomicin acts with greater specificity than lactacystin (Kim et al., 1999) (Vigouroux et al., 2003) (Fenteany et al., 1995) (Meng et al., 1999). Aβ has been demonstrated to selectively inhibit the chymotrypsin-like activity of the proteasome, although not through a direct binding to the catalytic site (Gregori et al., 1995; Gregori et al., 1997). This study was carried out *in vitro* therefore it is unclear whether exposing cells to extracellular Aβ would result in the same specificity of proteasome activity inhibition, supposing that the cells can internalise small quantities of Aβ. However we postulated that inhibiting the same proteasome peptidase activity as Aβ, would increase the potential effects of Aβ on the cellular system. We used low concentrations of both epoxomicin and lactacystin to avoid inhibiting the other two peptidases activities. As the degradation of tau protein is unaffected by inhibition of the chymotrypsin-like activity (Cardozo and Michaud, 2002), we speculated that Aβ might cause an increase in tau insolubility through the generation of specific toxic products from the impaired proteasome degradation process. Furthermore we hypothesised that inhibiting specifically the chymotrypsin-like activity without Aβ, may reproduce the effects of Aβ. The whole experiment was carried out on differentiated neuroblastoma cells as all three proteasome inhibitors inhibit the cell cycle and cause apoptosis, and we used very low concentrations of all inhibitors compared to other studies. Unfortunately we observe a significant variability in levels of insoluble tau detected after sequential extraction. This variability allowed us only to distinguish an “all or nothing” effect on tau insolubility as seen with Aβ but not to evaluate lesser effects due to the different proteasome inhibitors used.

However we can conclude that all three inhibitors do not have major effects on Aβ mediated tau insolubility.

4.4 Study of tau phosphorylation in P301L tau mouse brains

Our group has observed a specific phosphorylation state of soluble tau in P301L tau brains (Gotz et al., 2001a). The purpose of this study was to identify all the phosphorylation epitopes in the tau protein in our mouse model. We aimed to identify these phosphorylation sites without specific antibodies, in order to locate potential new tau phosphorylations. As tau phosphorylation has a role in determining the binding of tau to microtubules and potentially the propensity of tau to form fibrils, our objective was to investigate by MS, tau phosphorylation specifically in soluble AD type tau and not NFT tau (Alonso et al., 2001). Köpke et al. (Kopke et al., 1993) have published a method to specifically separate AD phosphorylated tau (AD-P tau) from soluble normal cytosolic tau and NFT tau. This method uses a series of centrifugation steps and solubilises the AD-P tau in 8 M urea. Finally AD-P tau is separated from non-hyperphosphorylated AD tau by phosphocellulose chromatography. We carried out the whole extraction with brains from old P301L tau mice, but we could not detect the presence of tau by Western blotting in any of the fractions eluted out of the phosphocellulose column. This is probably caused by too low quantities of AD type tau in the mouse brains as compared to the AD patient brains used in the original extraction. Thereafter we stopped our extraction before the chromatography step. First we looked at the 200,000 x g pellet extracted in urea on 2-D gels. The Western blot of this 2-D show numerous tau species suggesting several sites of phosphorylation. Unfortunately the pattern on 2-D gels after Silver staining demonstrated a wide variety of other proteins are present in this fraction and we could only identify one spot as tau. Centrifugation of the urea soluble fraction to remove more contaminants did not significantly improve the background.

We can conclude that this method is not adapted to extracting AD-P tau from our mouse model in the present form and we suggest that it would be worthwhile carrying out an immunoprecipitation of tau from the urea soluble fraction to enrich AD-tau in order to detect these on 2-D gels without Western blotting.

4.5 PipOFF system

The PipOFF system established by Fussenegger et al. (Fussenegger et al., 2000) was tested in a variety of mammalian cells (CHO-K1, BHK-21, HeLa). In order to assess whether our constructs were adapted for expression in the mouse system, we demonstrated with success the expression and inhibition of YFP expression using the PipOFF system in mouse fibroblasts. However transactivation of YFP expression or another reporter gene such as GFP and LacZ, was not obtained in transgenic mice having integrated both the PIT construct and the construct containing PPIR8 controlling the reporter gene. We modified out initial constructs by changing the promoter controlling PIT expression to the stronger promoter CMV/β-actin and also modifying the reporter gene, but we still did not observe the expression of the reporter gene through transactivation with PIT. When generating double transgenic mice through co-injection of both PIT and reporter constructs and single transgenic mice with only the CMV/β-actin-PIT construct, we observed very few positive founders and none after single injection of CMV/β-actin-PIT. On the contrary, generation rates of PPIR8-YFP or PPIR8-GFP founders were normal. Therefore we can conclude that there is most probably an insertion problem of the PIT construct into the mouse genome. We could not detect the expression of the reporter in any of the double transgenics that we produced. However PIT was possibly present in the only double positive EF1α -PIT and PPIR8-YFP transgenic mouse that transmitted the constructs to her offspring. Therefore it is difficult to conclude whether the PipOFF system in itself does not work in the mouse model or whether the lack of reporter expression is due to the absence of PIT transcription. It would be interesting to carry out an RT-PCR for PIT in the double positive transgenic lines to establish if the PIT gene is being transcribed into mRNA but not translated into protein.

In conclusion, our study shows that the PipOFF system in its present form is not adapted to function in the mouse model. Prof. Fussenegger's group has since produced several other transgene regulatory expression systems such as macrolide-based transgene control and gas-inducible transgene expression systems (Weber et al., 2002) (Weber et al., 2004). These systems have been shown to work in the mouse when implanting CHO cells containing the system, intraperitoneally. It would be interesting to see whether transgenic mice can be generated with these new systems and whether these systems would be functional.

REFERENCES

Ackmann, M., Wiech, H., and Mandelkow, E. (2000). Nonsaturable binding indicates clustering of tau on the microtubule surface in a paired helical filament-like conformation. J Biol Chem *275*, 30335-30343.

Aksenov, M. Y., Tucker, H. M., Nair, P., Aksenova, M. V., Butterfield, D. A., Estus, S., and Markesbery, W. R. (1999). The expression of several mitochondrial and nuclear genes encoding the subunits of electron transport chain enzyme complexes, cytochrome c oxidase, and NADH dehydrogenase, in different brain regions in Alzheimer's disease. Neurochem Res *24*, 767-774.

Allen, B., Ingram, E., Takao, M., Smith, M. J., Jakes, R., Virdee, K., Yoshida, H., Holzer, M., Craxton, M., Emson, P. C.*, et al.* (2002). Abundant tau filaments and nonapoptotic neurodegeneration in transgenic mice expressing human P301S tau protein. J Neurosci *22*, 9340-9351.

Alonso, A., Zaidi, T., Novak, M., Grundke-Iqbal, I., and Iqbal, K. (2001). Hyperphosphorylation induces self-assembly of tau into tangles of paired helical filaments/straight filaments. Proc Natl Acad Sci U S A *98*, 6923-6928.

Alonso, A. C., Zaidi, T., Grundke-Iqbal, I., and Iqbal, K. (1994). Role of abnormally phosphorylated tau in the breakdown of microtubules in Alzheimer disease. Proc Natl Acad Sci U S A *91*, 5562-5566.

Anandatheerthavarada, H. K., Biswas, G., Robin, M. A., and Avadhani, N. G. (2003). Mitochondrial targeting and a novel transmembrane arrest of Alzheimer's amyloid precursor protein impairs mitochondrial function in neuronal cells. J Cell Biol *161*, 41-54.

Andreadis, A. (2005). Tau gene alternative splicing: expression patterns, regulation and modulation of function in normal brain and neurodegenerative diseases. Biochim Biophys Acta *1739*, 91-103.

Andreadis, A., Brown, W. M., and Kosik, K. S. (1992). Structure and novel exons of the human tau gene. Biochemistry *31*, 10626-10633.

Arriagada, P. V., Growdon, J. H., Hedley-Whyte, E. T., and Hyman, B. T. (1992). Neurofibrillary tangles but not senile plaques parallel duration and severity of Alzheimer's disease. Neurology *42*, 631-639.

Banks, J. F., Jr., and Whitehouse, C. M. (1996). Electrospray ionization mass spectrometry. Methods Enzymol *270*, 486-519.

Barghorn, S., Zheng-Fischhofer, Q., Ackmann, M., Biernat, J., von Bergen, M., Mandelkow, E. M., and Mandelkow, E. (2000). Structure, microtubule interactions, and paired helical filament aggregation by tau mutants of frontotemporal dementias. Biochemistry *39*, 11714-11721.

Behl, C., Davis, J. B., Lesley, R., and Schubert, D. (1994). Hydrogen peroxide mediates amyloid beta protein toxicity. Cell *77*, 817-827.

Beites, C. L., Xie, H., Bowser, R., and Trimble, W. S. (1999). The septin CDCrel-1 binds syntaxin and inhibits exocytosis. Nat Neurosci *2*, 434-439.

Berggren, K. N., Schulenberg, B., Lopez, M. F., Steinberg, T. H., Bogdanova, A., Smejkal, G., Wang, A., and Patton, W. F. (2002). An improved formulation of SYPRO Ruby protein gel stain: comparison with the original formulation and with a ruthenium II tris (bathophenanthroline disulfonate) formulation. Proteomics *2*, 486-498.

Bierer, L. M., Hof, P. R., Purohit, D. P., Carlin, L., Schmeidler, J., Davis, K. L., and Perl, D. P. (1995). Neocortical neurofibrillary tangles correlate with dementia severity in Alzheimer's disease. Arch Neurol *52*, 81-88.

Blanchard, V., Moussaoui, S., Czech, C., Touchet, N., Bonici, B., Planche, M., Canton, T., Jedidi, I., Gohin, M., Wirths, O*., et al.* (2003). Time sequence of maturation of dystrophic neurites associated with Abeta deposits in APP/PS1 transgenic mice. Exp Neurol *184*, 247-263.
Bonnes-Taourel, D., Guerin, M. C., Torreilles, J., Ceballos-Picot, I., and de Paulet, A. C. (1993). 4-Hydroxynonenal content lower in brains of 25 month old transgenic mice carrying the human CuZn superoxide dismutase gene than in brains of their non-transgenic littermates. J Lipid Mediat *8*, 111-120.
Bowling, A. C., Mutisya, E. M., Walker, L. C., Price, D. L., Cork, L. C., and Beal, M. F. (1993). Age-dependent impairment of mitochondrial function in primate brain. J Neurochem *60*, 1964-1967.
Braak, H., and Braak, E. (1991). Neuropathological stageing of Alzheimer-related changes. Acta Neuropathol (Berl) *82*, 239-259.
Braak, H., and Braak, E. (1995). Staging of Alzheimer's disease-related neurofibrillary changes. Neurobiol Aging *16*, 271-278; discussion 278-284.
Budd, S. L., Castilho, R. F., and Nicholls, D. G. (1997). Mitochondrial membrane potential and hydroethidine-monitored superoxide generation in cultured cerebellar granule cells. FEBS Lett *415*, 21-24.
Bussiere, T., Hof, P. R., Mailliot, C., Brown, C. D., Caillet-Boudin, M. L., Perl, D. P., Buee, L., and Delacourte, A. (1999). Phosphorylated serine422 on tau proteins is a pathological epitope found in several diseases with neurofibrillary degeneration. Acta Neuropathol (Berl) *97*, 221-230.
Butterfield, D. A., Boyd-Kimball, D., and Castegna, A. (2003). Proteomics in Alzheimer's disease: insights into potential mechanisms of neurodegeneration. J Neurochem *86*, 1313-1327.
Cardozo, C., and Michaud, C. (2002). Proteasome-mediated degradation of tau proteins occurs independently of the chymotrypsin-like activity by a nonprocessive pathway. Arch Biochem Biophys *408*, 103-110.
Casley, C. S., Canevari, L., Land, J. M., Clark, J. B., and Sharpe, M. A. (2002). Beta-amyloid inhibits integrated mitochondrial respiration and key enzyme activities. J Neurochem *80*, 91-100.
Castegna, A., Aksenov, M., Thongboonkerd, V., Klein, J. B., Pierce, W. M., Booze, R., Markesbery, W. R., and Butterfield, D. A. (2002). Proteomic identification of oxidatively modified proteins in Alzheimer's disease brain. Part II: dihydropyrimidinase-related protein 2, alpha-enolase and heat shock cognate 71. J Neurochem *82*, 1524-1532.
Castegna, A., Thongboonkerd, V., Klein, J. B., Lynn, B., Markesbery, W. R., and Butterfield, D. A. (2003). Proteomic identification of nitrated proteins in Alzheimer's disease brain. J Neurochem *85*, 1394-1401.
Check, E. (2002). Nerve inflammation halts trial for Alzheimer's drug. Nature *415*, 462.
Chevallet, M., Wagner, E., Luche, S., van Dorsselaer, A., Leize-Wagner, E., and Rabilloud, T. (2003). Regeneration of peroxiredoxins during recovery after oxidative stress: only some overoxidized peroxiredoxins can be reduced during recovery after oxidative stress. J Biol Chem *278*, 37146-37153.
Collins, T. J., Berridge, M. J., Lipp, P., and Bootman, M. D. (2002). Mitochondria are morphologically and functionally heterogeneous within cells. Embo J *21*, 1616-1627.
Comporti, M. (1987). Glutathione depleting agents and lipid peroxidation. Chem Phys Lipids *45*, 143-169.
Crouch, S. P., Kozlowski, R., Slater, K. J., and Fletcher, J. (1993). The use of ATP bioluminescence as a measure of cell proliferation and cytotoxicity. J Immunol Methods *160*, 81-88.

Crystal, H., Dickson, D., Fuld, P., Masur, D., Scott, R., Mehler, M., Masdeu, J., Kawas, C., Aronson, M., and Wolfson, L. (1988). Clinico-pathologic studies in dementia: nondemented subjects with pathologically confirmed Alzheimer's disease. Neurology *38*, 1682-1687.
Dabir, D. V., Trojanowski, J. Q., Richter-Landsberg, C., Lee, V. M., and Forman, M. S. (2004). Expression of the small heat-shock protein alphaB-crystallin in tauopathies with glial pathology. Am J Pathol *164*, 155-166.
Davey, G. P., and Clark, J. B. (1996). Threshold effects and control of oxidative phosphorylation in nonsynaptic rat brain mitochondria. J Neurochem *66*, 1617-1624.
Davey, G. P., Peuchen, S., and Clark, J. B. (1998). Energy thresholds in brain mitochondria. Potential involvement in neurodegeneration. J Biol Chem *273*, 12753-12757.
David, D. C., Hauptmann, S., Scherping, I., Schuessel, K., Keil, U., Rizzu, P., Ravid, R., Drose, S., Brandt, U., Muller, W. E.*, et al.* (2005). Proteomic and functional analysis reveal a mitochondrial dysfunction in P301L tau transgenic mice. J Biol Chem.
David, D. C., Layfield, R., Serpell, L., Narain, Y., Goedert, M., and Spillantini, M. G. (2002). Proteasomal degradation of tau protein. J Neurochem *83*, 176-185.
Dei, R., Takeda, A., Niwa, H., Li, M., Nakagomi, Y., Watanabe, M., Inagaki, T., Washimi, Y., Yasuda, Y., Horie, K.*, et al.* (2002). Lipid peroxidation and advanced glycation end products in the brain in normal aging and in Alzheimer's disease. Acta Neuropathol (Berl) *104*, 113-122.
Delacourte, A., David, J. P., Sergeant, N., Buee, L., Wattez, A., Vermersch, P., Ghozali, F., Fallet-Bianco, C., Pasquier, F., Lebert, F.*, et al.* (1999). The biochemical pathway of neurofibrillary degeneration in aging and Alzheimer's disease [see comments]. Neurology *52*, 1158-1165.
Delacourte, A., Sergeant, N., Champain, D., Wattez, A., Maurage, C. A., Lebert, F., Pasquier, F., and David, J. P. (2002). Nonoverlapping but synergetic tau and APP pathologies in sporadic Alzheimer's disease. Neurology *59*, 398-407.
DeTure, M., Ko, L. W., Easson, C., and Yen, S. H. (2002). Tau assembly in inducible transfectants expressing wild-type or FTDP-17 tau. Am J Pathol *161*, 1711-1722.
Diehl, J., Grimmer, T., Drzezga, A., Riemenschneider, M., Forstl, H., and Kurz, A. (2004). Cerebral metabolic patterns at early stages of frontotemporal dementia and semantic dementia. A PET study. Neurobiol Aging *25*, 1051-1056.
Djafarzadeh, R., Kerscher, S., Zwicker, K., Radermacher, M., Lindahl, M., Schagger, H., and Brandt, U. (2000). Biophysical and structural characterization of proton-translocating NADH-dehydrogenase (complex I) from the strictly aerobic yeast Yarrowia lipolytica. Biochim Biophys Acta *1459*, 230-238.
Ebneth, A., Godemann, R., Stamer, K., Illenberger, S., Trinczek, B., and Mandelkow, E. (1998). Overexpression of tau protein inhibits kinesin-dependent trafficking of vesicles, mitochondria, and endoplasmic reticulum: implications for Alzheimer's disease. J Cell Biol *143*, 777-794.
Edbauer, D., Winkler, E., Regula, J. T., Pesold, B., Steiner, H., and Haass, C. (2003). Reconstitution of gamma-secretase activity. Nat Cell Biol *5*, 486-488.
Encinas, M., Iglesias, M., Liu, Y., Wang, H., Muhaisen, A., Cena, V., Gallego, C., and Comella, J. X. (2000). Sequential treatment of SH-SY5Y cells with retinoic acid and brain-derived neurotrophic factor gives rise to fully differentiated, neurotrophic factor-dependent, human neuron-like cells. J Neurochem *75*, 991-1003.
Esterbauer, H., and Cheeseman, K. H. (1990). Determination of aldehydic lipid peroxidation products: malonaldehyde and 4-hydroxynonenal. Methods Enzymol *186*, 407-421.
Feinstein, S. C., and Wilson, L. (2005). Inability of tau to properly regulate neuronal microtubule dynamics: a loss-of-function mechanism by which tau might mediate neuronal cell death. Biochim Biophys Acta *1739*, 268-279.

Fellgiebel, A., Siessmeier, T., Scheurich, A., Winterer, G., Bartenstein, P., Schmidt, L. G., and Muller, M. J. (2004). Association of elevated phospho-tau levels with Alzheimer-typical 18F-fluoro-2-deoxy-D-glucose positron emission tomography findings in patients with mild cognitive impairment. Biol Psychiatry *56*, 279-283.
Fenn, J. B., Mann, M., Meng, C. K., Wong, S. F., and Whitehouse, C. M. (1989). Electrospray ionization for mass spectrometry of large biomolecules. Science *246*, 64-71.
Fenteany, G., Standaert, R. F., Lane, W. S., Choi, S., Corey, E. J., and Schreiber, S. L. (1995). Inhibition of proteasome activities and subunit-specific amino-terminal threonine modification by lactacystin. Science *268*, 726-731.
Ferrari, A., Hoerndli, F., Baechi, T., Nitsch, R. M., and Gotz, J. (2003). Beta-amyloid induces PHF-like tau filaments in tissue culture. J Biol Chem *278*, 40162-40168.
Ferrer, I., Boada Rovira, M., Sanchez Guerra, M. L., Rey, M. J., and Costa-Jussa, F. (2004). Neuropathology and pathogenesis of encephalitis following amyloid-beta immunization in Alzheimer's disease. Brain Pathol *14*, 11-20.
Finckh, U., Kuschel, C., Anagnostouli, M., Patsouris, E., Pantes, G. V., Gatzonis, S., Kapaki, E., Davaki, P., Lamszus, K., Stavrou, D., and Gal, A. (2005). Novel mutations and repeated findings of mutations in familial Alzheimer disease. Neurogenetics.
Fisher, G. H., D'Aniello, A., Vetere, A., Cusano, G. P., Chavez, M., and Petrucelli, L. (1992). Quantification of D-aspartate in normal and Alzheimer brains. Neurosci Lett *143*, 215-218.
Foster, N. L., Wilhelmsen, K., Sima, A. A., Jones, M. Z., D'Amato, C. J., and Gilman, S. (1997). Frontotemporal dementia and parkinsonism linked to chromosome 17: a consensus conference. Conference Participants. Ann Neurol *41*, 706-715.
Fukata, Y., Itoh, T. J., Kimura, T., Menager, C., Nishimura, T., Shiromizu, T., Watanabe, H., Inagaki, N., Iwamatsu, A., Hotani, H., and Kaibuchi, K. (2002). CRMP-2 binds to tubulin heterodimers to promote microtubule assembly. Nat Cell Biol *4*, 583-591.
Fussenegger, M. (2001). The impact of mammalian gene regulation concepts on functional genomic research, metabolic engineering, and advanced gene therapies. Biotechnol Prog *17*, 1-51.
Fussenegger, M., Morris, R. P., Fux, C., Rimann, M., von Stockar, B., Thompson, C. J., and Bailey, J. E. (2000). Streptogramin-based gene regulation systems for mammalian cells. Nat Biotechnol *18*, 1203-1208.
Games, D., Adams, D., Alessandrini, R., Barbour, R., Berthelette, P., Blackwell, C., Carr, T., Clemens, J., Donaldson, T., Gillespie, F., and et al. (1995). Alzheimer-type neuropathology in transgenic mice overexpressing V717F beta-amyloid precursor protein. Nature *373*, 523-527.
Gatz, M., Pedersen, N. L., Berg, S., Johansson, B., Johansson, K., Mortimer, J. A., Posner, S. F., Viitanen, M., Winblad, B., and Ahlbom, A. (1997). Heritability for Alzheimer's disease: the study of dementia in Swedish twins. J Gerontol A Biol Sci Med Sci *52*, M117-125.
Giannakopoulos, P., Herrmann, F. R., Bussiere, T., Bouras, C., Kovari, E., Perl, D. P., Morrison, J. H., Gold, G., and Hof, P. R. (2003). Tangle and neuron numbers, but not amyloid load, predict cognitive status in Alzheimer's disease. Neurology *60*, 1495-1500.
Gitler, D., Takagishi, Y., Feng, J., Ren, Y., Rodriguiz, R. M., Wetsel, W. C., Greengard, P., and Augustine, G. J. (2004). Different presynaptic roles of synapsins at excitatory and inhibitory synapses. J Neurosci *24*, 11368-11380.
Glenner, G. G., and Wong, C. W. (1984). Alzheimer's disease: initial report of the purification and characterization of a novel cerebrovascular amyloid protein. Biochem Biophys Res Commun *120*, 885-890.

Goate, A., Chartier-Harlin, M. C., Mullan, M., Brown, J., Crawford, F., Fidani, L., Giuffra, L., Haynes, A., Irving, N., James, L., and et al. (1991). Segregation of a missense mutation in the amyloid precursor protein gene with familial Alzheimer's disease. Nature *349*, 704-706.
Goedert, M., Spillantini, M. G., Jakes, R., Crowther, R. A., Vanmechelen, E., Probst, A., Gotz, J., Burki, K., and Cohen, P. (1995). Molecular dissection of the paired helical filament. Neurobiol Aging *16*, 325-334.
Goldbaum, O., Oppermann, M., Handschuh, M., Dabir, D., Zhang, B., Forman, M. S., Trojanowski, J. Q., Lee, V. M., and Richter-Landsberg, C. (2003). Proteasome inhibition stabilizes tau inclusions in oligodendroglial cells that occur after treatment with okadaic acid. J Neurosci *23*, 8872-8880.
Gotz, J. (2001). Tau and transgenic animal models. Brain Res Brain Res Rev *35*, 266-286.
Gotz, J., Chen, F., Barmettler, R., and Nitsch, R. M. (2001a). Tau Filament Formation in Transgenic Mice Expressing P301L Tau. J Biol Chem *276*, 529-534.
Gotz, J., Chen, F., van Dorpe, J., and Nitsch, R. M. (2001b). Formation of neurofibrillary tangles in P301L tau transgenic mice induced by Abeta 42 fibrils. Science *293*, 1491-1495.
Gotz, J., Probst, A., Spillantini, M. G., Schafer, T., Jakes, R., Burki, K., and Goedert, M. (1995). Somatodendritic localization and hyperphosphorylation of tau protein in transgenic mice expressing the longest human brain tau isoform. Embo J *14*, 1304-1313.
Gotz, J., Schild, A., Hoerndli, F., and Pennanen, L. (2004a). Amyloid-induced neurofibrillary tangle formation in Alzheimer's disease: insight from transgenic mouse and tissue-culture models. Int J Dev Neurosci *22*, 453-465.
Gotz, J., Streffer, J. R., David, D., Schild, A., Hoerndli, F., Pennanen, L., Kurosinski, P., and Chen, F. (2004b). Transgenic animal models of Alzheimer's disease and related disorders: Histopathology, behavior and therapy. Mol Psychiatry *9*, 664-683.
Gotz, J., Tolnay, M., Barmettler, R., Chen, F., Probst, A., and Nitsch, R. M. (2001c). Oligodendroglial tau filament formation in transgenic mice expressing G272V tau. Eur J Neurosci *13*, 2131-2140.
Gregori, L., Fuchs, C., Figueiredo-Pereira, M. E., Van Nostrand, W. E., and Goldgaber, D. (1995). Amyloid beta-protein inhibits ubiquitin-dependent protein degradation in vitro. J Biol Chem *270*, 19702-19708.
Gregori, L., Hainfeld, J. F., Simon, M. N., and Goldgaber, D. (1997). Binding of amyloid beta protein to the 20 S proteasome. J Biol Chem *272*, 58-62.
Griffin, T. J., and Aebersold, R. (2001). Advances in proteome analysis by mass spectrometry. J Biol Chem *276*, 45497-45500.
Grimmer, T., Diehl, J., Drzezga, A., Forstl, H., and Kurz, A. (2004). Region-specific decline of cerebral glucose metabolism in patients with frontotemporal dementia: a prospective 18F-FDG-PET study. Dement Geriatr Cogn Disord *18*, 32-36.
Gutteridge, J. M. (1984). Lipid peroxidation initiated by superoxide-dependent hydroxyl radicals using complexed iron and hydrogen peroxide. FEBS Lett *172*, 245-249.
Gutteridge, J. M., Beard, A. P., and Quinlan, G. J. (1983). Superoxide-dependent lipid peroxidation. Problems with the use of catalase as a specific probe for fenton-derived hydroxyl radicals. Biochem Biophys Res Commun *117*, 901-907.
Gygi, S. P., Rist, B., Gerber, S. A., Turecek, F., Gelb, M. H., and Aebersold, R. (1999a). Quantitative analysis of complex protein mixtures using isotope-coded affinity tags. Nat Biotechnol *17*, 994-999.
Gygi, S. P., Rochon, Y., Franza, B. R., and Aebersold, R. (1999b). Correlation between protein and mRNA abundance in yeast. Mol Cell Biol *19*, 1720-1730.

Hardy, J. A., and Higgins, G. A. (1992). Alzheimer's disease: the amyloid cascade hypothesis. Science *256*, 184-185.
Hartley, D. M., Walsh, D. M., Ye, C. P., Diehl, T., Vasquez, S., Vassilev, P. M., Teplow, D. B., and Selkoe, D. J. (1999). Protofibrillar intermediates of amyloid beta-protein induce acute electrophysiological changes and progressive neurotoxicity in cortical neurons. J Neurosci *19*, 8876-8884.
Hartzler, A. W., Zhu, X., Siedlak, S. L., Castellani, R. J., Avila, J., Perry, G., and Smith, M. A. (2002). The p38 pathway is activated in Pick disease and progressive supranuclear palsy: a mechanistic link between mitogenic pathways, oxidative stress, and tau. Neurobiol Aging *23*, 855-859.
Hasegawa, M., Jakes, R., Crowther, R. A., Lee, V. M., Ihara, Y., and Goedert, M. (1996). Characterization of mAb AP422, a novel phosphorylation-dependent monoclonal antibody against tau protein. FEBS Lett *384*, 25-30.
Hensley, K., Carney, J. M., Mattson, M. P., Aksenova, M., Harris, M., Wu, J. F., Floyd, R. A., and Butterfield, D. A. (1994). A model for beta-amyloid aggregation and neurotoxicity based on free radical generation by the peptide: relevance to Alzheimer disease. Proc Natl Acad Sci U S A *91*, 3270-3274.
Higuchi, M., Ishihara, T., Zhang, B., Hong, M., Andreadis, A., Trojanowski, J., and Lee, V. M. (2002). Transgenic mouse model of tauopathies with glial pathology and nervous system degeneration. Neuron *35*, 433-446.
Hillenkamp, F., Karas, M., Beavis, R. C., and Chait, B. T. (1991). Matrix-assisted laser desorption/ionization mass spectrometry of biopolymers. Anal Chem *63*, 1193A-1203A.
Hock, C., Konietzko, U., Papassotiropoulos, A., Wollmer, A., Streffer, J., von Rotz, R. C., Davey, G., Moritz, E., and Nitsch, R. M. (2002). Generation of antibodies specific for beta-amyloid by vaccination of patients with Alzheimer disease. Nat Med *8*, 1270-1275.
Hock, C., Konietzko, U., Streffer, J. R., Tracy, J., Signorell, A., Muller-Tillmanns, B., Lemke, U., Henke, K., Moritz, E., Garcia, E.*, et al.* (2003). Antibodies against beta-Amyloid Slow Cognitive Decline in Alzheimer's Disease. Neuron *38*, 547-554.
Hoerndli, F., David, D., and Gotz, J. (2005). Functional Genomics Meets Neurodegenerative Disorders. Prog Neurobiol *in revision*.
Hoffmann, R., Lee, V. M., Leight, S., Varga, I., and Otvos, L., Jr. (1997). Unique Alzheimer's disease paired helical filament specific epitopes involve double phosphorylation at specific sites. Biochemistry *36*, 8114-8124.
Holcomb, L., Gordon, M. N., McGowan, E., Yu, X., Benkovic, S., Jantzen, P., Wright, K., Saad, I., Mueller, R., Morgan, D.*, et al.* (1998). Accelerated Alzheimer-type phenotype in transgenic mice carrying both mutant amyloid precursor protein and presenilin 1 transgenes. Nat Med *4*, 97-100.
Hoving, S., Gerrits, B., Voshol, H., Muller, D., Roberts, R. C., and van Oostrum, J. (2002). Preparative two-dimensional gel electrophoresis at alkaline pH using narrow range immobilized pH gradients. Proteomics *2*, 127-134.
Hsiao, K., Chapman, P., Nilsen, S., Eckman, C., Harigaya, Y., Younkin, S., Yang, F., and Cole, G. (1996). Correlative memory deficits, Abeta elevation, and amyloid plaques in transgenic mice. Science *274*, 99-102.
Hutton, M., Lendon, C. L., Rizzu, P., Baker, M., Froelich, S., Houlden, H., Pickering-Brown, S., Chakraverty, S., Isaacs, A., Grover, A.*, et al.* (1998). Association of missense and 5'-splice-site mutations in tau with the inherited dementia FTDP-17. Nature *393*, 702-705.

Inagaki, N., Chihara, K., Arimura, N., Menager, C., Kawano, Y., Matsuo, N., Nishimura, T., Amano, M., and Kaibuchi, K. (2001). CRMP-2 induces axons in cultured hippocampal neurons. Nat Neurosci *4*, 781-782.
Ingram, E. M., and Spillantini, M. G. (2002). Tau gene mutations: dissecting the pathogenesis of FTDP-17. Trends Mol Med *8*, 555-562.
Ishihara, T., Hong, M., Zhang, B., Nakagawa, Y., Lee, M. K., Trojanowski, J. Q., and Lee, V. M. (1999). Age-dependent emergence and progression of a tauopathy in transgenic mice overexpressing the shortest human tau isoform. Neuron *24*, 751-762.
Ishihara, T., Zhang, B., Higuchi, M., Yoshiyama, Y., Trojanowski, J. Q., and Lee, V. M. (2001). Age-Dependent Induction of Congophilic Neurofibrillary Tau Inclusions in Tau Transgenic Mice. Am J Pathol *158*, 555-562.
Jagust, W. J., Seab, J. P., Huesman, R. H., Valk, P. E., Mathis, C. A., Reed, B. R., Coxson, P. G., and Budinger, T. F. (1991). Diminished glucose transport in Alzheimer's disease: dynamic PET studies. J Cereb Blood Flow Metab *11*, 323-330.
Jeon, S. G., Bahn, J. H., Jang, J. S., Park, J., Kwon, O. S., Cho, S. W., and Choi, S. Y. (2000). Human brain GABA transaminase tissue distribution and molecular expression. Eur J Biochem *267*, 5601-5607.
Jicha, G. A., Lane, E., Vincent, I., Otvos, L., Jr., Hoffmann, R., and Davies, P. (1997). A conformation- and phosphorylation-dependent antibody recognizing the paired helical filaments of Alzheimer's disease. J Neurochem *69*, 2087-2095.
Jin, L. W., Masliah, E., Iimoto, D., Deteresa, R., Mallory, M., Sundsmo, M., Mori, N., Sobel, A., and Saitoh, T. (1996). Neurofibrillary tangle-associated alteration of stathmin in Alzheimer's disease. Neurobiol Aging *17*, 331-341.
Kamenetz, F., Tomita, T., Hsieh, H., Seabrook, G., Borchelt, D., Iwatsubo, T., Sisodia, S., and Malinow, R. (2003). APP processing and synaptic function. Neuron *37*, 925-937.
Karas, M., and Hillenkamp, F. (1988). Laser desorption ionization of proteins with molecular masses exceeding 10,000 daltons. Anal Chem *60*, 2299-2301.
Karelson, E., Bogdanovic, N., Garlind, A., Winblad, B., Zilmer, K., Kullisaar, T., Vihalemm, T., Kairane, C., and Zilmer, M. (2001). The cerebrocortical areas in normal brain aging and in Alzheimer's disease: noticeable differences in the lipid peroxidation level and in antioxidant defense. Neurochem Res *26*, 353-361.
Keil, U., Bonert, A., Marques, C. A., Scherping, I., Weyermann, J., Strosznajder, J. B., Muller-Spahn, F., Haass, C., Czech, C., Pradier, L.*, et al.* (2004). Amyloid beta-induced changes in nitric oxide production and mitochondrial activity lead to apoptosis. J Biol Chem *279*, 50310-50320.
Keller, J. N., Hanni, K. B., and Markesbery, W. R. (2000). Impaired proteasome function in Alzheimer's disease. J Neurochem *75*, 436-439.
Keller, J. N., Pang, Z., Geddes, J. W., Begley, J. G., Germeyer, A., Waeg, G., and Mattson, M. P. (1997). Impairment of glucose and glutamate transport and induction of mitochondrial oxidative stress and dysfunction in synaptosomes by amyloid beta-peptide: role of the lipid peroxidation product 4-hydroxynonenal. J Neurochem *69*, 273-284.
Kenessey, A., Yen, S. H., Liu, W. K., Yang, X. R., and Dunlop, D. S. (1995). Detection of D-aspartate in tau proteins associated with Alzheimer paired helical filaments. Brain Res *675*, 183-189.
Kenney, A. M., and Kocsis, J. D. (1998). Peripheral axotomy induces long-term c-Jun amino-terminal kinase-1 activation and activator protein-1 binding activity by c-Jun and junD in adult rat dorsal root ganglia In vivo. J Neurosci *18*, 1318-1328.

Kim, K. B., Myung, J., Sin, N., and Crews, C. M. (1999). Proteasome inhibition by the natural products epoxomicin and dihydroeponemycin: insights into specificity and potency. Bioorg Med Chem Lett *9*, 3335-3340.
Kim, S. H., Vlkolinsky, R., Cairns, N., Fountoulakis, M., and Lubec, G. (2001). The reduction of NADH ubiquinone oxidoreductase 24- and 75-kDa subunits in brains of patients with Down syndrome and Alzheimer's disease. Life Sci *68*, 2741-2750.
Kinoshita, A., Kinoshita, M., Akiyama, H., Tomimoto, H., Akiguchi, I., Kumar, S., Noda, M., and Kimura, J. (1998). Identification of septins in neurofibrillary tangles in Alzheimer's disease. Am J Pathol *153*, 1551-1560.
Kinoshita, A., Noda, M., and Kinoshita, M. (2000). Differential localization of septins in the mouse brain. J Comp Neurol *428*, 223-239.
Klose, J. (1975). Protein mapping by combined isoelectric focusing and electrophoresis of mouse tissues. A novel approach to testing for induced point mutations in mammals. Humangenetik *26*, 231-243.
Kopke, E., Tung, Y. C., Shaikh, S., Alonso, A. C., Iqbal, K., and Grundke-Iqbal, I. (1993). Microtubule-associated protein tau. Abnormal phosphorylation of a non-paired helical filament pool in Alzheimer disease. J Biol Chem *268*, 24374-24384.
Korolainen, M. A., Goldsteins, G., Alafuzoff, I., Koistinaho, J., and Pirttila, T. (2002). Proteomic analysis of protein oxidation in Alzheimer's disease brain. Electrophoresis *23*, 3428-3433.
Krijgsveld, J., Ketting, R. F., Mahmoudi, T., Johansen, J., Artal-Sanz, M., Verrijzer, C. P., Plasterk, R. H., and Heck, A. J. (2003). Metabolic labeling of C. elegans and D. melanogaster for quantitative proteomics. Nat Biotechnol *21*, 927-931.
Krohn, A. J., Wahlbrink, T., and Prehn, J. H. (1999). Mitochondrial depolarization is not required for neuronal apoptosis. J Neurosci *19*, 7394-7404.
Landino, L. M., Robinson, S. H., Skreslet, T. E., and Cabral, D. M. (2004a). Redox modulation of tau and microtubule-associated protein-2 by the glutathione/glutaredoxin reductase system. Biochem Biophys Res Commun *323*, 112-117.
Landino, L. M., Skreslet, T. E., and Alston, J. A. (2004b). Cysteine oxidation of tau and microtubule-associated protein-2 by peroxynitrite: modulation of microtubule assembly kinetics by the thioredoxin reductase system. J Biol Chem *279*, 35101-35105.
Lewis, J., Dickson, D. W., Lin, W.-L., Chisholm, L., Corral, A., Jones, G., Yen, S.-H., Sahara, N., Skipper, L., Yager, D.*, et al.* (2001). Enhanced neurofibrillary degeneration in transgenic mice expressing mutant Tau and APP. Science *293*, 1487-1491.
Lewis, J., McGowan, E., Rockwood, J., Melrose, H., Nacharaju, P., Van Slegtenhorst, M., Gwinn-Hardy, K., Murphy, P. M., Baker, M., Yu, X.*, et al.* (2000). Neurofibrillary tangles, amyotrophy and progressive motor disturbance in mice expressing mutant (P301L) tau protein. Nat Genet *25*, 402-405.
Li, Y. J., Oliveira, S. A., Xu, P., Martin, E. R., Stenger, J. E., Scherzer, C. R., Hauser, M. A., Scott, W. K., Small, G. W., Nance, M. A.*, et al.* (2003). Glutathione S-transferase omega-1 modifies age-at-onset of Alzheimer disease and Parkinson disease. Hum Mol Genet *12*, 3259-3267.
Liu, R., Liu, I. Y., Bi, X., Thompson, R. F., Doctrow, S. R., Malfroy, B., and Baudry, M. (2003). Reversal of age-related learning deficits and brain oxidative stress in mice with superoxide dismutase/catalase mimetics. Proc Natl Acad Sci U S A *100*, 8526-8531.
Loo, D. T., Copani, A., Pike, C. J., Whittemore, E. R., Walencewicz, A. J., and Cotman, C. W. (1993). Apoptosis is induced by beta-amyloid in cultured central nervous system neurons. Proc Natl Acad Sci U S A *90*, 7951-7955.

Lopez Salon, M., Pasquini, L., Besio Moreno, M., Pasquini, J. M., and Soto, E. (2003). Relationship between beta-amyloid degradation and the 26S proteasome in neural cells. Exp Neurol *180*, 131-143.
Lorenzo, A., Yuan, M., Zhang, Z., Paganetti, P. A., Sturchler-Pierrat, C., Staufenbiel, M., Mautino, J., Vigo, F. S., Sommer, B., and Yankner, B. A. (2000). Amyloid beta interacts with the amyloid precursor protein: a potential toxic mechanism in Alzheimer's disease. Nat Neurosci *3*, 460-464.
Lovell, M. A., Ehmann, W. D., Butler, S. M., and Markesbery, W. R. (1995). Elevated thiobarbituric acid-reactive substances and antioxidant enzyme activity in the brain in Alzheimer's disease. Neurology *45*, 1594-1601.
Lovell, M. A., Xie, C., Gabbita, S. P., and Markesbery, W. R. (2000). Decreased thioredoxin and increased thioredoxin reductase levels in Alzheimer's disease brain. Free Radic Biol Med *28*, 418-427.
Lovell, M. A., Xie, C., and Markesbery, W. R. (1998). Decreased glutathione transferase activity in brain and ventricular fluid in Alzheimer's disease. Neurology *51*, 1562-1566.
Lowry, O. H., Rosebrough, N. J., Farr, A. L., and Randall, R. J. (1951). Protein measurement with the Folin phenol reagent. J Biol Chem *193*, 265-275.
Mandelkow, E. M., Stamer, K., Vogel, R., Thies, E., and Mandelkow, E. (2003). Clogging of axons by tau, inhibition of axonal traffic and starvation of synapses. Neurobiol Aging *24*, 1079-1085.
Masliah, E., Hansen, L., Adame, A., Crews, L., Bard, F., Lee, C., Seubert, P., Games, D., Kirby, L., and Schenk, D. (2005). Abeta vaccination effects on plaque pathology in the absence of encephalitis in Alzheimer disease. Neurology *64*, 129-131.
Masters, C. L., Simms, G., Weinman, N. A., Multhaup, G., McDonald, B. L., and Beyreuther, K. (1985). Amyloid plaque core protein in Alzheimer disease and Down syndrome. Proc Natl Acad Sci U S A *82*, 4245-4249.
McKhann, G., Drachman, D., Folstein, M., Katzman, R., Price, D., and Stadlan, E. M. (1984). Clinical diagnosis of Alzheimer's disease: report of the NINCDS-ADRDA Work Group under the auspices of Department of Health and Human Services Task Force on Alzheimer's Disease. Neurology *34*, 939-944.
McShea, A., Zelasko, D. A., Gerst, J. L., and Smith, M. A. (1999). Signal transduction abnormalities in Alzheimer's disease: evidence of a pathogenic stimuli. Brain Res *815*, 237-242.
Meng, L., Mohan, R., Kwok, B. H., Elofsson, M., Sin, N., and Crews, C. M. (1999). Epoxomicin, a potent and selective proteasome inhibitor, exhibits in vivo antiinflammatory activity. Proc Natl Acad Sci U S A *96*, 10403-10408.
Mielke, R., Schroder, R., Fink, G. R., Kessler, J., Herholz, K., and Heiss, W. D. (1996). Regional cerebral glucose metabolism and postmortem pathology in Alzheimer's disease. Acta Neuropathol (Berl) *91*, 174-179.
Mirra, S. S., Gearing, M., McKeel, D. W., Jr., Crain, B. J., Hughes, J. P., van Belle, G., and Heyman, A. (1994). Interlaboratory comparison of neuropathology assessments in Alzheimer's disease: a study of the Consortium to Establish a Registry for Alzheimer's Disease (CERAD). J Neuropathol Exp Neurol *53*, 303-315.
Mizuno, Y., and Ohta, K. (1986). Regional distributions of thiobarbituric acid-reactive products, activities of enzymes regulating the metabolism of oxygen free radicals, and some of the related enzymes in adult and aged rat brains. J Neurochem *46*, 1344-1352.
Molloy, M. P., Herbert, B. R., Walsh, B. J., Tyler, M. I., Traini, M., Sanchez, J. C., Hochstrasser, D. F., Williams, K. L., and Gooley, A. A. (1998). Extraction of membrane proteins by differential

solubilization for separation using two-dimensional gel electrophoresis. Electrophoresis *19*, 837-844.
Mukaetova-Ladinska, E. B., Garcia-Siera, F., Hurt, J., Gertz, H. J., Xuereb, J. H., Hills, R., Brayne, C., Huppert, F. A., Paykel, E. S., McGee, M.*, et al.* (2000). Staging of cytoskeletal and beta-amyloid changes in human isocortex reveals biphasic synaptic protein response during progression of Alzheimer's disease. Am J Pathol *157*, 623-636.
Mullan, M., Crawford, F., Axelman, K., Houlden, H., Lilius, L., Winblad, B., and Lannfelt, L. (1992). A pathogenic mutation for probable Alzheimer's disease in the APP gene at the N-terminus of beta-amyloid. Nat Genet *1*, 345-347.
Mullis, K. B. (1990). Target amplification for DNA analysis by the polymerase chain reaction. Ann Biol Clin (Paris) *48*, 579-582.
Nagy, Z., Jobst, K. A., Esiri, M. M., Morris, J. H., King, E. M., MacDonald, B., Litchfield, S., Barnetson, L., and Smith, A. D. (1996). Hippocampal pathology reflects memory deficit and brain imaging measurements in Alzheimer's disease: clinicopathologic correlations using three sets of pathologic diagnostic criteria. Dementia *7*, 76-81.
Nakagawa, T., Zhu, H., Morishima, N., Li, E., Xu, J., Yankner, B. A., and Yuan, J. (2000). Caspase-12 mediates endoplasmic-reticulum-specific apoptosis and cytotoxicity by amyloid-beta. Nature *403*, 98-103.
Nebot, C., Moutet, M., Huet, P., Xu, J. Z., Yadan, J. C., and Chaudiere, J. (1993). Spectrophotometric assay of superoxide dismutase activity based on the activated autoxidation of a tetracyclic catechol. Anal Biochem *214*, 442-451.
Nicoll, J. A., Wilkinson, D., Holmes, C., Steart, P., Markham, H., and Weller, R. O. (2003). Neuropathology of human Alzheimer disease after immunization with amyloid-beta peptide: a case report. Nat Med *9*, 448-452.
Nordberg, J., and Arner, E. S. (2001). Reactive oxygen species, antioxidants, and the mammalian thioredoxin system. Free Radic Biol Med *31*, 1287-1312.
Oddo, S., Caccamo, A., Shepherd, J. D., Murphy, M. P., Golde, T. E., Kayed, R., Metherate, R., Mattson, M. P., Akbari, Y., and LaFerla, F. M. (2003). Triple-transgenic model of Alzheimer's disease with plaques and tangles. Intracellular abeta and synaptic dysfunction. Neuron *39*, 409-421.
Odetti, P., Garibaldi, S., Norese, R., Angelini, G., Marinelli, L., Valentini, S., Menini, S., Traverso, N., Zaccheo, D., Siedlak, S.*, et al.* (2000). Lipoperoxidation is selectively involved in progressive supranuclear palsy. J Neuropathol Exp Neurol *59*, 393-397.
O'Farrell, P. H. (1975). High resolution two-dimensional electrophoresis of proteins. J Biol Chem *250*, 4007-4021.
Orgogozo, J. M., Gilman, S., Dartigues, J. F., Laurent, B., Puel, M., Kirby, L. C., Jouanny, P., Dubois, B., Eisner, L., Flitman, S.*, et al.* (2003). Subacute meningoencephalitis in a subset of patients with AD after Abeta42 immunization. Neurology *61*, 46-54.
Orlowski, M. (1990). The multicatalytic proteinase complex, a major extralysosomal proteolytic system. Biochemistry *29*, 10289-10297.
Orosz, F., Wagner, G., Liliom, K., Kovacs, J., Baroti, K., Horanyi, M., Farkas, T., Hollan, S., and Ovadi, J. (2000). Enhanced association of mutant triosephosphate isomerase to red cell membranes and to brain microtubules. Proc Natl Acad Sci U S A *97*, 1026-1031.
Paglia, D. E., and Valentine, W. N. (1967). Studies on the quantitative and qualitative characterization of erythrocyte glutathione peroxidase. J Lab Clin Med *70*, 158-169.
Parker, W. D., Jr., Parks, J., Filley, C. M., and Kleinschmidt-DeMasters, B. K. (1994). Electron transport chain defects in Alzheimer's disease brain. Neurology *44*, 1090-1096.

Paxinos, K. B. J. F. a. G. (1997). The mouse brain in stereotaxic coordinates (San Diego, Academic Press Inc.).
Pennanen, L., Welzl, H., D'Adamo, P., Nitsch, R. M., and Gotz, J. (2004). Accelerated extinction of conditioned taste aversion in P301L tau transgenic mice. Neurobiol Dis *15*, 500-509.
Perez, M., Cuadros, R., Smith, M. A., Perry, G., and Avila, J. (2000). Phosphorylated, but not native, tau protein assembles following reaction with the lipid peroxidation product, 4-hydroxy-2-nonenal. FEBS Lett *486*, 270-274.
Probst, A., Gotz, J., Wiederhold, K. H., Tolnay, M., Mistl, C., Jaton, A. L., Hong, M., Ishihara, T., Lee, V. M., Trojanowski, J. Q.*, et al.* (2000). Axonopathy and amyotrophy in mice transgenic for human four-repeat tau protein. Acta Neuropathol (Berl) *99*, 469-481.
Rabilloud, T., Carpentier, G., and Tarroux, P. (1988). Improvement and simplification of low-background silver staining of proteins by using sodium dithionite. Electrophoresis *9*, 288-291.
Ramsden, M., Henderson, Z., and Pearson, H. A. (2002). Modulation of Ca2+ channel currents in primary cultures of rat cortical neurones by amyloid beta protein (1-40) is dependent on solubility status. Brain Res *956*, 254-261.
Ramsden, M., Plant, L. D., Webster, N. J., Vaughan, P. F., Henderson, Z., and Pearson, H. A. (2001). Differential effects of unaggregated and aggregated amyloid beta protein (1-40) on K(+) channel currents in primary cultures of rat cerebellar granule and cortical neurones. J Neurochem *79*, 699-712.
Rasmussen, U. F., and Rasmussen, H. N. (2000). Human quadriceps muscle mitochondria: a functional characterization. Mol Cell Biochem *208*, 37-44.
Roher, A. E., Lowenson, J. D., Clarke, S., Wolkow, C., Wang, R., Cotter, R. J., Reardon, I. M., Zurcher-Neely, H. A., Heinrikson, R. L., Ball, M. J., and et al. (1993). Structural alterations in the peptide backbone of beta-amyloid core protein may account for its deposition and stability in Alzheimer's disease. J Biol Chem *268*, 3072-3083.
Ross, P. L., Huang, Y. N., Marchese, J. N., Williamson, B., Parker, K., Hattan, S., Khainovski, N., Pillai, S., Dey, S., Daniels, S.*, et al.* (2004). Multiplexed protein quantitation in saccharomyces cerevisiae using amine-reactive isobaric tagging reagents. Mol Cell Proteomics *3*, 1154-1169.
Russo, C., Dolcini, V., Salis, S., Venezia, V., Violani, E., Carlo, P., Zambrano, N., Russo, T., and Schettini, G. (2002). Signal transduction through tyrosine-phosphorylated carboxy-terminal fragments of APP via an enhanced interaction with Shc/Grb2 adaptor proteins in reactive astrocytes of Alzheimer's disease brain. Ann N Y Acad Sci *973*, 323-333.
Santens, P., De Bleecker, J., Goethals, P., Strijckmans, K., Lemahieu, I., Slegers, G., Dierckx, R., and De Reuck, J. (2001). Differential regional cerebral uptake of (18)F-fluoro-2-deoxy-D-glucose in Alzheimer's disease and frontotemporal dementia at initial diagnosis. Eur Neurol *45*, 19-27.
Schagger, H., and Ohm, T. G. (1995). Human diseases with defects in oxidative phosphorylation. 2. F1F0 ATP-synthase defects in Alzheimer disease revealed by blue native polyacrylamide gel electrophoresis. Eur J Biochem *227*, 916-921.
Schenk, D. (2002). Amyloid-beta immunotherapy for Alzheimer's disease: the end of the beginning. Nat Rev Neurosci *3*, 824-828.
Scheufler, C., Brinker, A., Bourenkov, G., Pegoraro, S., Moroder, L., Bartunik, H., Hartl, F. U., and Moarefi, I. (2000). Structure of TPR domain-peptide complexes: critical elements in the assembly of the Hsp70-Hsp90 multichaperone machine. Cell *101*, 199-210.
Schneider, A., Biernat, J., von Bergen, M., Mandelkow, E., and Mandelkow, E. M. (1999). Phosphorylation that detaches tau protein from microtubules (Ser262, Ser214) also protects it against aggregation into Alzheimer paired helical filaments. Biochemistry *38*, 3549-3558.

Schonberger, S. J., Edgar, P. F., Kydd, R., Faull, R. L., and Cooper, G. J. (2001). Proteomic analysis of the brain in Alzheimer's disease: molecular phenotype of a complex disease process. Proteomics *1*, 1519-1528.
Schuessel, K., Leutner, S., Cairns, N. J., Muller, W. E., and Eckert, A. (2004). Impact of gender on upregulation of antioxidant defence mechanisms in Alzheimer's disease brain. J Neural Transm *111*, 1167-1182.
Schuessel, K., Schafer, S., Bayer, T. A., Czech, C., Pradier, L., Muller-Spahn, F., Muller, W. E., and Eckert, A. (2005). Impaired Cu/Zn-SOD activity contributes to increased oxidative damage in APP transgenic mice. Neurobiol Dis *18*, 89-99.
Selkoe, D. J. (1998). The cell biology of beta-amyloid precursor protein and presenilin in Alzheimer's disease. Trends Cell Biol *8*, 447-453.
Senior, K. (2002). Dosing in phase II trial of Alzheimer's vaccine suspended. Lancet Neurol *1*, 3.
Sergeant, N., Wattez, A., Galvan-valencia, M., Ghestem, A., David, J. P., Lemoine, J., Sautiere, P. E., Dachary, J., Mazat, J. P., Michalski, J. C.*, et al.* (2003). Association of ATP synthase alpha-chain with neurofibrillary degeneration in Alzheimer's disease. Neuroscience *117*, 293-303.
Shevchenko, A., Wilm, M., Vorm, O., and Mann, M. (1996). Mass spectrometric sequencing of proteins silver-stained polyacrylamide gels. Anal Chem *68*, 850-858.
Sims, N. R., Finegan, J. M., Blass, J. P., Bowen, D. M., and Neary, D. (1987). Mitochondrial function in brain tissue in primary degenerative dementia. Brain Res *436*, 30-38.
Small, D. H., Mok, S. S., and Bornstein, J. C. (2001). OPINIONAlzheimer's disease and Abeta toxicity: from top to bottom. Nat Rev Neurosci *2*, 595-598.
Song, S., Kim, S. Y., Hong, Y. M., Jo, D. G., Lee, J. Y., Shim, S. M., Chung, C. W., Seo, S. J., Yoo, Y. J., Koh, J. Y.*, et al.* (2003). Essential role of E2-25K/Hip-2 in mediating amyloid-beta neurotoxicity. Mol Cell *12*, 553-563.
Spillantini, M. G., Van Swieten, J. C., and Goedert, M. (2000). Tau gene mutations in frontotemporal dementia and parkinsonism linked to chromosome 17 (FTDP-17). Neurogenetics *2*, 193-205.
Spittaels, K., Van den Haute, C., Van Dorpe, J., Bruynseels, K., Vandezande, K., Laenen, I., Geerts, H., Mercken, M., Sciot, R., Van Lommel, A.*, et al.* (1999). Prominent axonopathy in the brain and spinal cord of transgenic mice overexpressing four-repeat human tau protein. Am J Pathol *155*, 2153-2165.
Stamer, K., Vogel, R., Thies, E., Mandelkow, E., and Mandelkow, E. M. (2002). Tau blocks traffic of organelles, neurofilaments, and APP vesicles in neurons and enhances oxidative stress. J Cell Biol *156*, 1051-1063.
Steen, H., and Mann, M. (2004). The ABC's (and XYZ's) of peptide sequencing. Nat Rev Mol Cell Biol *5*, 699-711.
Stoll, L., Schubert, T., and Muller, W. E. (1992). Age-related deficits of central muscarinic cholinergic receptor function in the mouse: partial restoration by chronic piracetam treatment. Neurobiol Aging *13*, 39-44.
Sumpter, P. Q., Mann, D. M., Davies, C. A., Yates, P. O., Snowden, J. S., and Neary, D. (1986). An ultrastructural analysis of the effects of accumulation of neurofibrillary tangle in pyramidal neurons of the cerebral cortex in Alzheimer's disease. Neuropathol Appl Neurobiol *12*, 305-319.
Tanemura, K., Akagi, T., Murayama, M., Kikuchi, N., Murayama, O., Hashikawa, T., Yoshiike, Y., Park, J. M., Matsuda, K., Nakao, S.*, et al.* (2001). Formation of filamentous tau aggregations in transgenic mice expressing V337M human tau. Neurobiol Dis *8*, 1036-1045.
Tani, K., Shibata, M., Kawase, K., Kawashima, H., Hatsuzawa, K., Nagahama, M., and Tagaya, M. (2003). Mapping of functional domains of gamma-SNAP. J Biol Chem *278*, 13531-13538.

Tatebayashi, Y., Miyasaka, T., Chui, D. H., Akagi, T., Mishima, K., Iwasaki, K., Fujiwara, M., Tanemura, K., Murayama, M., Ishiguro, K.*, et al.* (2002). Tau filament formation and associative memory deficit in aged mice expressing mutant (R406W) human tau. Proc Natl Acad Sci U S A *99*, 13896-13901.
Taylor, E. R., Hurrell, F., Shannon, R. J., Lin, T. K., Hirst, J., and Murphy, M. P. (2003). Reversible glutathionylation of complex I increases mitochondrial superoxide formation. J Biol Chem *278*, 19603-19610.
Thal, D. R., Rub, U., Orantes, M., and Braak, H. (2002). Phases of A beta-deposition in the human brain and its relevance for the development of AD. Neurology *58*, 1791-1800.
Tien, M., Svingen, B. A., and Aust, S. D. (1981). Superoxide dependent lipid peroxidation. Fed Proc *40*, 179-182.
Tilleman, K., Van den Haute, C., Geerts, H., van Leuven, F., Esmans, E. L., and Moens, L. (2002). Proteomics analysis of the neurodegeneration in the brain of tau transgenic mice. Proteomics *2*, 656-665.
Tsuji, T., Shiozaki, A., Kohno, R., Yoshizato, K., and Shimohama, S. (2002). Proteomic profiling and neurodegeneration in Alzheimer's disease. Neurochem Res *27*, 1245-1253.
Turrens, J. F., and Boveris, A. (1980). Generation of superoxide anion by the NADH dehydrogenase of bovine heart mitochondria. Biochem J *191*, 421-427.
Ursini, F., Maiorino, M., and Gregolin, C. (1985). The selenoenzyme phospholipid hydroperoxide glutathione peroxidase. Biochim Biophys Acta *839*, 62-70.
Vassar, R., Bennett, B. D., Babu-Khan, S., Kahn, S., Mendiaz, E. A., Denis, P., Teplow, D. B., Ross, S., Amarante, P., Loeloff, R.*, et al.* (1999). Beta-secretase cleavage of Alzheimer's amyloid precursor protein by the transmembrane aspartic protease BACE. Science *286*, 735-741.
Vercauteren, F. G., Clerens, S., Roy, L., Hamel, N., Arckens, L., Vandesande, F., Alhonen, L., Janne, J., Szyf, M., and Cuello, A. C. (2004). Early dysregulation of hippocampal proteins in transgenic rats with Alzheimer's disease-linked mutations in amyloid precursor protein and presenilin 1. Brain Res Mol Brain Res *132*, 241-259.
Vigouroux, S., Furukawa, Y., Farout, L., S, J. K., Briand, M., and Briand, Y. (2003). Peptidase activities of the 20/26S proteasome and a novel protease in human brain. J Neurochem *84*, 392-396.
Wagner, E., Luche, S., Penna, L., Chevallet, M., Van Dorsselaer, A., Leize-Wagner, E., and Rabilloud, T. (2002). A method for detection of overoxidation of cysteines: peroxiredoxins are oxidized in vivo at the active-site cysteine during oxidative stress. Biochem J *366*, 777-785.
Walzer, M. A., Hejna, M. J., Lorens, S. A., and Lee, J. M. (2003). A induced tau pathology in mutant P301L mice. Paper presented at: Society for Neuroscience (New Orleans).
Weber, W., Fux, C., Daoud-el Baba, M., Keller, B., Weber, C. C., Kramer, B. P., Heinzen, C., Aubel, D., Bailey, J. E., and Fussenegger, M. (2002). Macrolide-based transgene control in mammalian cells and mice. Nat Biotechnol *20*, 901-907.
Weber, W., Rimann, M., Spielmann, M., Keller, B., Daoud-El Baba, M., Aubel, D., Weber, C. C., and Fussenegger, M. (2004). Gas-inducible transgene expression in mammalian cells and mice. Nat Biotechnol *22*, 1440-1444.
Yang, H., Zheng, G., Peng, X., Qiang, B., and Yuan, J. (2003). D-Amino acids and D-Tyr-tRNA(Tyr) deacylase: stereospecificity of the translation machine revisited. FEBS Lett *552*, 95-98.
Yao, Y., Zhukareva, V., Sung, S., Clark, C. M., Rokach, J., Lee, V. M., Trojanowski, J. Q., and Pratico, D. (2003). Enhanced brain levels of 8,12-iso-iPF2alpha-VI differentiate AD from frontotemporal dementia. Neurology *61*, 475-478.

Yoo, B. C., Cairns, N., Fountoulakis, M., and Lubec, G. (2001a). Synaptosomal proteins, beta-soluble N-ethylmaleimide-sensitive factor attachment protein (beta-SNAP), gamma-SNAP and synaptotagmin I in brain of patients with Down syndrome and Alzheimer's disease. Dement Geriatr Cogn Disord *12*, 219-225.
Yoo, B. C., Kim, S. H., Cairns, N., Fountoulakis, M., and Lubec, G. (2001b). Deranged expression of molecular chaperones in brains of patients with Alzheimer's disease. Biochem Biophys Res Commun *280*, 249-258.
Yoshida, H., Watanabe, A., and Ihara, Y. (1998). Collapsin response mediator protein-2 is associated with neurofibrillary tangles in Alzheimer's disease. J Biol Chem *273*, 9761-9768.
Younes, M., and Siegers, C. P. (1980). Lipid peroxidation as a consequence of glutathione depletion in rat and mouse liver. Res Commun Chem Pathol Pharmacol *27*, 119-128.

ABBREVIATIONS

aa: amino acid
Aβ: beta-amyloid peptide
$A\beta_{1-42}$: beta-amyloid peptide 1-42
$A\beta_{42-1}$: reverse beta-amyloid peptide 42-1
ACN: acetonitrile
AD: Alzheimer's disease
AD-P tau: AD hyperphosphorylated tau
APP: amyloid precursor protein
APS: ammonium persulfate
CBD: corticobasal degeneration
DBQ: n-decylubiquinone
ddH_2O: double deionised water
DMEM: Dulbecco's modified Eagle's medium
DRP-2: dihydropyrimidinase related protein 2
DTT: dithiothreitol
ESI: electrospray ionisation
FA: formic acid
FAD: familial form of AD
FCCP: carbonyl-cyanide-p-trifluoro-methoxy-phenylhydrazone
FTD: frontotemporal dementia
FTDP-17: frontotemporal dementia with parkinsonism linked to chromosome 17
GAPDH: glyceraldehyde-3-phosphate dehydrogenase
GFAP: glial fibrillary acidic protein
GFP: green fluorescent protein
GPx: glutathione peroxidase
GR: glutathione reducatase
GRB2: growth factor receptor-bound protein 2
γ-SNAP: γ-soluble N-ethylmaleimide-sensitive factor (NSF) attachment protein
GST: glutathione S-transferase
HAR: hexaammineruthenium(III)-chloride
HS: horse serum
IEF: isoelectrical focusing
IPG: immobilised pH gradients
LC: liquid chromatography
MALDI-TOF: matrix assisted laser desorption ionisation time of flight
MAP: microtubule associated protein
MDA: malondialdehyde
MRI: magnetic resonance imaging
MS: mass spectrometry
MudPIT: multidimensional protein identification technology
MW: molecular weight
NFT: neurofibrillary tangles
PCR: polymerase chain reaction
PDGF: platelet-derived growth factor
PET: Positron emission tomography

PFA: paraformaldehyde
PHF: paired helical filaments
PHGPx: phospholipid hydroperoxide glutathione peroxidase
PI: pristinamycin
pI: isoelectrical point
PIT: pristinamycin-inhibited transactivator
PPIR: pristinamycin-responsive promoter
PMF: peptide mass fingerprint
PrP: prion protein
PS1: presenilin 1
PSP: progressive supranuclear palsy
ptr: pristinamycin resistance determinant
ROS: reactive oxygen species
RT: room temperature
SB: caprylyl sulfobetaine
SDS: sodium dodecyl sulfate
SILAC: isotope labeling with amino acids in cell culture
SNPs: single nucleotide polymorphisms
SOD: superoxide dismutase
TBP: tributylphosphine
2-D: two-dimensional
2-DE: two-dimensional electrophoresis
TFA: trifluoroacetic acid
TPI: triosephosphate isomerase
Vh: volts x hours
WT: wild-type
YFP: yellow fluorescent protein

ACKNOWLEDGMENTS

I am foremost indebted to my parents who encouraged me to follow my own path and supported me right throughout my studies. To my father who died of cancer two years ago, I cannot begin to express the extent of my gratitude for his constant love and patient advice even until the very end. I also want to thank my mother for her understanding and still trying to be there for me during these difficult times.

This thesis would not have been possible without the supervision of Dr. Jürgen Götz. I would especially like to thank him for his genuine support, help and kindness. He has always been ready to listen unwearyingly to my various scientific dilemmas.

I am indebted to all the members of the Division of Psychiatry Research for their help and for providing such a great work environment and atmosphere. I am particularly grateful to Raphael Poirier for his witty humour, his suggestions and also of course his company. I want to thank Luis Pennanen for his constant support, easy going attitude and for being such a great friend. I am also much obliged to Frederic Hoerndli, Dr. Feng Chen and Andreas Schild for helpful comments on my work during our group meetings.

I would like to thank the Functional Genomics Center Zürich for providing access to the MALDI TOF/TOF apparatus, GelPix robot and Proteomweaver software. I would especially like to thank Dr. Peter Gehrig in the FGCZ for helping me with the MALDI mass spectrometry of the spots and constantly improving the accuracy of the measurements, allowing us to detect even the faintest spots. Also at the FGCZ, Dorothea Rutishauser and Frank Potthast have both helped me with respectively the ESI mass spectrometry and computer related problems.

I am greatly indebted to Eva Moritz for her constant smile and support. She has enormously helped me by providing immunostaining related protocols and especially by cutting and staining the sections needed to check the site of Aβ injection in the mice.
I am much obliged to Daniel Schuppli for all the cloning for the PipOFF system and especially the generation of the transgenic mice with the different constructs. I would also like to thank Jerôme Bosset for performing the transfection of the mouse fibroblasts with the Gene Gun.
I am very appreciative of the work done by the group of Dr. Anne Eckert in Frankfurt on the mitochondrial and oxidative stress disorder in the P301L tau mice.

I am grateful to Dr. Robert Layfield for patiently listening to my research related questions and for helpful suggestions.

Finally, I would like to thank Prof. Josef Jiricny for kindly accepting me as an external student and for helpful comments on my work. I am also thankful to Dr. Luc Buée for agreeing to be the independent external expert and for refereeing my thesis.
I am grateful to Prof. Roger Nitsch for allowing me to carry out this thesis in his department.

CURRICULUM VITAE

Surname: **David**

First name: **Della Crystal**

Date and place of Birth: 8 June 1978 in Durban, South Africa.

Nationality: British

Languages: Bilingual English/French. Fluent in German.

E-mail: della.david@bli.unizh.ch

STUDIES:

1998-2001: Ecole Superieure de Biotechnologie de Strasbourg (ESBS), Université Louis Pasteur, Strasbourg, France.

Obtained the French/German/Swiss bioengineer diploma and the D.E.A. (Diplôme d'Etudes Approfondies) in molecular and cell biology with the grade Bien.

Part of this bilingual course is carried out in the universities of Freiburg, Karlsruhe and Basel.

See web site: http://www-esbs.u-strasbg.fr/

Attended neurobiology lectures at Strasbourg University, ULP.

1997-1998: Montpellier University - selected for special class of intensive preparation for Grande Ecole. Principal subjects were biochemistry, physiology and molecular biology. Obtained the two year university degree DEUG (Diplome d'Etudes Universitaires Generales), grade Bien and Assez-Bien.

1989-1996: Secondary school Gérard Philipe (Bagnols-sur-Cèze, France), took the science Baccalaureate in June 1996.

TRAINING PERIODS:

November 2001-June 2005: Ph. D. in the laboratory of Dr. Götz, University of Zürich, investigating with the help of proteomics, a cellular and mouse model of Alzheimer's disease.
January-September 2001: Internship under the direction of Dr. Layfield in Dr. Spillantini's laboratory working on neurodegeneration in the Brain Repair Centre, Cambridge, UK. Diploma title: The degradation of tau by the proteasome.
June-July 2000: Internship in the laboratory of Regeneration and Developmental Neurobiology of Prof. Faissner, CNRS unite UPR 1352, Neurochemistry Centre, Strasbourg, France.
August 1999: Internship in the laboratory of Neuronal Specification directed by Prof. Goetz, Max Planck Institute for Neurobiology, Martinsried, Germany.
June-July 1999: Internship in the laboratory of Functional Neuromorphology of Prof. Bons, on Alzheimer pathology in the lemur *Microcebus murinus*, Ecole Pratique des Hautes Etudes (EPHE), Montpellier, France.

PUBLICATIONS:

David DC, Hauptmann S, Scherping I, Schuessel K, Keil U, Rizzu P, Ravid R, Dröse S, Brandt U, Müller WE, Eckert E, Gotz J (2005) Proteomic and functional analysis reveal a mitochondrial dysfunction in P301L tau transgenic mice. *J. Biol. Chem*., in press.
David DC, Layfield R, Serpell L, Narain Y, Goedert M, Spillantini MG (2002) Proteasomal degradation of tau protein. *J. Neurochem*. 83, 176-185.

Reviews:
David D, Hoerndli F, Gotz J (2005) Functional Genomics Meets Neurodegenerative Disorders. *Prog. Neurobiol.* in press.
Chen F, **David D**, Ferrari A, Gotz J. (2004) Posttranslational modifications of tau--role in human tauopathies and modeling in transgenic animals. *Curr. Drug Targets*. 5, 503-515. Review.
Gotz J, Streffer JR, **David D**, Schild A, Hoerndli F, Pennanen L, Kurosinski P, Chen F (2004) Transgenic animal models of Alzheimer's disease and related disorders: histopathology, behavior and therapy. *Mol Psychiatry*. 9, 664-683. Review.

Chen F, Ferrari A, Schild A, Kurosinski P, **David D**, Hoerndli F, Pennanen L, Kins S, van Dorpe J, Nitsch RM, Götz J (2003) Amyloid-induced neurofibrillary tangle formation. In: Alzheimer's disease and related disorders: Research advances (editors: K. Iqbal, B. Winblad; Ana Aslan International Foundation).

MEETINGS ATTENDED:

February 2005: Winter Brain symposium, Sils Maria, Switzerland
October 2004: Society for Neuroscience 2004 annual meeting, San Diego, USA
October 2004: ZNZ symposium, Zürich, Switzerland
August 2003: Arolla Workshop, Growth control in development and disease, Arolla, Switzerland
May 2003: Alzheimer's and Parkinson's diseases, 6th International conference, Seville, Spain
April 2003: Sixth International Workshop on Proteasomes, Clermont-Ferrand, France
October 2002: High resolution biopolymer mass spectrometry, GDCh course, Konstanz, Germany
February 2002: NCCR Neural Plasticity and Repair Symposium, Kartause Ittingen, Switzerland
November 2001: Proceedings of the 1st Annual Conference of the Swiss Proteomics Society, Geneva, Switzerland
September 2001: International Meeting on Proteome Analysis, München, Germany
April 2001: British Neuroscience Association, Harrogate, UK
March 2001: Brain Repair Centre spring school on plasticity and stem cells, Cambridge, UK
March 2000: Neuropathology and Genetics of Dementia, St Moritz, Switzerland
December 1999: Neurex, Basel, Switzerland